University of Technology, Sydney

AN ADAPTIVE TUNABLE VIBRATION ABSORBER USING MAGNETORHEOLOGICAL ELASTOMERS FOR VIBRATION CONTROL OF VEHICLE POWERTRAINS

By

Nga Hoang

Submitted in fulfilment of the requirements for the degree of

Doctor of Philosophy

Faculty of Engineering and Information Technology

June, 2011

CERTIFICATE OF AUTHORSHIP/ORIGINALITY

I certify that the work in this thesis has not previously been submitted for a degree nor has it been submitted as part of requirements for a degree except as fully acknowledged within the text.

I also certify that the thesis has been written by me. Any help that I have received in my research work and the preparation of the thesis itself has been acknowledged. In addition, I certify that all information sources and literature used are indicated in the thesis.

Signed Production Note:
Signature removed prior to publication.

Nga Hoang

Acknowledgments

I would like to thank my principal supervisor Professor Nong Zhang for his supervision and support during my thesis. His helpful advice is invaluable for me not only in the PhD course but also in my further studies.

I would also like to thank my co-supervisor Dr. Haiping Du for his guidance. Under his supervision my research skills have improved significantly. His careful review has also helped me a lot during this work. It is my pleasure to work with him.

The support from Professor Weihua Li and Tongfei Tian, University of Wollongong is greatly appreciated. The author also would like to thank Professor Peter Watterson, Chris Chapman, Michael Tran and Lifu Wang for their technical support during the experimental testing stage.

A special thanks to Dr. Wade Smith and my colleagues Paul Walker, Jin Zhang, Salisa Abdul Rahman, Yoo Shin Kim, Jing Zhao and Robert Heal for their great friendship at the University of Technology, Sydney.

I would like to sincerely thank Vietnam's Overseas Scholarship Program (Project 322), Vietnam International Education Development, Vietnam's Ministry of Education and Training for the doctoral scholarship. Also, the financial support by the Australian Research Council (ARC LP0775445) is gratefully acknowledged.

Special thanks to my parents, sisters and brothers and other members of my family for their support and encouragement. Particularly, thanks to my son, Viet Hoang, and my little daughter, Ngan Hoang for their love.

Finally, I would like to give special thanks to my wife, Thi Yen Hoang, who has stood by me through all circumstances of ups and downs. Thank you for your understanding and support.

Sydney 9-6-2011

Nga Hoang

TABLE OF CONTENTS

Abstract

Powertrains are a crucial subsystem of vehicles and are also a source of the vibration. Because of the wide range of operating frequencies of powertrain, the likelihood of the engine working speed being in the resonance area is very high. Moreover, the resonance cannot be avoided when the engine speed passes through one or more modal powertrain frequencies in the transient stage. An example of the transient stage is that the engine accelerates from idle to top working speeds. Consequently, powertrains may experience a high level of vibration.

This thesis presents the development of torsional adaptive tunable vibration absorber (ATVA) using magnetorheological elastomers (MREs) for powertrain vibration control. The effectiveness of the ATVA is examined by both methods: numerical simulations and experimental testing.

The MRE is a smart material consisting of a host matrix and magnetic particles and the MRE material is promising for constructing ATVAs because its elastic moduli and damping can be controlled magnetically. Consequently, a MRE-based ATVA can work in a wide frequency range instead of a narrow bandwidth as a traditional vibration absorber does.

The principal idea of this thesis is that by tuning the MRE-based ATVA modal frequency and by choosing the ATVA location, powertrain modal frequencies can be actively shifted away from the resonant area for either steady or transient states. Numerical simulations are conducted to show the ATVA's effectiveness. In addition, the application of multiple ATVAs for dealing with multi-harmonic excitations is numerically examined. The numerical simulations are also used to facilitate the ATVA design, in which, the effect of ATVA parameters such as moment of inertia, stiffness and damping is investigated.

A MRE material is fabricated to develop an ATVA for experimental validation. With the MRE measured properties, an ATVA is designed and manufactured. Both designed and experimental results of ATVA modal frequency are in a good agreement. The ATVA can work in a frequency range from 10.75 to 16.5Hz (53% in relative change).

To validate the ATVA's effectiveness, experimental testing is conducted for a powertrain test rig at the University of Technology, Sydney. The powertrain fitted with the ATVA is experimentally investigated. The experimental results show that with the ATVA the powertrain modal frequencies can be shifted far away from the resonant area. This finding confirms that the ATVA works effectively. The torsional MRE-based ATVA is a new device for vehicle powertrain vibration reduction.

Abbreviations

ATVA	Adaptive Tuned Vibration Absorber
TVA	Tunable vibration absorber
AT	Automatic transmission
MT	Manual transmission
TC	Torque converter
ICD	Internal Crankshaft Damper
BSD	Balanceshaft Damper
DMF	Dual Mass Flywheel
ICE	Internal combustion engine
DOF	Degree of freedom
SDOF	Single degree of freedom
MDOF	Multi degrees of freedom
EOM	Equation of motion
ODE	Ordinary differential equation
SMA	Shape memory alloy
MR	Magnetorheological
MRE	Magnetorheological elastomer
MRF	Magnetorheological fluid
FFT	Fast Fourier Transformation
SSA	State-switched absorbers
UTS	University of Technology, Sydney

List of Symbols

a	constant, length
A	area, cross section area
A	system matrix
b	constant, length
B	magnetic flux density
c_A	ATVA damping coefficient
c	damping coefficient
c_{ij}	damping coefficient
C	damping matrix
d	distance, diameter
h	real part of complex eigenvalue
E	Young's modulus
F	force
G	shear modulus
$\hat{G}$	complex shear modulus
G'	storage modulus
G''	loss modulus
H	magnetic field intensity
I	electric current
i	integer
I	identity matrix
J	moment of inertia
J	inertia matrix
J_A	moment of inertia of dynamic absorber
k_i	torsional spring coefficient
k_{ij}	stiffness coefficient
K	stiffness matrix
k_A	stiffness coefficient of dynamic absorber, MRE stiffness
l, l_i	length
m	mass
n	an integer

N	number of degrees of freedom, number of turn of electric coil
Q_i	i^{th} generalized force
R	dissipation function, radius
R	matrix of transfer functions
R_i	inner radius
R_O	outer radius
t	time
T	torque, kinetic energy
T_i	kinetic energy of i^{th} body
V	potential energy
V_i	potential energy of i^{th} spring
x	vibration response
X	vibration amplitude, vibration complex amplitude
$\overline{X}$	vibration amplitude
W	width
z	state vector
α	angle, constant
β	angle, constant
γ	dynamic harmonic strain
ΔF	increment in F
Δl	increment in l
ε	strain
ς	damping ratio
ς_A	ATVA damping ratio
θ	angular displacement
θ	vector of angular displacement
θ_i	i^{th} angular displacement
Θ	vector amplitude of θ
λ	eigenvalue
μ	mass ratio, inertia ratio
ϕ	magnetic flux, phase angle
ω	frequency
ω_i	i^{th} natural frequency

ω_n	natural frequency
ω_d	damped frequency
Ω	excitation frequency, forcing frequency
ρ	mass density

List of Figures

List of Tables

Chapter 1 INTRODUCTION

1.1 Overview of this work

This thesis presents the development of torsional adaptive tunable vibration absorber (ATVA) using magnetorheological elastomers (MREs) for vibration reduction of vehicle powertrains, in which the MRE is a smart material with variable stiffness under application of an external magnetic field.

A vehicle powertrain is a term referring to a crucial component of automobiles for delivering power from engine to vehicle tires. In general, it consists of an engine, a torque converter (TC) for automatic transmission (AT) or a clutch for manual transmission (MT), a transmission gearbox and driveline components such as differentials and wheel tires. Obviously, the powertrain system is a major source of vibration for a vehicle and the system has several natural frequencies in a wide range of frequencies, [1-3]. In addition, the torque fluctuation of the engine is periodic due to dynamic characteristics of the internal combustion engine (ICE). As a result, the powertrain is subjected to multi-frequency excitations [4, 5]. Because the engine speed range is large, the resonance phenomenon may be unavoidable. In particular, when the engine speed accelerates from 700-1000 r.p.m (idle speed) to 5000-6500 r.p.m (top working speed) it will pass through one or more powertrain natural frequencies. Consequently, the vibration of the powertrain could increase significantly if the acceleration time is not rapid enough, and this vibration reduces the comfort performance of vehicle. In addition, the vibration of the powertrain contributes to the noise, vibration and harshness of vehicles and needs to be minimised.

Dynamic absorbers or tunable vibration absorbers (TVAs) have been an effective device for minimising mechanical vibrations for engineering applications such as structures and mechanisms. The theory and application of the device have been introduced for a long time, [5-7]. Basically, a TVA is an auxiliary system attached to the primary system when the resonance occurs to absorb undesirable vibrations. When the forcing frequency (also the excitation frequency) is close to or coincides with the natural frequency of the primary system, TVA, a mass-spring-damper system, characterised by a mass (moment of inertia), stiffness and damping coefficients are tuned to make sure that TVA frequency also coincides with the forcing frequency. As a result, the frequency of the primary system will be shifted far away from the excitation frequency and the vibration of the primary system will be reduced significantly. However, one drawback of the traditional TVA is that this device can work effectively only in a narrow bandwidth. In other words, the TVA may not work effectively for vibration control of mechanical systems which have a wide range of operating frequencies, such as the powertrain. Thus, ATVAs are an effective solution to deal with the drawback of traditional TVAs. The main difference between traditional TVA and ATVA is that there is an adaptive element in the ATVA so that its frequency range can be varied widely. The magnetorheological elastomer is a potential material to be used for developing such an element for ATVAs.

Magnetorheological elastomers (MREs) are a smart material in the MR family that includes MR fluids, foams and elastomers. One vital feature of MREs is that their mechanical properties such as elastic moduli and damping can be properly controlled by a magnetic field. Consequently, both stiffness and damping of MREs can be controlled rapidly by an external magnetic field, and thus, MREs have been used to develop adaptive tuned vibration absorbers (ATVAs), [8-10].

1.2 Motivation and significance of the thesis

Even though, a great number of MRE-based ATVAs have been studied, the use of these MRE-based ATVAs has only applied to single degree of freedom (SDOF) systems. The application of the ATVAs for multi degree of freedom (MDOF) systems such as the powertrain system is an area that has not been fully addressed so far.

The motivation of this thesis is to develop a torsional ATVA using MREs for torsional vibration control of powertrains, which are an essential component in automotive engineering. The principal idea of the thesis is that by tuning the MRE-based ATVA frequency properly and by choosing its location correctly, powertrain frequencies can be actively controlled away from the resonant area for either steady or transient states. As a result, the powertrain vibration can be reduced significantly. The effectiveness of the MRE-based ATVA will be validated by both numerical simulations and experimental testing. This MRE-based ATVA will be a new device for vibration reduction of powertrains.

1.3 Objectives of the thesis

The thesis objectives include:

- To gain a comprehensive understanding of relevant research topics by investigation into previous research to identify the gap in current knowledge.
- To numerically investigate the MRE-based ATVA effectiveness for powertrain vibration reduction for both steady and transient states. Also, the application of ATVA for powertrain vibration reduction in single or multi-frequency excitation is examined.
- To measure the mechanical properties of a MRE material. The measured properties of the MRE include Young's modulus and damping ratio. These MRE properties will be used to design an ATVA. Also, theory models of the properties are derived to facilitate the ATVA design.
- To propose an ATVA design using the MRE for vibration control of a powertrain test rig at the Dynamics Laboratory, Faculty of Engineering and Information Technology, University of Technology, Sydney (UTS). Accordingly, both mechanical and magnetic parameters are designed.
- To measure the frequency of the ATVA using the MRE, in which, the dependence of ATVA frequency on magnetic flux density (or electric current) is presented.
- To conduct the experimental validation to show the ATVA's effectiveness for shifting the frequency of the UTS powertrain test rig.

1.4 Contributions

- Investigation into MREs, powertrain, ATVA to obtain a comprehensive understanding of key research topics.
- Numerical simulations for several applications of ATVA. Relevant examples are for powertrain steady state, powertrain transient state and using multi ATVAs for powertrain under multi-frequency excitation.
- Development of experimental testing for measuring a MRE property such as Young's modulus and damping ratio. Basing on experimental data, explicit functions of the properties are derived to facilitate the ATVA design.
- Development of ATVA using a MRE for powertrain vibration control.
- Experimental testing for measuring ATVA frequency under application of magnetic field.
- Experimental testing for validating the ATVA's effectiveness for shifting resonant frequencies of the UTS powertrain test rig.

1.5 Methodology

To achieve the objectives of the thesis, which include both numerical and experimental results, several methods are used in this work.

A lumped-mass model is used for investigation into powertrain systems before and after using ATVA. The equation of motion (EOM) of the powertrain is derived from Lagrange's equation in the matrix form. From the EOM, both the free and forced vibration of the powertrain can be obtained.

The free vibration of the powertrain can be determined from the eigenvalue problem of the system matrix which is formed from the inertia, stiffness and damping matrix of the powertrain. Searching the eigenvalue and eigenvector problems can be done by using basic functions of MATLAB software. As a result, powertrain mechanical vibration features such as natural frequencies, damped frequencies, damping ratio and mode shapes are determined.

In addition, there are also two methods, complex magnitude and integration methods, for solving the equation of motion of the powertrain to obtain the powertrain's forced

vibration. The complex magnitude method is used to calculate forced vibration responses of the powertrain when the excitation torque is harmonic. To be specific, in this thesis the steady state vibration of powertrains is determined by this method. Otherwise, when the excitation torque is not harmonic such as in the transient state, the integration method is used for numerically solving the forced vibration problem of powertrain. For this method, the EOM of the powertrain is re-written as a system of first-order ordinary differential equations. Then, MTLAB module ODE45 is used to compute the forced vibration response of powertrain. In this work, the integration method is used to determine the transient state vibration of powertrains.

Ohm's law for the magnetic circuit is used to design the magnetic circuit of ATVA. With the specification of the UTS powertrain test rig, ATVA geometry parameters are calculated and chosen. As a result, parameters of magnetic circuit such as magnetic reluctance, magnetic flux, magnetic flux density and number of turns of electromagnetic coils can be determined.

Experimental verification is conducted to validate the ATVA's effectiveness. The ATVA is tested for a powertrain test rig at the Dynamics Laboratory, Faculty of Engineering and Information Technology, University of Technology, Sydney, Australia. There are three states for the experimental testing. The first state is to measure the mechanical properties of a MRE. The second state is to measure the ATVA frequency. The last stage is to experimentally validate the effectiveness of ATVA for shifting frequency of UTS powertrain test rig.

To measure Young's modulus of the MRE the tensile and compression device INSTRON 1026, is used. This device is connected to the National Instrument module to transfer data to the computer. The data acquisition is conducted by Labview software version 8.6, and, the magnetic flux density is measured by instrument Gaussmeter 610. The ATVA design is conducted by using the effective tool SolidWorks 2006 SP4.1. For measuring free vibration response, a Dynamic Signal Analyser device is used. Also, two kinds of sensors, accelerometer and torque transducer, are used to pick up and transfer the signal to the Analyser for measuring the ATVA frequency and the UTS powertrain test rig frequency, respectively.

1.6 Outlines of thesis

This work consists of ten chapters, summarised below:

Chapter 2: This chapter conducts a literature survey for this work, in which, information and knowledge of relevant research topics are investigated. The research topics include torsional vibration, powertrains and vibration of powertrains, magnetorheological elastomers, TVAs, ATVAs and ATVAs using MREs. The gap in current knowledge is also identified.

Chapter 3: This chapter briefly presents the fundamental features of MREs. Two models of MREs, which are essential for mechanical vibration problems, are reported. In addition, the equivalent stiffness of MRE layers for the two main types of vibration motion (translation and rotation) is presented for MRE-based ATVA design.

Chapter 4: A mathematic background of traditional dynamic absorbers is presented. A model of two degrees of freedom is investigated to show the effectiveness of dynamic absorbers for dealing with mechanical resonances. A case study is demonstrated. The optimal turning parameters of dynamic absorbers are also presented.

Chapter 5: Numerical simulations are conducted in this chapter to show the effectiveness of the ATVA using a soft MRE for powertrain vibration reduction for steady state. In this chapter, equations of motion of powertrain with and without ATVA are derived. Also, free and forced vibrations of powertrain under single harmonics excitation are reported. In addition, the effect of ATVAs parameters (such as inertia, stiffness and damping) on powertrain vibration control is examined.

Chapter 6: The numerical simulation of dual ATVA using MREs is carried out to demonstrate the ATVA's effectiveness for steady state vibration reduction of powertrain under multi-frequency excitation. In this chapter, the dual ATVA is used to deal with multi resonances at the same time and both the free and forced vibrations of the powertrain are numerically investigated.

Chapter 7: In this chapter, the use of ATVA for reducing powertrain transient vibration is demonstrated. The transient process of powertrain vibration examined is the

acceleration of engine speed. In the transient process, the excitation frequency of engine fluctuation is variable rather than constant as the steady state. In the transient state, the ATVA is also used to deal with the resonance, which definitely occurs when the powertrain engine accelerates from idle to top working speeds. By tuning ATVA frequency, powertrain modal frequency is shifted out of the resonant area. Thus, the powertrain transient vibration is reduced significantly.

Chapter 8: This chapter proposes an ATVA design to experimentally validate the effectiveness of ATVA for shifting the frequency of the UTS powertrain test rig. To design the ATVA, a MRE material is fabricated and experimentally tested to obtain dynamic properties such as Young's modulus and damping ratio. With the MRE measured properties, a MRE-based ATVA is designed.

Chapter 9: This chapter provides experimental validation for the ATVA using a MRE. An actual ATVA is developed in the UTS mechanical workshop. The ATVA frequency range is then measured to validate the ATVA design. The ATVA's effectiveness is experimentally validated for shifting the frequency of the UTS powertrain test rig. The frequency of UTS powertrain test rig before and after adding the ATVA is measured and compared to confirm the ATVA's effectiveness.

Chapter 10: Lastly, the summary of thesis is presented. The contribution of this thesis is reviewed and concluded and recommendations for further studies are proposed.

Chapter 2 LITERATURE REVIEW

2.1 Introduction

This chapter provides background information, which involves several research topics of this thesis. Firstly, the chapter presents brief background of torsional vibration, the powertrain system and its vibration. Secondly, this is a brief introduction to traditional TVAs and ATVAs, which are an upgraded version of TVAs. A detailed review of MREs and ATVAs using MREs is then provided. From the literature review, the gap in the current knowledge is identified. As a result, the definition of this thesis is highlighted as given in Chapter 1.

2.2 Torsional vibration

Torsional vibration is a typical form of mechanical vibration. This vibration involves angular vibration of the rotor of a machine. The theory of torsional vibration has been reported in classic books of mechanical vibration for a long time. For example, Walker [11] presented a comprehensive study about the torsional vibration of turbomachinery. In this study, the author classified and characterised the torsional vibration. Torsional fatigue was also mentioned in this study and the author pointed out that the main reason for the failure of rotating machines is the torsional vibration of the rotating shaft. In addition, the author indicated that both steady and transient vibration state vibration should be calculated for torsional vibration systems.

In line with Walker, the torsional vibration of rotating machinery was summarised

by Wachel and Szenasi [4]. The authors stated that the significance of torsional vibration for rotating machinery is so important that there are API codes for the torsional vibration of rotating machines (API 611, 617, 610). The API codes specify that any torsional vibration frequency should be at least 10% below or above that of the operating speed. In addition, during calculations at least 5% should be added. The study also suggested that the analysis of torsional vibration is an important stage which should be performed carefully. Moreover, the author reported that a system with a wide operating speed (such as a system with a reciprocating engine) will increase the likelihood of coincidence between the operating speed and torsional vibration frequency. Furthermore, these authors indicated that the resonance may not be avoided when the engine speed is accelerated to pass through the natural frequency of the rotating system. Thus, the authors also recommended that for such systems, considerations should be given to the torsional vibration.

The model of the rectilinear vibration and the torsional vibration is shown in Figures 2.1a) and b).

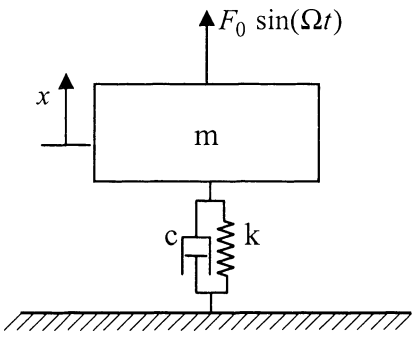

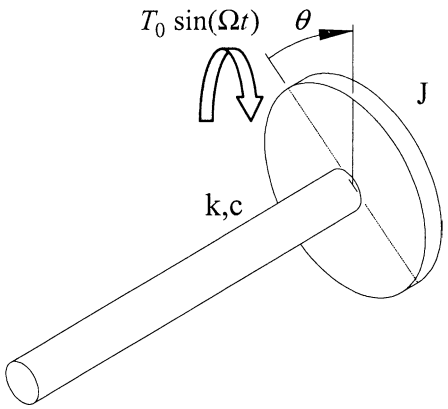

a) Rectilinear SDOF system b) Equivalent torsional vibration SOF system

Figure 2.1. A simple torsional vibration

Even though the physics nature of the two problems is different, the mathematic model of both rectilinear and torsional vibrations is the same, see the references by Wachel and Szenasi [4] and Friswell et al [12] for more detail.

The equivalence between two models of SDOF system in Figures 2.1a, b is summarised in Table 2.1.

Table 2.1. Equivalent model of rectilinear and torsional vibration [4]

	Rectilinear vibration		torsional vibration	
	Symbol	Unit	Symbol	Unit
time	t	s	t	s
displacement	x	m	θ	rad
velocity	$\dot{x}$	m/s	$\dot{\theta}$	rad/s
acceleration	$\ddot{x}$	m/s^2	$\ddot{\theta}$	rad/s^2
stiffness coefficient	k	N/m	k	Nm/rad
damping coefficient	c	Ns/m	c	Nms/rad
kinetic energy	$\frac{1}{2}m\dot{x}^2$	Nm	$\frac{1}{2}J\dot{\theta}^2$	Nm
potential energy	$\frac{1}{2}kx^2$	Nm	$\frac{1}{2}k\theta^2$	Nm
force (torque)	$F = m\ddot{x}$	N	$T = J\ddot{\theta}$	Nm
work	$\int Fdx$	Nm	$\int Td\theta$	Nm
natural frequency	$\omega_n = \sqrt{k/m}$	rad/s	$\omega_n = \sqrt{k/J}$	rad/s
damped frequency	$\omega_d = \omega_n\sqrt{1-\varsigma^2}$	rad/s	$\omega_d = \omega_n\sqrt{1-\varsigma^2}$	rad/s
damping ratio	$\varsigma = \frac{c}{2m\omega_n}$	rad/s	$\varsigma = \frac{c}{2J\omega_n}$	rad/s
equation of motion	$m\ddot{x} + c\dot{x} + kx = F_0\sin(\Omega t)$		$J\ddot{\theta} + c\dot{\theta} + k\ddot{\theta} = T_0\sin(\Omega t)$	

2.3 Powertrain system and its torsional vibration

A powertrain system is a crucial component of vehicles. The detailed description of powertrain systems and their components were mentioned in a great deal of study [13-17]. Two references, Shaver [13] and Kienckle and Nielsen [14] presented components of manual transmission powertrain systems. Crouse [15] and Larew [16] described automatic transmission powertrain components. In addition, the dynamic models of powertrain for both MT and AT were reported by Gillespie [17].

A typical powertrain system is shown in Figures 2.2 and 2.3.

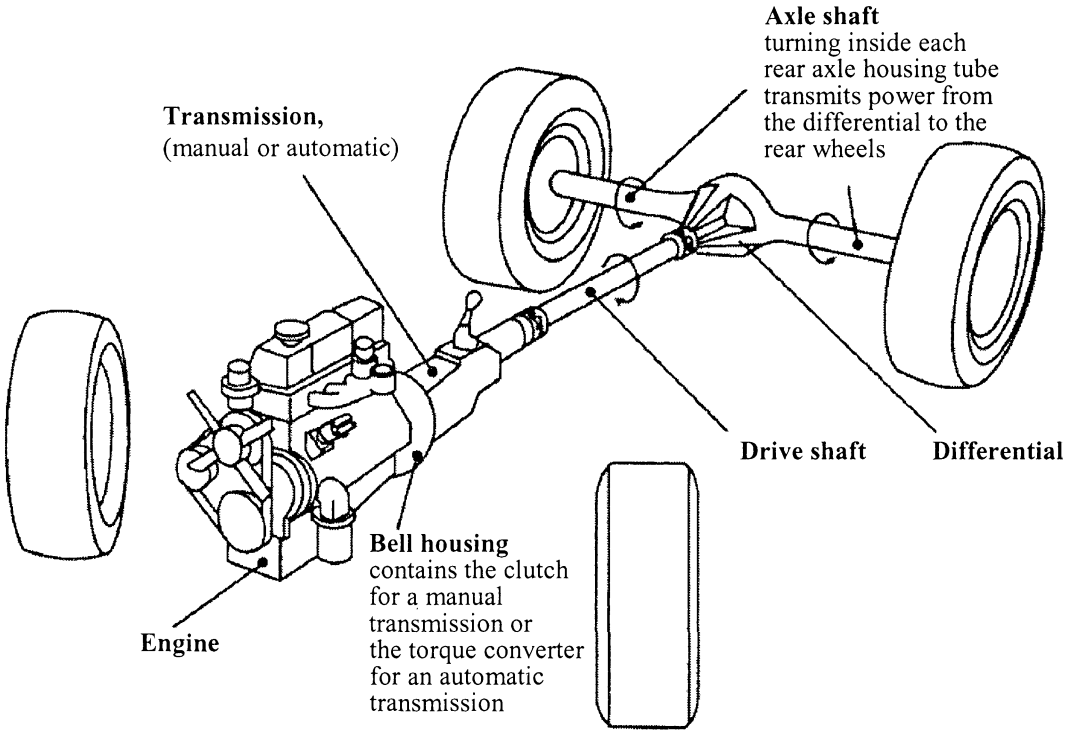

Figure 2.2. Primary components of a powertrain system [17]

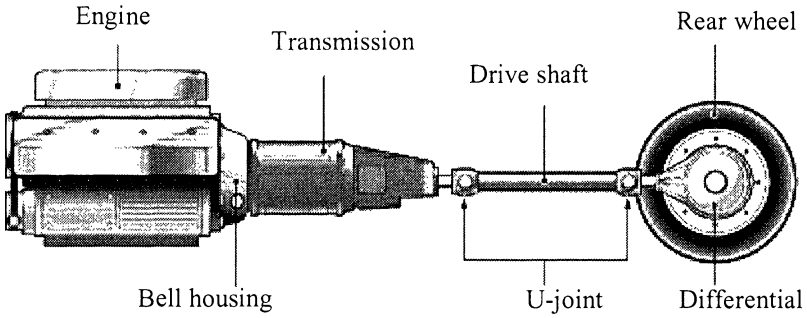

Figure 2.3. Side view of a powertrain system [18]

According to Gillespie [17], the powertrain consists of primary elements as follows:

- **Engine:** provides the power for vehicles. It is noted that ICEs are used in most vehicles. In this study it is assumed that vehicle engines mentioned are ICEs.
- **Bell housing**: covers either the clutch for a manual transmission or the torque converter for an automatic transmission.
- **Transmission**, manual or automatic, has a gearset to provide a number of gear ratios used to set the optimal engine speed according to vehicle speed.

- **Driveshaft:** transmits power from the transmission to the differential. The Universal joints (U-joints) allow the driveshaft to ride up and down to the rear axle.
- **Differential:** turns the power, which is from the driveshaft, at a right angle. The differential also allows one wheel to rotate faster or slower than the other.
- **Axle shaft:** This transmits the power from the differential to the rear wheels.

In a vehicle powertrain there are a number of gear ratios, which are used to set the optimal engine speed according to vehicle speed. Obviously, the powertrain is a main source of torsional vibration because the system has potential vibration sources such as the engine and gear sets.

Study about torsional vibration of powertrain is a broad area which has been of interest to a great deal of researchers. A series of studies about the torsional vibrations of powertrains and their components is presented in references [19-24]. In this series, torsional vibration in the powertrain system, fundamental features of the powertrain system and torsional vibration modelling are reported. Reik [19] presented the fundamental features of the internal combustion engine of powertrains and introduced several torsional vibration models of powertrain systems. In particular, the author pointed out that several possible resonance points in powertrain over a range of engine speed. In a further, study Reik [20] presented several methods to eliminate the torsional vibrations of powertrains; for example, the use of propeller shaft dampers and centrifugal pendulum were mentioned. Karl [21] described the torsional vibration of a tractor for both steady and transient vibration stages and the author also proposed a torsional vibration model for the tractor powertrain.

More recently, Hwang et al [25] investigated a Ford rear-wheel-drive with a four-speed automatic powertrain. They developed a torsional vibration model to determine the torsional characteristics of a vehicle powertrain such as natural frequencies and mode shapes. These authors indicated that the fundamental frequency of the powertrain versus axle stiffness is about 5.5Hz to 7.0 Hz for the third gear and 6.75 Hz to 8.0 Hz for the fourth gear. In recent years, Crowther [1] and Zhang et al [2] studied transient and free

vibrations of an automatic powertrain BTR four-speed 93 LE. Their results pointed out that the first powertrain fundamental frequency for the second gear is 7.0 Hz and for the third gear is 8.8 Hz. The second powertrain fundamental frequencies are 28.6Hz and 28.0Hz for the second and third gear respectively.

Couderc et al [3] simulated and tested a manual powertrain and reported that the gear rattle vibration mode with frequency 68.3 Hz is a potential vibration source. The authors also showed that there are many natural frequencies in a wide range in the powertrain system. In addition, the authors reported that the torque fluctuation is periodic due to the ICE dynamic characteristics so that the powertrain is subjected to multi-frequency excitations. Because the engine speed range is large, the resonance phenomena may not be avoided.

Wang [26] developed a test rig for a vehicle powertrain. The test rig consists of an ICE, an automatic transmission and a driveline component, which includes a propeller (drive shaft), differential and vehicle wheels. Several analytical models of torsional vibration were proposed to investigate both free and forced vibration of the test rig. As a result, features of mechanical torsional vibration of the tests rig such as natural frequency and mode shapes were investigated.

Although there has been a great deal of study about powertrain vibration, effective solutions for vibration reduction of the powertrain have not been fully addressed in either theory or practice because of the complexity of the powertrain system.

Fredriksson et al [27] proposed a model of a powertrain and conducted experimental testing for vibration control of a real heavy truck. In this study, an active controller was used for vibration reduction of the powertrain. However, the limitation of the study is that it did not show how to deal with the resonance of the powertrain for both the steady state and transient state. As a result, the powertrain modal frequency shifting by an active controller was not reported.

Imtiaz [28] used different control strategies for controlling a powertrain system, which

was modelled as a SDOF system. Although many attempts were made, this study shows two main drawbacks. Firstly, the SDOF model for powertrain may not correctly reflect the mechanical vibration behaviour of a powertrain. Secondly, the experimental testing was not conducted for a real powertrain system.

Schankin et al [29] used a damper for rotating shaft torsional vibration. In this study, an actuator and coupling were used for damping the torsional vibration of the shaft. However, these studies did not show how powertrain frequencies shift. Also, the mathematic background of these studies was not provided.

More recently, a range of products by the international LuK Group for vibration reduction of powertrains was introduced in [30]. In this range, the powertrain vibration control is concentrated on the powertrain's components such as the engine flywheel or clutch. Examples of these dampers are Internal Crankshaft Damper (ICD), Balanceshaft Damper (BSD) or Dual Mass Flywheel (DMF). Although the use of ICDs, BSDs and DMFs are effective for damping the vibration of separated components, the drawback of the products is that these devices are only passive dampers. In addition, the powertrain modal frequency cannot be shifted significantly by using the dampers; thus, these devices may not deal with the resonances, which often happen for powertrain systems. For instance, when a powertrain's engine accelerates from idle speed to top working speed, a passive damper may no longer be effective. Therefore, the resonance, which occurs when the engine speed passes through one or several powertrain frequencies, cannot be avoided for powertrain vibration control.

2.4 Traditional TVAs

The dynamic absorber or tunable vibration absorber (TVA), which was briefly introduced in Chapter 1, is a useful device for reducing unwanted mechanical vibrations and it is used widely in mechanical vibration control. A summary of the theory, application and parameter optimisation of TVAs was reported by Sun et al [31].

It is noted that TVAs are an effective solution for mechanical vibration reduction. These TVAs are used for not only SDOF systems but also MDOF systems. Many studies

about using TVAs for MDOF systems have been reported in references [32-40].

Ram and Elhay [32] presented the mathematic background of a MDOF dynamic absorber for MDOF systems. They also pointed out that SDOF dynamic absorbers, which have been used so far for vibration control, are a particular instant of MDOF dynamic absorber. Hadi et al [33] used the genetic algorithm to optimize a dynamic absorber design for a MDOF system structure. Ozer and Royston [34] extended Den Hartog's method to find the optimal parameters of a dynamic absorber added to an undamped MDOF system. In their further study, Ozer and Royston [35] applied Sherman-Morrison matrix inversion formula for optimisation parameters of a dynamic absorber attached to a damped MDOF system. In addition, Kitis et al [36] found an optimal design of a dynamic absorber, which is added to a damped MDOF system. This finding was base on numerical methods and is demonstrated for a 22 DOF system in the case study. In particular, Brennan and Dayou [40] used a TVA for shifting the frequencies of global modes of vibration.

One drawback of TVAs is that these devices can only work effectively in a narrow frequency range. Consequently, this limits the application of TVAs to many engineering mechanisms, such as powertrain systems, which have a wide range of operating frequency.

There are a number of studies on how to broaden the frequency range for traditional TVAs. The ATVA is part of next generation built on traditional TVAs. Basically, there is an adaptive element, which is embedded in the ATVA and is used to vary the ATVA frequency. As a result, an ATVA can work in a wider frequency range than a traditional TVA does.

Bonello et al [41] developed an ATVA using a variable stiffness element, which is formed from two parallel curved beams. These beams have a curvature that can be adjusted and hence the ATVA stiffness can be tuned. The frequency of this device can be changed by tuning the voltage applied to the piezoelectric materials, which are fitted in the parallel beams. The performance of the ATVA with piezo-actuated curved beams

is in a good agreement with both the theoretical and experimental testing data. The device is shown to be tunable over the frequency range 36–56 Hz.

Davis and Lesieutre [42] also used a piezoelectric ceramic material as a varying stiffness element to develop a TVA for vibration control. For this ATVA, the effective stiffness of the piezoelectric element is controlled by electric current. As a result, the frequency of the ATVA can be tuned. The author reported that the frequency range of the prototype of TVAs is 290-350 Hz.

Franchek et al [43] used a series of variable length coil spring to develop a dynamic absorber for a 4 degree-of-freedom system. The stiffness of the absorber can be controlled by changing a certain factors such as the wire diameter, spring diameter and the number of spring coils. The effectiveness of the dynamic absorber was experimentally tested and the authors reported that this dynamic absorber has a frequency range from 5.9 to 7.7Hz.

Flatau et al [44] implemented a magnetostrictive material called Terfenol-D for developing a TVA. The elastic modulus of the magnetostrictive material was controlled electrically because of stiffening of the crystal lattice under the application of a magnetic field. Experimental results were conducted and these authors reported that the frequency range of the Terfenol-D TVA is 1375 Hz and 2010 Hz.

Walsh and Lamancusa [45] developed an ATVA which has variable stiffness by introducing a compound leaf spring for minimizing the transient vibration for a SDOF application with time-varying excitation frequency. In the study, a spring design was proposed and the spring feature was then experimentally investigated. The author reported that by using the compound leaf spring, the relative stiffness of the ATVA was increased up to 45 times.

Another solution for changing the stiffness when developing ATVA is to use shape memory alloys (SMAs) [46-49]. Basically, the elastic modulus of SMAs can be tuned if the temperature of the SMA material is controlled. Thus, the frequency of ATVA using the SMA can be changed.

Williams et al [47] use a SMA for developing an ATVA. The SMA elastic modulus can be controlled by tuning the heat of the SMA spring element. Subsequently, the frequency of the absorber can be controlled. The experimental testing from the work reported that the SMA dynamic absorber frequency can be increased 15% (from 83.5 to 98Hz). In a further study, Williams et al [48] used a SMA element for a cantilever beam to develop an ATVA. These authors reported that the device can work in a frequency range from 38.5 to 46.5Hz. Rustighi et al [49] also presented a dynamic absorber using a SMA. By varying the electric applied current, the temperature of the SHA can be controlled. As a result, the elastic modulus can be varied. It was reported that the frequency range of the SMA absorber is 52-66Hz.

Although many attempts have been made to broaden the stiffness of ATVAs for vibration control, these devices still have some drawbacks such as complicated structures and slow responses. In addition, the increase in temperature may affect working conditions for mechanical systems.

2.5 Magnetorheological elastomers

Magnetorheological elastomers (MREs) are a smart material in the MR family that includes MR fluids (MRF) and elastomers. The most important feature of the MR family is that its mechanical properties can be controlled rapidly by an external magnetic field. An overview study about the MR family was reported by Carlson et al [9]. The authors also pointed out that MRFs are mainly used for torque transfer devices such as MR clutches or MR brakes. A number of examples of using MRFs for engineering applications can be seen in references [50, 51-53]. While MRFs have been used for developing MR clutches or MR brakes, it has been reported that MREs are promising material for constructing stiffness-varying devices such as ATVAs [8, 9-10].

Typically, MREs are composed of a host gel material, micro-size iron additives and an oil component, which serves as plasticisers. One vital feature of MREs called the MR effect is that their mechanical properties such as elastic moduli (including Young's modulus E and shear modulus G) can be properly controlled by a magnetic field [8-10].

Obviously, the mechanical property of the MRE depends on a number of factors. The relevant factors are the magnetic field, polymer matrices, the magnetic particle sizes, the volume fraction of particles, strain regimes and so on [8-10, 54-57]. Because stiffness and damping of MREs can be controlled rapidly by a magnetic field, MREs have been an interest in many studies. Having the ability of tuning stiffness and damping, which are two of three key components of mechanical vibrations (together with mass or inertia moment), MREs are clearly promising material for constructing ATVAs.

It has also been reported that the properties of MREs depend on the distribution of magnetic particles inside MREs [8-9]. As a result, MREs can be divided into isotropic MREs and anisotropic MREs. Isotropic MREs are MRE material in which magnetic particles homogeneously distributed. In contrast, anisotropic MRE materials are MREs that have aligned particles in which the magnetic particles are cured by a magnetic field for cross-linking these particles so that the columnar structures of the particles are formed. In other words, the preparation of isotropic MR elastomers and anisotropic MR elastomers is similar. The only difference is that the curing takes place in a magnetic field for magnetic particles for the anisotropic MREs but not for isotropic MREs [8].

Although the study of MREs is receiving a great deal of interest, to the author's knowledge, MREs might be classified as three generations so far. The first generation is traditional MREs, the second generation is enhanced MREs, and the thirdt generation is new MREs. These generations of MREs will be introduced in following sections.

2.5.1 Traditional MREs

Generally, the increment in elastic modulus in traditional MREs under MR effect is about 50-60% [8-10, 54, 55-57]. Jolly et al [54] reported that the increment in elastic modulus in regular MREs under MR effect is about 50-60%. Davis [52] used the Finite Element Method (FEM) to examine typical elastomers and reported that the increase in shear modulus at saturation of magnetic field is 50%. In addition, this author reported that the optimum volume faction of magnetic particles is 27%.

Zhou [10] used experimental testing to investigate MRE properties. The author used a

MRE material, which plays a role as a spring-damper element in a mass-spring-damper system. The free vibration of the mass was investigated. By measuring the decay response of the mass, the natural frequency, damped frequency and damping ratio can be measured. As a result, the shear modulus and damping ratio were obtained. The experimental results show that the increase in shear modulus could be 60% while the zero-field damping ratio is 0.24 and the change of the damping ratio is slight.

Kaliko [8] did a great deal of experimental testing for measuring the stiffness and damping properties of MREs. The properties of both isotropic and anisotropic MREs were investigated. In addition, several factors that affect MREs properties were examined: magnetic field, strain regimes and fraction volumes of magnetic particles. In addition, the author experimentally investigated MRE properties under both static load and dynamic load. According to the experimental results, the author reported that for anisotropic MRE material the maximal increase in stiffness is 60% in dynamic loading and 100% in static loading.

2.5.2 Enhanced MREs

The second generation of MRE are enhanced MREs. These MREs are enhanced by using techniques that increase the MR effect to overcome the shortcomings of traditional MREs. There have been an increasing number of studies to broaden the MRE stiffness range [58-64].

Lokander, M. and Stenberg [58, 59] produced an enhanced isotropic MRE. In these studies, the MR elastomers were enhanced by embedding large irregular particles into nitrile rubber without curing of the MRE matrix by a magnetic field. As a result, isotropic MREs were created. The properties of MRE were also experimentally studied and according to these authors, the large-size particles are a key factor that increases the MR effect.

Hu et al [60] fabricated a MRE material, which was enhanced by polyurethane (PU) silicone rubber (Si-rubber). The authors reported that by choosing an optimal ratio between the PU and Si-rubber and by improving the compatibility between the PU and Si-rubber, the MR effect is better than that of MREs which are based on either pure PU

or Si-rubber in the same testing conditions. According to the authors, the maximum increase in shear modulus is up to 0.5 MPa under the application of a magnetic field 0.2T.

Chen et al [61] fabricated several MRE samples with enhancement of different carbon black content. In this study, the mechanical properties of the MREs were experimentally investigated. These authors reported that the addition of the carbon black to the MR matrix results in a high MR effect. As a result, the maximum increase in shear modulus is 104%. Jiang et al [62] developed several anisotropic rubber-based MREs with three types of surfactants to enhance the MR effect for MREs. The authors reported that with enhanced surface activity of magnetic particles, the increase in modulus could be raised up to 188% due to the MR effect.

Farshad and Benine [63] developed a sample of a magnetoactive elastomer with particle-filled silicone rubber. Composite elastomer samples with different types of micron-size particles and various volume fractions were experimentally tested. The authors pointed out that the maximum increase in tensile modulus and compression modulus is 200% for the former and more than 300% for the latter.

Zhang et al [64] proposed a theoretical model for fabricating special MREs. To fabricate the MREs, the magnetizable soft material including nano-size ferrite powders inside a polymer gel is created first, after which carbonyl iron particles wetted by polymer chains are coated on the soft material. The authors investigate the MR effect of the MREs by introducing a theory model to calculate the shear modulus of the MREs. The new fabrication process makes the MREs increase in elastic modulus extensively.

2.5.3 New MREs

In recent years, a new generation of MRE has been developed with a significant MR effect [65-71]. In general, the fabrication process of the new MREs has three main features. Firstly, the host matrix is chosen as a highly elastic polymer, polymerised from special components such as silicone oligomer with hydride groups. Secondly, the magnetic particles are a mixture of small and large micro-size powders which have

previously been processed to remove moisture from the particle surfaces. These particles are homogeneously dispersed in the host matrix. Lastly, the mixed material of host polymer matrix and particles is polymerised at a temperature 100-150^{0}C with the additional effect of a super high frequency electromagnetic field at 2.4GHz for enhancing the polymerisation rate and avoiding filler sedimentation. With the fabrication process, MREs from the new generation have significant increase in elastic modulus.

Stepanov et al [69] introduced the tangential Young's modulus for describing the non-linear behaviour of a new soft MRE. Their experimental results reported that for a MRE sample with a magnetic filler content of volume 37%, the maximum increase in the modulus, when the strain is small (less than 4%), is up to 100 times.

In line with this result, Abramchuk et al [70] measured the shear modulus for a soft MRE in a small strain regime. This MRE material is based on a silicone polymer matrix and the ferrous filler content by volume is 27.6%. For the first time, this appears to present a relationship between the elastic modulus and magnetic field intensity where the increase in shear modulus is about 10000% (100 times).

Chertovich et al [71], in particular, presented two new MRE samples: hard and soft. The two new MRE samples were experimentally investigated and the shear modulus and damping of these MR samples were measured. From the experimental results, the authors reported that the increase in shear modulus may be up to 420 times in a magnetic filed of only 0.3T.

The new generation of MREs obviously has a significant increase in elastic modulus compared to other MREs so far. The new MREs will be a promising material for constructing a new generation of MRE-based ATVAs because these ATVAs can work in a much larger range of frequency than traditional TVAs.

2.6 Adaptive tunable vibration absorber using MREs

In parallel with developing MREs, there is a great deal of study on the use of MREs for

developing ATVAs. As MREs are a smart material whose elastic moduli can be magnetically controlled, they have been used widely for developing ATVAs [72-81].

Ginder et al [72] appear to be the first authors to develop ATVAs using MREs. They used MREs as variable-spring-rate element and the MRE used in this study includes a natural rubber matrix and magnetic particles. The content of the particles has 27% by volume in the natural rubber matrix. To enhance the MR effect, the MRE sample was cured at a magnetic field of 0.8 Tesla at 150^0C in 15 minutes and an ATVA was developed and experimentally tested. The experimental results stated that the frequency range of the ATVA is 500 to 610 Hz under a magnetic field of 0.56 Tesla. In a further study, Ginder et al [73] developed a MRE-based ATVA for which the authors reported a frequency range of 580-710Hz under a magnetic field of 0.56 Tesla.

Deng et al [74] developed an ATVA for a beam with two supported ends. The MRE has silicone rubber matrix and carbonyl iron particles. The mass ratio of the magnetic particles is 70% and the size of particles is 3–5 μm. The MRE sample was cured in a magnetic field of 1T for 24h. The authors reported that this ATVA could work effectively in a frequency range from 55 to 81.25 Hz (relative frequency change of 49%) in a magnetic field, which is produced by an electromagnetic coil with a DC current of 1.5A. In a further study of a modification of the ATVA, Deng and Gong [75] developed an ATVA using MREs and the authors reported that the ATVA frequency could be tuned from 27.5Hz to 40Hz (45% increase in frequency).

Ni et al [76] proposed a concept design for a novel ATVA using a MRE working in a combination of shear and squeeze mode. The ATVA's effectiveness for vibration control was investigated by numerical simulation. The study reported that with the enhancement of squeeze mode, the increase in frequency of the ATVA using the MRE is about 40%.

A series of studies about state-switched absorbers (SSAs) using MREs was reported by references [77-81]. Albanese and Cunefare [78] presented a SSA using a MRE material and found that, with iron particles by volume 35%, the MRE material has the largest MR effect and the natural frequency of the SSA could be tuned from 45Hz to 183 Hz (360% increase in frequency shift). In line with these authors, Lerner [79] investigated

the MRE properties for the longitudinal mode of a SSA and reported that the frequency change in the longitudinal mode is 360%. Albanese [80] and Lerner and Cunefare [81] tested the SSA operating in different working modes with an increase in the frequency range of 183%, 473% and 510% for shear, longitudinal and squeeze modes respectively.

2.7 Identification of gap in current knowledge

To date, the MRE has been used for developing ATVAs to reduce vibration for SDOF applications only. In fact, most real world structures and mechanisms are MDOF systems. This shortcoming limits the application of the unique MRE material in many engineering problems. In addition, no ATVA using MREs has been developed for dealing with vibration reduction of mechanical torsional vibration systems, which is a major fraction of engineering vibration problems, of which vehicle powertrain is a typical example. The motivation of this thesis is to develop a torsional MRE-based ATVA for vibration control for a vehicle powertrain as presented in Chapter 1.

2.8 Summary

This chapter provided a background to related topics of this thesis. After presenting an overview of torsional vibration, powertrain systems and their primary components and powertrain vibration control were presented. A review of TVAs, ATVAs was also reported. In addition, a broad range of study of MREs, which are promising material for constructing ATVAs, was reviewed. In particular, the using of MREs for developing ATVA was presented and the gap of knowledge was identified. It was found that the development of ATVA using MREs for powertrain vibration control is an unsolved problem. As a result, the objective of this thesis was proposed, as in Chapter 1.

Chapter 3 THE MR ELASTOMER, ITS MODELS AND APPLICATION FOR DEVELOPING ATVAs

3.1 Introduction

This chapter briefly introduces a few fundamental features of MREs. It focuses on mechanical properties of MREs that relate to stiffness and damping, the two essential factors for constructing ATVAs. Two models of MREs, viscous and viscoelastic will be presented. According to these models, the properties of MREs will be experimentally investigated. This chapter also reviews several typical MREs which have been reported by previous studies. Specifically, two particular MREs of the new MRE generation, one that uses viscous model and the other that uses viscoelastic model, will be introduced. These particular MREs will be used for the numerical simulation of a MRE-based ATVA to show the capability of MREs for developing an ATVA in later chapters.

3.2 Fundamental features of MREs

MR elastomers consist of three fundamental components: a host matrix material, magnetic particles and oil that serves as plasticisers. The MR effect depends on the types and ratio of these components. In other words, with the same fabrication process, the MRE properties can be controlled by varying the fraction of the components [8, 9].

One technique which has been used to enhance the MRE effect is to cure the fabricated MRE material in a magnetic field. With this enhancement, the cross linking of magnetic particles is created. Images of magnetic particles with and without cross linking are shown in Figure 3.1 a) and b).

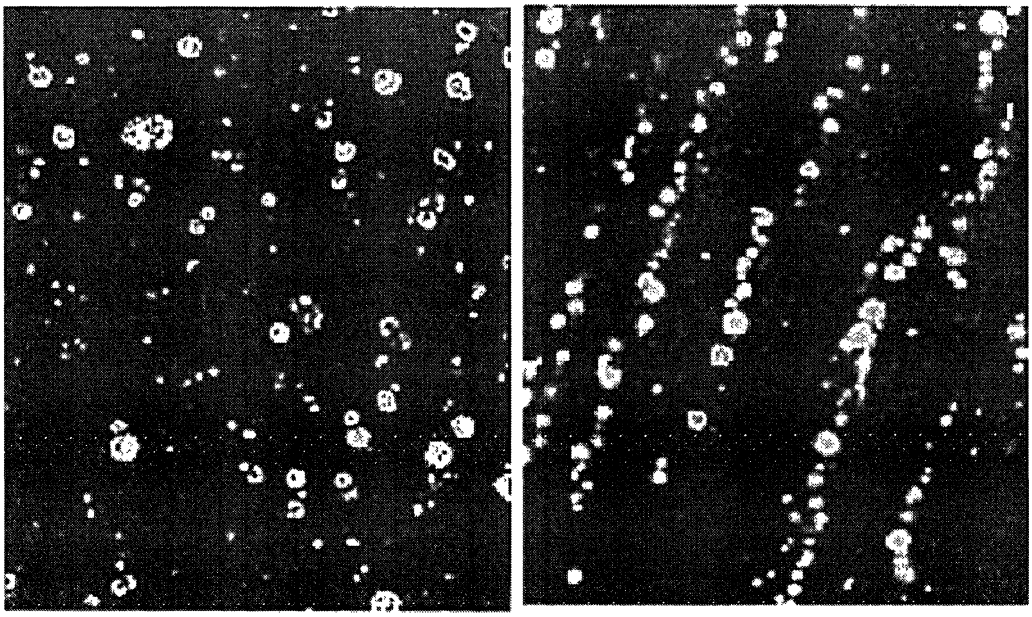

a) Without magnetic field b) With magnetic field

Figure 3.1. Image of magnetic particles in host matrix [54]

It can be seen that after curing, parallel particle chains are created as shown in Figure 3.1b).

To investigate the MRE properties, a great deal of study has been presented so far. To predict the properties, it is assumed that MREs are filled by spherical rigid particles. In addition, it is assumed that these particles are randomly distributed. Using these assumptions, the shear modulus of the MRE can be calculated by Davis [55]:

$$G_{ran} = G_0(1 + 2.5\phi + 14.1\phi^2) \tag{3.1}$$

G_0 is unfilled elastomer shear modulus, ϕ is the volume fraction of the particles.

If a magnetic field is applied to MREs, their elastic moduli change. Due to the MR effect there is a change of shear modulus ΔG. The MR shear modulus can be calculated by equation:

$$G = G_{ran} + \Delta G \tag{3.2}$$

The change of shear modulus, ΔG, has been studied by both theoretical and experimental methods.

Davis [55] used FEM to investigate the change of shear modulus. In this study, the author reported that the maximum increase in shear modulus of MRE is 50% at volume fraction of magnetic particles is 27%. The increase in shear modulus is shown in Figure 3.2.

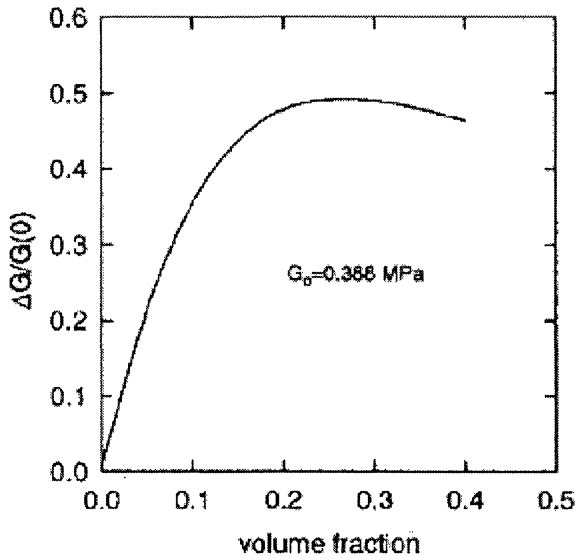

Figure 3.2. The predicted ratio of the change in modulus ΔG [55]

The study of MRE is quite a large area of smart material engineering but, to the author's knowledge, for mechanical vibration problems, the stiffness and damping of MREs are two the most important properties. Thus, in this chapter, the focus is on the two properties of MREs. So far, two models, namely viscous and viscoelastic, have been used to investigate the mechanical vibration features of MREs. These models also involve in two types of loading for MRE samples: static and dynamic loadings [8, 10].

3.3 MRE viscous model

This model treats the MRE as a spring-damping element. A model for testing MRE properties is shown in Figure 3.3.

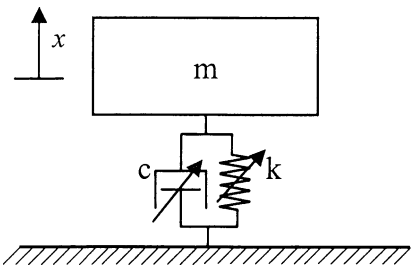

Figure 3.3. Components of MRE viscous model

The stiffness and damping of the MRE can be determined from this equation:

$$m\ddot{x} + c\dot{x} + kx = 0 \tag{3.3}$$

In which m is the effective mass, k and c are the stiffness and damping coefficients of MRE as shown in Figure 3.3.

Because the damping coefficient is dependent on the dimension of the MRE specimen, a dimensionless damping ratio is used to investigate mechanical damping instead, according to Kallio [8].

$$\varsigma = \frac{c}{C_c} \tag{3.4}$$

In which:

$$C_c = 2\omega_n m \tag{3.5}$$

is the critical damping and

$$\omega_n = \sqrt{k/m} \tag{3.6}$$

is the natural frequency of the system.

It is noted that by measuring the decay vibration of the mass m, the natural frequency, damped frequency and damping ratio can be obtained. To be specific, the damping ratio can be calculated as:

$$\varsigma = \frac{\delta}{\sqrt{(2\pi)^2 + \delta^2}} \tag{3.7}$$

Here,

$$\delta = \ln(x_1/x_2) \tag{3.8}$$

In the equation (3.8) δ is the logarithmic decrement. x_1, x_2 are vibration amplitudes measured one cycle for the vibration of the mass.

The damped frequency and natural frequency have the following relationship:

$$\omega_d = \omega_n\sqrt{1-\varsigma^2} \tag{3.9}$$

In summary, if the decay vibration of the mass m is measured, by using equations from (3.4) to (3.9) of the viscous model, MRE properties can be obtained.

The viscous model is used by a great number of studies to investigate MRE properties. For example, Zhou [10] used this model to measure MRE properties. This author used the viscous model to experimentally investigate the mechanical

properties of a MRE. The MRE has 27% ferrous particles by volume embedded in a silicone rubber matrix. By measuring the free vibration of the mass as discussed above, the change of shear modulus and damping ratio were calculated and are shown in Figures 3.4 and 3.5.

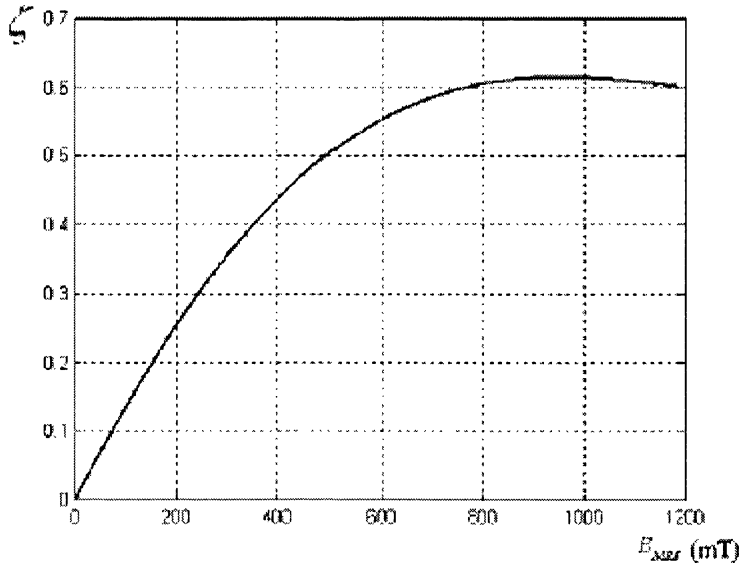

Figure 3.4. The ratio $\xi = \Delta G / G_0$ under application of magnetic flux density [10]

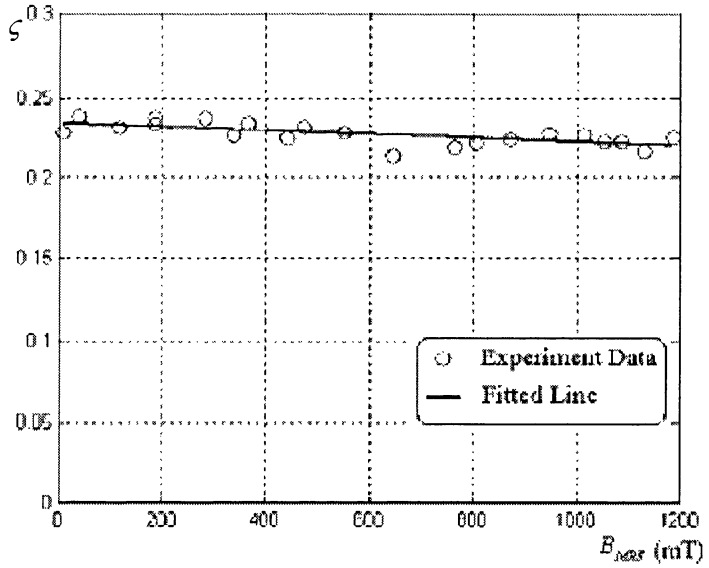

Figure 3.5. Damping ratio ς under application of magnetic field [10]

It can be seen that that the damping ratio is a slightly decreasing line (about 10%) when the magnetic field increases. The zero-field damping ratio ς_{A0} =0.24 was measured.

Another study using the viscous model is the work reported by Abramchuk et al [70]. In

this study, MREs are isotropic and belong to the new MRE generation, which was reported in Chapter 2.

According to these authors, the composition of MREs is a highly elastic polymer matrix and magnetic particles, which are suspended in the polymer matrix. The polymer matrix of the host material is a liquid silicone rubber, which was produced by GNIIKhTEOS (Institute of Chemistry and Technology of Organoelement Compounds, Russia). The matrix consists of two components. The first component is a silicone oligomer with vinyl groups and the second is a silicone oligomer with hydride groups. After the two components were mixed, the polymer matrix of the MRE was created by the following chemical reaction with the presence of platinum as a catalyst.

$$\sim Si - CH = CH_2 + H - Si \sim \xrightarrow{Pt\ catalyst} \sim Si - CH_2 = CH_2 - H - Si \sim$$

There are two types of magnetic particles: the magnetite powder (Fe_3O_4) and ferrous powder (Fe). These powders have sizes ranging from 0.2-0.3 μm and 2-3 μm, respectively. In addition, the elastic properties of the MREs can be controlled by varying the fraction between two rubber components and by adding silicone oil, which serves as a plasticiser.

The authors investigated five MRE samples. The specification of these samples is shown in Table 3.1.

Table 3.1. Shear modulus of filled samples without magnetic field

MRE sample	Magnetic type	Fraction of filler volume	Shear modulus (kPa)
Sample 1	Fe	27.6	3.5
Sample 2	Fe	22.3	2.95
Sample 3	Fe	7.1	4.56
Sample 4	Fe_3O_4	14.0	2.19
Sample 5	Fe_3O_4	24.3	4.48

It is noted that the fabrication process of MREs consists of three main steps. Firstly, the mixture of the silicone rubber and magnetic particles is ground by a mechanical mortar.

Secondly, the ferrous powder is homogeneously dispersed into the polymer matrix and the air bubbles are removed from the volume of the sample. Finally, the mixture material was injected into moulds and polymerised for two hours at a temperature of 100 to 150^{0}C.

It is assumed that the MRE material is operated in the small strain regime and the relationship between Young's modulus and shear modulus in this regime is linear so that the tensile test is conducted and the shear modulus G can be calculated from following equation:

$$\sigma = G(\lambda - \frac{1}{\lambda^2}) \tag{3.10}$$

Where σ is the nominal stress; $\lambda = l / l_0$ is the relative compression length; l is the length of the deformed sample and l_0 is the initial length of undeformed length, see reference [70] for more detail.

The change of shear modulus of the five MRE samples is shown in Figure 3.6.

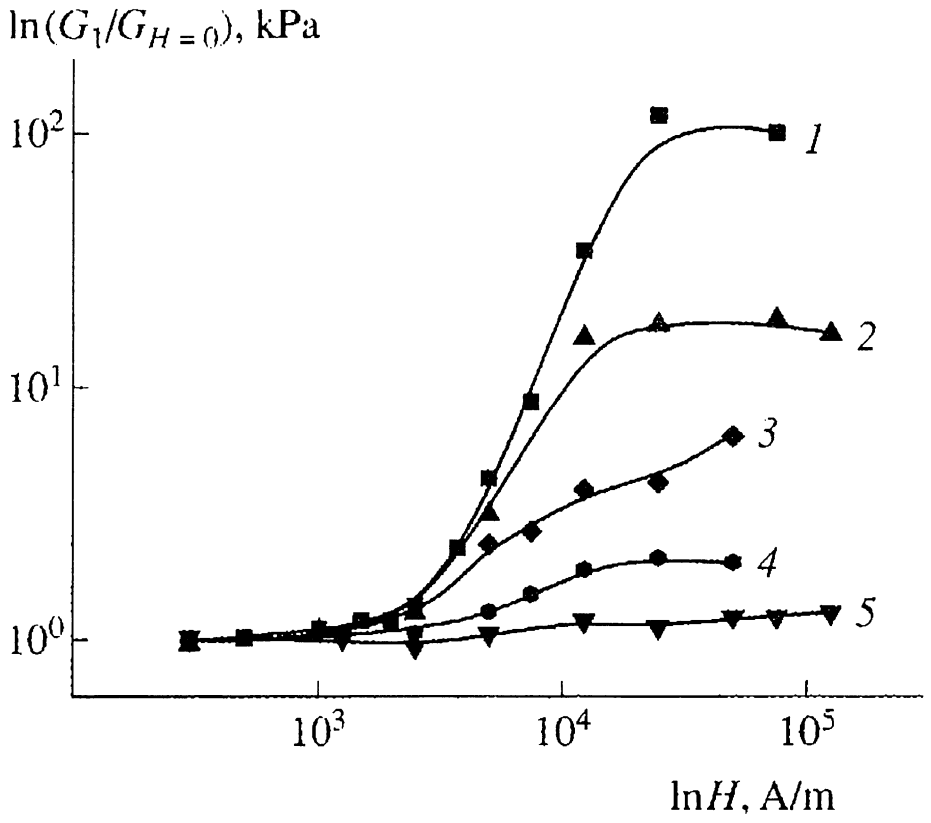

Figure 3.6. Shear modulus of MREs relative to magnetic field intensity H [70]

It can be seen in Figure 3.6 that Sample 1, with 27.6%Fe by volume, has the largest MR

effect. According to Abramchuk et al [70], the increase in shear modulus is up to 100 times if the strain is small. Thus, Sample 1 as shown in Table 3.1 and Figure 3.6 will be used to numerically validate the application of ATVA using MRE for vibration control to demonstrate the ability for MREs to construct ATVAs, which will be discussed in Chapter 5 and Chapter 6.

3.4 MRE Viscoelastic model

The viscoelastic model is used to investigate the properties of MREs under dynamic loading. In order to measure MRE properties, a harmonic strain γ is used as follows:

$$\gamma = \gamma_0 \sin(\omega t) \tag{3.11}$$

According to Kallio [8], there is a phase difference between the strain and the stress of MRE material. Thus, the stress can be expressed as:

$$\sigma = \sigma_0 \sin(\omega t + \delta) \tag{3.12}$$

Here, δ is the phase difference between the stress and the strain, ω is the frequency of strain oscillation and t is time,

The complex shear modulus of MRE can be calculated by:

$$G = G' + iG'' = G'(1 + \eta i) \tag{3.13}$$

G' and G'' are storage modulus and loss modulus, respectively and are calculated by:

$$G' = \frac{\sigma_0}{\gamma_0} \cos\delta \tag{3.14}$$

$$G'' = \frac{\sigma_0}{\gamma_0} \sin\delta \tag{3.15}$$

And η or $\tan\delta$ is called as the loss angle or loss factor of MRE and it is calculated by:

$$\eta = \tan\delta = \frac{G''}{G'} \tag{3.16}$$

The storage modulus and loss modulus represent the stiffness and internal damping respectively of MRE [8].

By measuring the stress of the MRE under dynamic loading, the mechanical properties of MRE can be determined by equations (3.13), (3.14), (3.15), and (3.16).

To date, there are an increasing number of studies using the viscoelastic model to examine MRE properties. For example, Jolly et al [54] used the model to investigate three samples of MREs.

The specification and the experimental results of the MRE samples are given in Table

3.2. It is noted that the MRE samples in Table 3.2 were tested with loading conditions: the magnitude and frequency of the strain are 1% and 2.0Hz, respectively.

Table 3.2. Experimental change in modulus at 1% strain and 2.0Hz [54]

MRE sample	zero-field modulus (MPa)	max change in modulus (MPa)
30% iron in volume	1.80	0.56 (31%)
20% iron in volume	0.74	0.29 (39%)
10% iron in volume	0.26	0.08 (30%)

The change of shear modulus is shown in Figure 3.7.

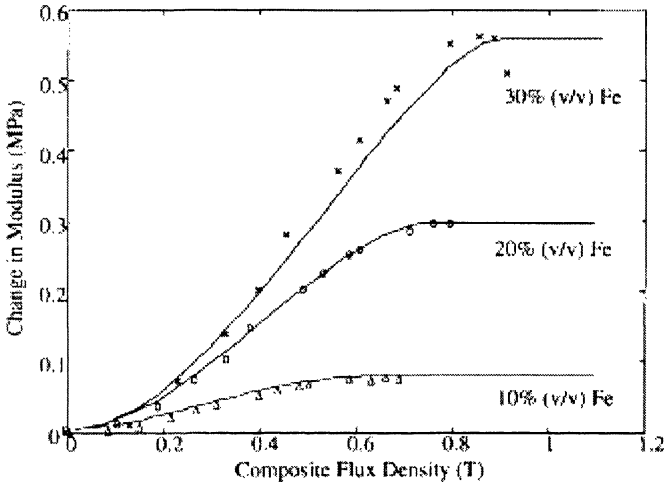

Figure 3.7. Change in shear modulus for several MRE samples [54]

And the loss factor is reported in Figure 3.8.

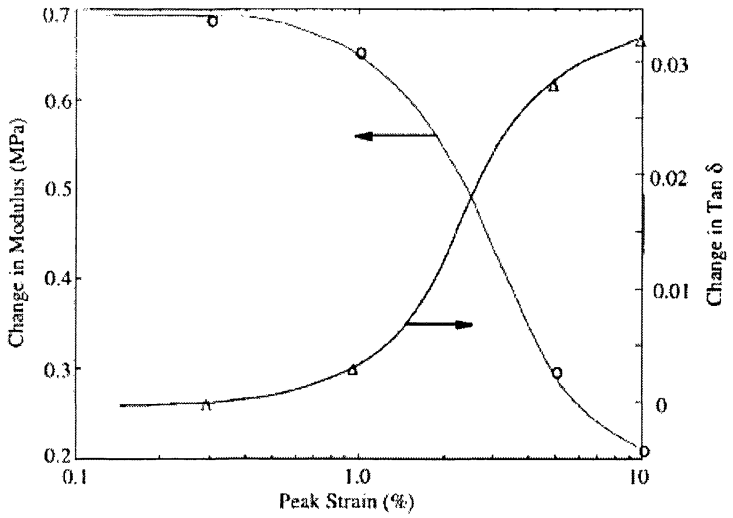

Figure 3.8. The effect of strain magnitude to shear modulus and loss factor [54]

Another study which used the viscoelastic model to investigate the MRE properties, is the work reported by Chertovich et al [71], which is presented in following section. The authors developed two MRE samples, soft and hard MRE samples, which are called Sample 1 and Sample 2, respectively. Sample 1 contains carbonyl iron particles of 3–5mm in size with 70 % by weight; this sample has a rather low modulus. Sample 2 has a higher fraction of magnetic filler (85% by weight). In addition, the magnetic fillers of Sample 2 were a mixture of small and large iron particles. The small and large particles have an average size of 3-5 μm and 40-50 μm respectively. The mixture of the magnetic fillers has fraction of 85% by weight, in which, the small and the large particles contain the fraction of 50% and 35% respectively.

The zero-field shear modulus of the two samples is shown in Table 3.3.

Table 3. 3. Shear modulus of two MRE samples

MRE sample	Zero-field shear modulus (kPa)
1	1.5
2	19

The fabrication process of the MREs consists of three main steps. Firstly, to enhance the MR effect, the magnetic fillers were initially processed by hydride containing silicone to remove moisture from the particle surface. Secondly, the iron powders are homogeneously dispersed into the polymer matrix. It is noted that the MRE samples created are isotropic. To measure the viscoelatic properties of the new MREs, cylindrical specimens (whose diameter and height are 10mm and 5mm respectively) were formed.

The viscoelastic behaviour of the two MRE samples was studied with the use of a rotational rheometer Rheostress RS 150L (HAAKEGmbH). As a result, properties of the MRE samples such as storage and loss moduli and loss factor can be determined.

The dependence of the storage modulus, loss modulus and the loss factor of MREs on the magnetic field are shown in Figures 3.9 and 3.10.

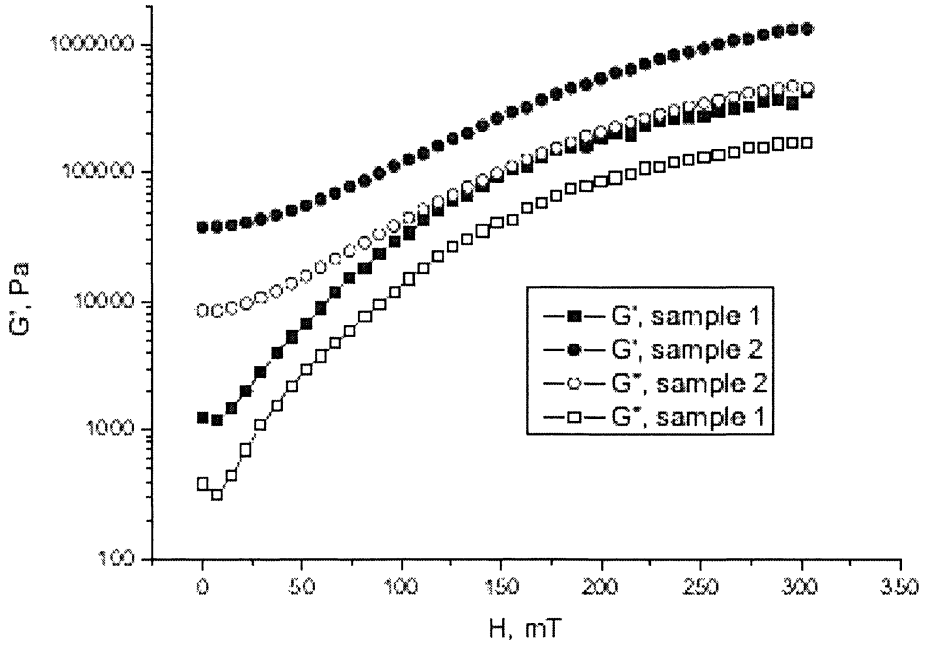

Figure 3.9. Storage and loss moduli of MRE Samples 1 and 2 [71]

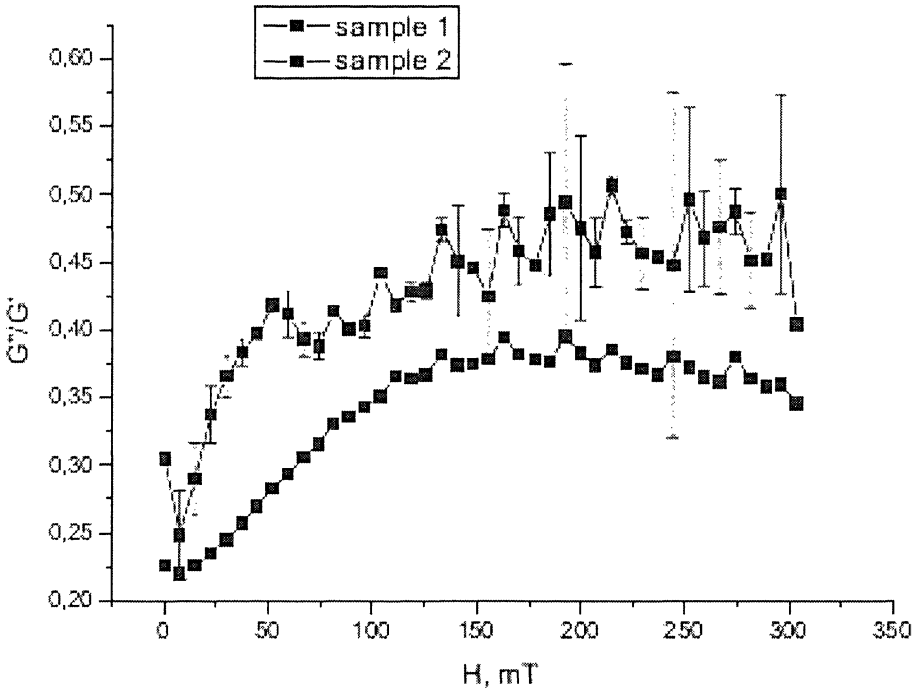

Figure 3.10. Loss factor of MRE Samples 1 and 2 [71]

It can be seen in Figures 3.9 and 3.10 that the hard MRE sample has a significant increase in shear modulus and also has low damping. Thus, this sample will be used for constructing an ATVA for vibration control of a powertrain, which will be presented in Chapter 7.

3.5 MRE equivalent stiffness for developing of ATVA

With two main forms of vibration motion, the translational and angular motions, there are two methods to calculate the equivalent stiffness for the MRE with respect to the two kinds of motions.

3.5.1 Translational motion of MRE sample

In this working mode, the MRE specimen plays a role as a translational spring as shown in Figure 3.11. Thus, its equivalent stiffness can be calculated by, [81]:

$$k = \frac{EA}{L} \tag{3.17}$$

Here, L and A are the length and cross section area of the MRE specimen respectively. E is the Young's modulus of the MRE material.

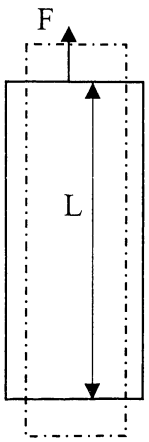

Figure 3.11. Translational motion mode of MRE specimen

If the MRE specimen translates in shear direction the equation (3.17) can be re-written in this form, [10, 74]:

$$k = \frac{GA}{L} \tag{3.18}$$

G is the shear modulus of MRE material.

3.5.2 Angular motion of MRE sample

The working mode of MREs is shown in Figure 3.12; the MRE layer acts as a torsional spring. According to Garcı´a et al [82], the equivalent dynamic torsional stiffness coefficient $\hat{k}$ of the MRE layer in the viscoelastic model is a complex quantity and it

can be calculated as:

$$\hat{k} = \frac{4\pi L a^2 b^2 \hat{G}}{b^2 - a^2} \tag{3.19}$$

In which $\hat{G}$ is the MRE complex shear modulus from the viscoelastic model. It is noted that equation (3.19) is also valid for the viscous model (for static stiffness and static shear modulus).

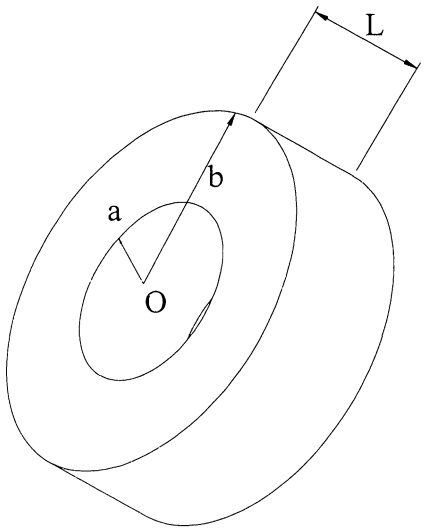

Figure 3.12. Angular motion mode of MREs

It is noted that the equations (3.17), (3.18) and (3.19) will be used to calculate equivalent stiffness for the design of an MRE-based ATVA.

3.6 Summary

This chapter presented the fundamental features of MREs that is related to mechanical vibration problems. The dependence of the elastic modulus and damping properties on the magnetic field were investigated. Two models (viscous and viscoelastic models) were used to measure the MRE properties and mechanical properties of few specific MREs were reported in this chapter. Finally, the equivalent stiffness of MREs for the two main types of vibration modes, translational and angular motions, was presented for constructing MRE-based ATVAs.

Chapter 4 MATHEMATICAL BACKGROUND OF DYNAMIC ABSORBERS

4.1 Introduction

This chapter presents the mathematical background of dynamic absorbers (or TVAs) for dealing with the resonance occurring in mechanical systems. The chapter begins by introducing the model of an undamped dynamic absorber for a SDOF system. The equation of motion of the resulting system is then derived and the forced vibrations of the system are determined. This is followed by using the damped dynamic absorbers for vibration control, and the effectiveness of traditional TVAs is demonstrated in a case study. Finally, the optimal parameters for TVAs are examined.

4.2 Undamped dynamic absorber

The dynamic absorber is a useful device for mechanical vibration reduction. It has been applied for more than hundred years (Den Hartog [5]). The model of the dynamic absorber can be seen in Figure 4.1.

In Figure 4.1, the primary system is modelled as a SDOF system with mass m_1 and stiffness coefficient k_1. If the frequency of the primary system $\omega_1 = \sqrt{k_1 / m_1}$ is the same or is close to the excitation frequency Ω, resonance occurs. To deal with the resonance, a dynamic absorber with parameters m_2 and k_2 is attached to the primary system. The parameters m_2 and k_2 are chosen such that the primary system excitation frequency is equal to the modal frequency of the TVA.

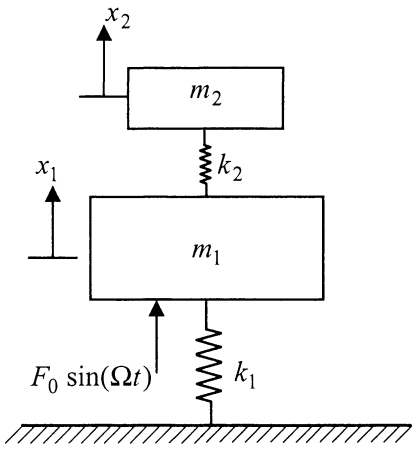

Figure 4.1. Undamped dynamic absorber

It can be seen that the EOM of the resulting system in Figure 4.1 can be expressed in following equations, [7]:

$$\begin{cases} m_1\ddot{x}_1 + k_1x_1 + k_2(x_1 - x_2) = F_0\sin(\Omega t) \\ m_2\ddot{x}_2 + k_2(x_2 - x_1) = 0 \end{cases} \tag{4.1}$$

It is obvious that the particular solution of the equation (4.1), the steady stage vibrations of the system, can be found by applying assumed harmonic response: $x_1(t) = X_1\sin(\Omega t)$, $x_2(t) = X_2\sin(\Omega t)$. The vibration of the primary system and the dynamic absorber can be solved:

$$X_1 = \frac{(k_2 - m_2\Omega^2)F_0}{(k_1 + k_2 - m_1\Omega^2)(k_2 - m_2\Omega^2) - k_2^2} \tag{4.2}$$

$$X_2 = \frac{k_2F_0}{(k_1 + k_2 - m_1\Omega^2)(k_2 - m_2\Omega^2) - k_2^2} \tag{4.3}$$

From equation (4.2), if the TVA is designed such that its natural frequency coincides with the excitation frequency Ω, such that $\omega_2 = \sqrt{\frac{k_2}{m_2}} \equiv \Omega$, the vibration of the primary system will be zero. As a result, from equation (4.3), the vibration of the auxiliary mass

m_2, $X_2 = -\frac{F_0}{k_2}$, that means:

$$F_0 = -X_2 k_2 \tag{4.4}$$

From equation (4.4) the principal of the dynamic absorber can be explained physically: if the elastic force of the TVA is equal to the excitation force but the direction is opposite, the primary system will be stationary.

It can be seen from equations (4.2) and (4.3) that although resonant frequency is removed, there are two new resonant peaks Ω_1 and Ω_2, at these frequencies the frequency response of the primary system will be infinity. Obviously, Ω_1 and Ω_2 can be determined by letting the dominator of equations (4.2) or (4.3) be zero. Ω_1 and Ω_2 can be calculated by the following equations, [7]:

$$\left(\frac{\Omega_{1,2}}{\omega_2}\right)^2 = \frac{1+(1+\frac{m_2}{m_1})(\frac{\omega_2}{\omega_1})^2 \mp \left\{\left[1+(1+\frac{m_2}{m_1})(\frac{\omega_2}{\omega_1})^2\right]^2 - 4(\frac{\omega_2}{\omega_1})^2\right\}^{1/2}}{2(\frac{\omega_2}{\omega_1})^2} \tag{4.5}$$

In particular, if $\omega_1 = \sqrt{\frac{k_1}{m_1}} = \omega_2 = \sqrt{\frac{k_2}{m_2}}$ and let $\mu = \frac{m_2}{m_1}$ be the mass ratio equation (4.5) becomes:

$$\left(\frac{\Omega_{1,2}}{\omega_2}\right)^2 = (1+\frac{\mu}{2}) \mp \sqrt{(1+\frac{\mu}{2})^2 - 1} \tag{4.6}$$

Equation (4.5) (or equation (4.6) in a particular case) shows that the excitation frequency Ω is between Ω_1 and Ω_2. In other words, the dynamic absorber has shifted the frequency of the primary system ω_1 by introducing two new frequencies Ω_1 and Ω_2. However, if the operating speed passes through Ω_1, for example, during the start-up or stopping of the machine, the large amplitude of vibration may occur. Thus, there is a need for damping for the dynamic absorber.

4.3 Damped dynamic absorber

The dynamic absorber in section (4.2) in this chapter removes the resonant frequency by introducing two new peaks so that the primary system experiences a large vibration level when the excitation frequency passes through the first peak. The amplitude of the

primary system can be reduced by adding damping to the dynamic absorber. The primary system and damped dynamic absorbers are shown in Figure 4.2.

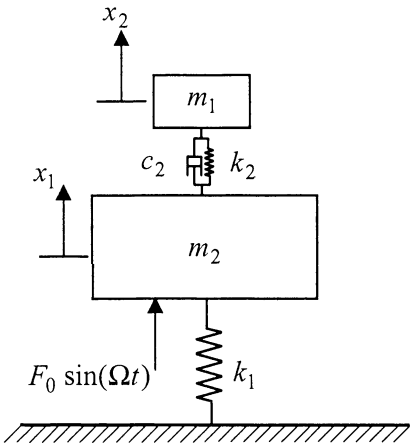

Figure 4.2. Damped dynamic absorber

The equation of the motion of the system can be written as:

$$\begin{cases} m_1\ddot{x}_1 + k_1x_1 + k_2(x_1 - x_2) + c_2(\dot{x}_1 - \dot{x}_2) = F_0\sin(\Omega t) \\ m_2\ddot{x}_2 + k_2(x_2 - x_1) + c_2(\dot{x}_2 - \dot{x}_1) = 0 \end{cases} \tag{4.7}$$

For more convenience, the particular solutions for equation (4.7) can be obtained by: $x_1(t) = \mathrm{Re}(X_1 e^{i\Omega t}) = \overline{X}_1 \sin(\Omega t - \phi_1)$; $x_2(t) = \mathrm{Re}(X_2 e^{i\Omega t}) = \overline{X}_2 \sin(\Omega t - \phi_2)$, in which $\overline{X}_1$ and $\overline{X}_2$ are amplitudes of motion of m_1 and m_2 respectively, ϕ_1 and ϕ_2 are phase angles.

The complex magnitudes X_1 and X_2 of masses m_1 and m_2 are solved as follows, [7]:

$$X_1 = \frac{(k_2 + ic_2\Omega - m_2\Omega^2)F_0}{\left[(k_1 - m_1\Omega^2)(k_2 - m_2\Omega^2) - m_2k_2\Omega^2\right] + ic_2\Omega(k_1 - m_1\Omega^2 - m_2\Omega^2)} \tag{4.8}$$

$$X_2 = \frac{(k_2 + ic_2\Omega)X_1}{(k_2 - m_2\Omega^2 + ic_2\Omega)} \tag{4.9}$$

It can be seen that the vibrations of masses m_1 and m_2 in the undamped case as shown in

equations (4.2) and (4.3) in section (4.1) relate to a particular case that was described in equations (4.8) and (4.9) with damping coefficient c_2=0.

For more convenience by defining:

$\mu = \frac{m_2}{m_1}$ as mass ratio

$\delta_{st} = F_0 / k_1$ as static deflection of the system

$\omega_a = \sqrt{\frac{k_2}{m_2}}$ as natural frequency of absorber

$\omega_n = \sqrt{\frac{k_1}{m_1}}$ as natural frequency of primary mass

$f = \omega_a / \omega_n$ as ratio of natural frequency

$g = \Omega / \omega_n$ as forced frequency ratio

$c_c = 2m_2\omega_n$ as critical damping

$\varsigma = c_2 / c_c$ as damping ratio

From the equations (4.8) and (4.9), amplitudes of vibration of m_1 and m_2 $\overline{X}_1$, $\overline{X}_2$ can be calculated in the following forms:

$$\frac{\overline{X}_1}{\delta_{st}} = \sqrt{\frac{(2\varsigma g)^2 + (g^2 - f^2)^2}{(2\varsigma g)^2(g^2 - 1 + \mu g^2)^2 + [\mu f^2 g^2 - (g^2 - 1)(g^2 - f^2)]^2}} \tag{4.10}$$

$$\frac{\overline{X}_2}{\delta_{st}} = \sqrt{\frac{(2\varsigma g)^2 + f^4}{(2\varsigma g)^2(g^2 - 1 + \mu g^2)^2 + [\mu f^2 g^2 - (g^2 - 1)(g^2 - f^2)]^2}} \tag{4.11}$$

See the references [5-7] for more detail.

The equation (4.10) shows that the vibration of the primary system fitted with the dynamic absorber is a function of parameters μ, f, g and ς.

The vibration of the primary system for a special case $\mu = 1/10$, f=1 for three values of damping ratio ς=0, 0.1 and 0.15 relative to forced frequency ratio g is shown in Figure 4.3.

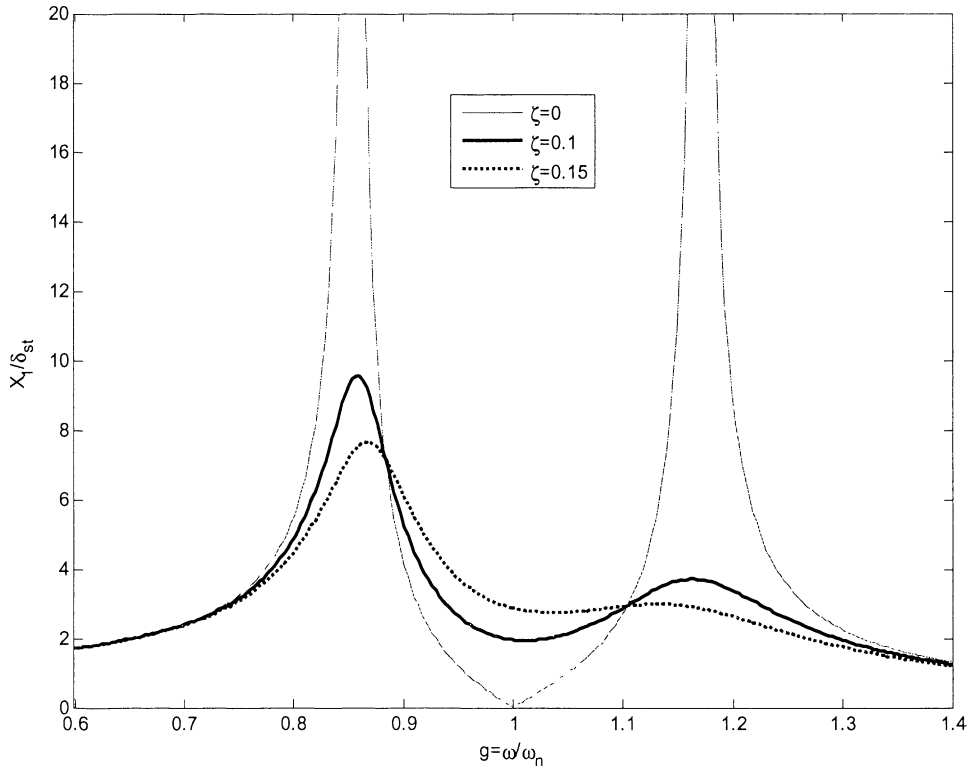

Figure 4.3. Frequency response of primary system for several values of damping ratio ς

It can be seen that the parameters of TVA can be optimised. According to Den Hartog, [5], for a mass ratio value μ, the damping ratio ς and optimal ratio of natural frequency f can be determined by:

$$f = \frac{1}{1+\mu} \tag{4.12}$$

And

$$\varsigma_{opt} = \sqrt{\frac{3\mu}{8(1+\mu)^3}} \tag{4.13}$$

At which the corresponding optimal value of $\frac{\overline{X}_1}{\delta_{st}}$ can be:

$$\frac{\overline{X}_1}{\delta_{st}} = \sqrt{1+\frac{2}{\mu}} \tag{4.14}$$

If $\mu = 1/10$ is set, the frequency responses of the primary system with the optimal value of the damping ratio and with damping ratio ς =0 are shown in Figure 4.4.

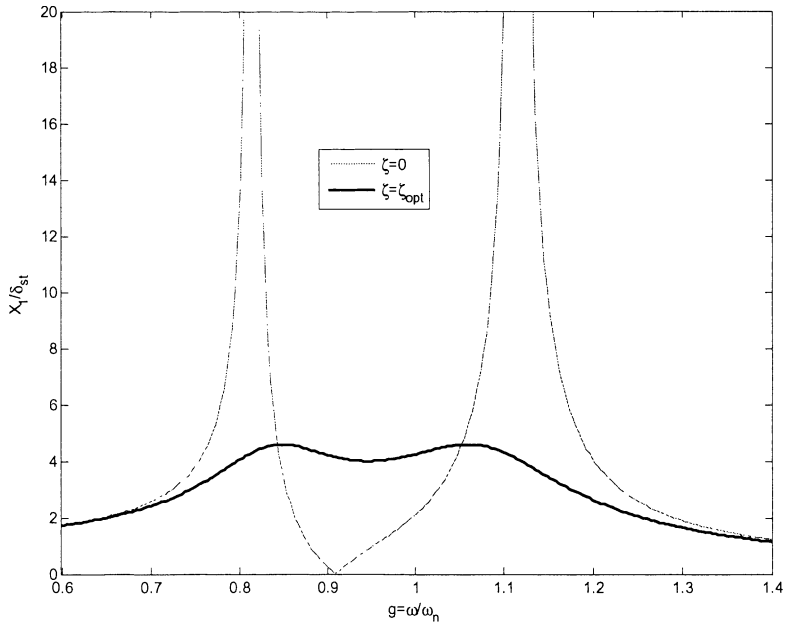

Figure 4.4. Frequency response of primary system with optimal values

It can be seen that with the optimal damping ratio, the frequency response at and around the resonant frequency is small and the responses at the two new frequencies, which are introduced after adding the TVAs, are also small.

It is noted that this chapter shows the mathematic background of traditional dynamic absorbers for vibration control of a SDOF system. The equations (4.12), (4.13) and (4.14) cannot apply for application of dynamic absorbers for MDOF system. To optimize the parameters of the dynamic absorber for MDOF system, the numerical methods must be used, which was discussed in [34, 35].

4.4 Summary

This chapter reviewed the mathematic background of TVAs, which are effective devices to absorb the undesirable vibration of mechanical systems whose natural frequencies coincide with or are close to the forcing frequency. The equation of motion of the system, which consists of the primary system and a TVA, was derived. From the derived equation of motion, the forced vibrations of the primary system and the TVA were determined analytically. Thus, the effectiveness of TVAs was presented. A general case was presented to demonstrate the effect of using TVAs for dealing with the mechanical resonance. In addition, for the example demonstrated, optimal parameters of TVAs were determined.

Chapter 5 ATVA FOR POWERTRAIN STEADY STATE VIBRATION REDUCTION

5.1 Introduction

The primary objective of this chapter is to demonstrate the ability of the ATVA using MREs for steady state vibration reduction of powertrains. In the steady state, the excitation frequency of the engine fluctuation torque of a powertrain is assumed as a constant.

The chapter begins with the introduction of a soft MRE, which was reported by Abramchuk et al [70] and was presented briefly in Chapter 3. The soft MRE is used in this simulation because its increase in elastic modulus is significant. As a result, the MRE-based ATVA can work in a wide frequency range that covers the frequency range of the powertrain. Consequently, the ability of the ATVA for vibration control of powertrain can be examined. A simplified powertrain model is then proposed as a 4 DOF system to examine the effectiveness of the MRE-based ATVA. With the simplified powertrain model, equations of motion of the powertrain with and without ATVA are derived. In this way, free and forced vibrations of the powertrain are determined. To deal with the resonance occurring in the powertrain a concept design of a MRE-based ATVA is proposed. As a result, numerical simulations can be conducted to validate the ATVA's effectiveness for powertrain vibration control. In addition, the effect of ATVA's parameters such as inertia, stiffness and damping is examined. Finally, the influence of ATVA location on the MRE-based ATVA's effectiveness is investigated.

5.2 A soft MRE and its characteristics

It is noted, as presented in Chapter 3, that Abramchuk et al [70] investigated the increase in shear modulus of five MRE samples, which were shown in Figure 3.6 in Chapter 3. Sample 1 has magnetic particles which are ferrous powders with 27.6% by volume, and the initial shear modulus of Sample 1 is 3.5kPa. Thus, Sample 1 is called a, soft MRE, and it is used to develop the concept design for the ATVA in this chapter.

Figure 5.1 shows the relative change of shear modulus (G/G_0), which depends on the magnetic field intensity. In this chapter, the change of shear modulus is obtained by mapping point-to-point and interpolating by Matlab software, in which G_0=3.5kPa is the initial shear modulus without magnetic field. It is noted that the relationship between G-H is displayed in the formation of logarithm (base 10).

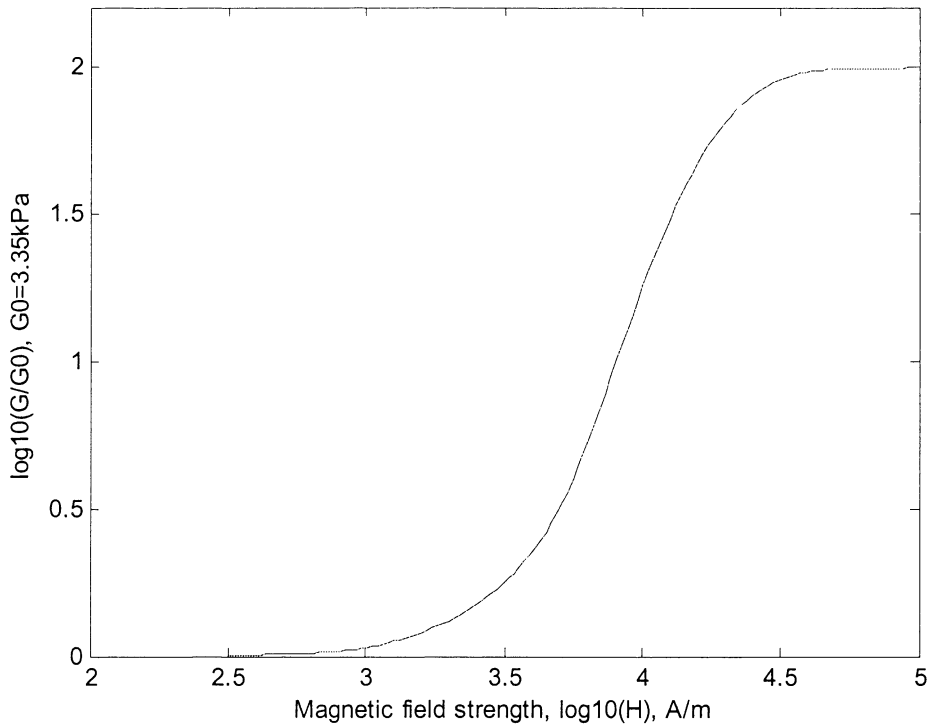

Figure 5.1. Shear modulus of the soft MRE [70]

It is assumed that the magnetic field intensity H (the maximum value is 100kA/m) can be produced by a magnetic field of coil with current I to supply for the MRE-based ATVA. The magnetic field intensity H depends on a number of factors such as turns of wire, the type of material in the coil and the ratio of the coil length to the coil width. For

convenience H is expressed in the form $H = \alpha I$, where α is the propositional coefficient. For instance, the magnetic field is assumed to be similar to one presented by Park et al, [84], α=12500/m was chosen, the relationship between the shear modulus G and input current I is shown in Figure 5.2.

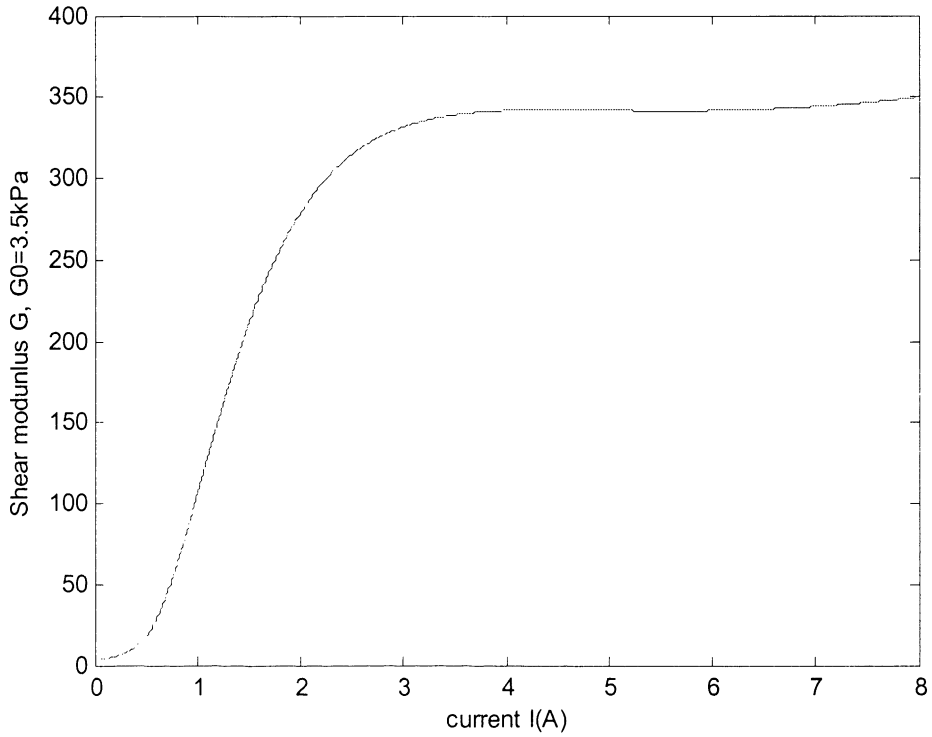

Figure 5.2. Dependence between shear modulus of the soft MRE and input current I

It is noted that the increase in shear modulus of the soft MRE is significant (more than 100 times). Thus, this MRE can provide a wide frequency to develop MRE-based ATVAs.

5.3 A novel ATVA for powertrain vibration control

5.3.1 A simplified powertrain model and its vibration characteristics

A simplified torsional vibration model of a powertrain, which consists of inertias, stiffness and damping as shown in Figure 5.3, is used to validate the ATVA's effectiveness. It is noted that the powertrain is modelled as a four-degree-of-freedom system, in which the engine is modelled by the first inertia. The second and third inertias represent the clutch or the torque converter (TC) and the gear box of transmission, respectively. The drive line components of the powertrain are modelled by

the fourth inertia. It is noted that the model of 4 DOFs was used by Reik [19, 20] to investigate the torsional vibration of powertrains.

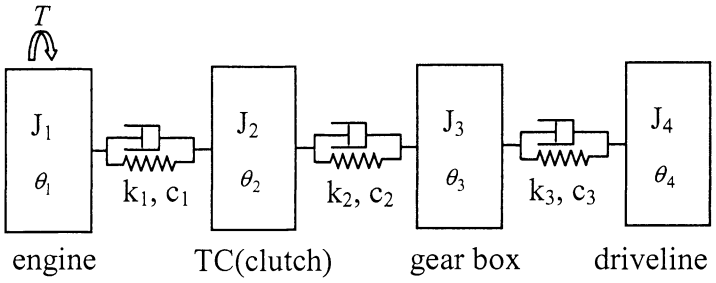

Figure 5.3. A simplified vehicle powertrain model

By using Lagrange's equation, it is straightforward to obtain the equation of motion of the system as:

$$\mathbf{J}\ddot{\boldsymbol{\theta}} + \mathbf{C}\dot{\boldsymbol{\theta}} + \mathbf{K}\boldsymbol{\theta} = \mathbf{T} \tag{5.1}$$

Where $\boldsymbol{\theta} = [\theta_1\ \theta_2\ \theta_3\ \theta_4]^T$, $\mathbf{T} = [T(t)\ 0\ 0\ 0]^T$ are vectors of generalized coordinates and external torque. The inertial matrix **J** and stiffness and damping matrices, **K** and **C,** have the following forms:

$$\mathbf{J} = \begin{bmatrix} J_1 & 0 & 0 & 0 \\ 0 & J_2 & 0 & 0 \\ 0 & 0 & J_3 & 0 \\ 0 & 0 & 0 & J_4 \end{bmatrix} \tag{5.2}$$

$$\mathbf{K} = \begin{bmatrix} k_1 & -k_1 & 0 & 0 \\ -k_1 & k_1+k_2 & -k_2 & 0 \\ 0 & -k_2 & k_2+k_3 & -k_3 \\ 0 & 0 & -k_3 & k_3 \end{bmatrix}; \mathbf{C} = \begin{bmatrix} c_1 & -c_1 & 0 & 0 \\ -c_1 & c_1+c_2 & -c_2 & 0 \\ 0 & -c_2 & c_2+c_3 & -c_3 \\ 0 & 0 & -c_3 & c_3 \end{bmatrix} \tag{5.3}$$

For more detail, see Appendix A1.

When an ATVA or ATVAs are added to a powertrain, the equation of motion of a powertrain fitted with ATVAs keeps the same form as equation (5.1) but $\boldsymbol{\theta}$, **T**, **J, K** and **C** change.

It is noted that the powertrain has a number of gear ratios which are used to set the

optimal engine speed according to vehicle speed. In this chapter, four gear ratios are investigated so there are four gear shifts. At each gear shift, associated gears are engaged to provide a fixed gear ratio called as the first gear, second gear, third gear and the fourth gear accordingly. In this case study, the free and steady state vibration of the system before and after adding the ATVA are investigated for the first, second, third and fourth gears. These gears are characterized by varying the stiffness coefficient k_2. When the powertrain modal frequency is in the resonant range, the ATVA is considered to work effectively if the powertrain natural frequencies can be shifted away from the resonant excitation frequency range so that powertrain's steady state response is reduced significantly.

Let J_1=0.82, J_2=0.22, J_3=0.4, J_4=8kgm^2; c_1=1.0, c_2=2.0, c_3=5.0Nms/rad; k_1=15000, k_3=3350Nm/rad. Where k_2=13000, 15000, 16000 and 18000 Nm/rad for the first, second, third and fourth gear of the gear box are used, respectively. With these parameters, the free vibration of the powertrain can be obtained by solving the equation (5.1) without the vector of excitation torque, please see Appendix A5 for more detail. As a result, the natural frequencies of powertrain and damping ratios ζ for the first, second, third and fourth gears of the gearbox respectively are shown in Table 5.1.

Table 5.1. Natural frequencies of a powertrain model for four gear shifts.

	first gear		second gear		third gear		fourth gear	
index	f (Hz)	ζ (%)	f (Hz)	ζ (%)	f (Hz)	ζ (%)	f (Hz)	ζ (%)
f_1	0[a]		0[a]		0[a]		0[a]	
f_2	7.5299[b]	2.89	7.5937	2.96	7.6199	2.99	7.6640	3.04
f_3	28.0366	3.27	28.7146[b]	3.05	29.0034	2.97	29.5017	2.82
f_4	62.3363	2.39	64.8331	2.35	66.0662	2.32	68.4972[b]	2.27

[a] the first natural frequency is zero due to the rigid body rotation of the whole system (without vibration)
[b] powertrain natural frequencies are used to validate the ATVA's effectiveness in this chapter.

Although the powertrain's natural frequencies vary for each gear shift, their vibration mode shapes have similar forms. For instance, Figure 5.4 shows the powertrain vibration mode shapes of the first gear of the gear box. It can be seen that the second

mode is sensitive to either the first, second or third inertia. In other words, the second frequency powertrain can be shifted significantly if an ATVA is added to these inertias. Meanwhile, the third and fourth modes seem to be sensitive only to the third and second inertia respectively.

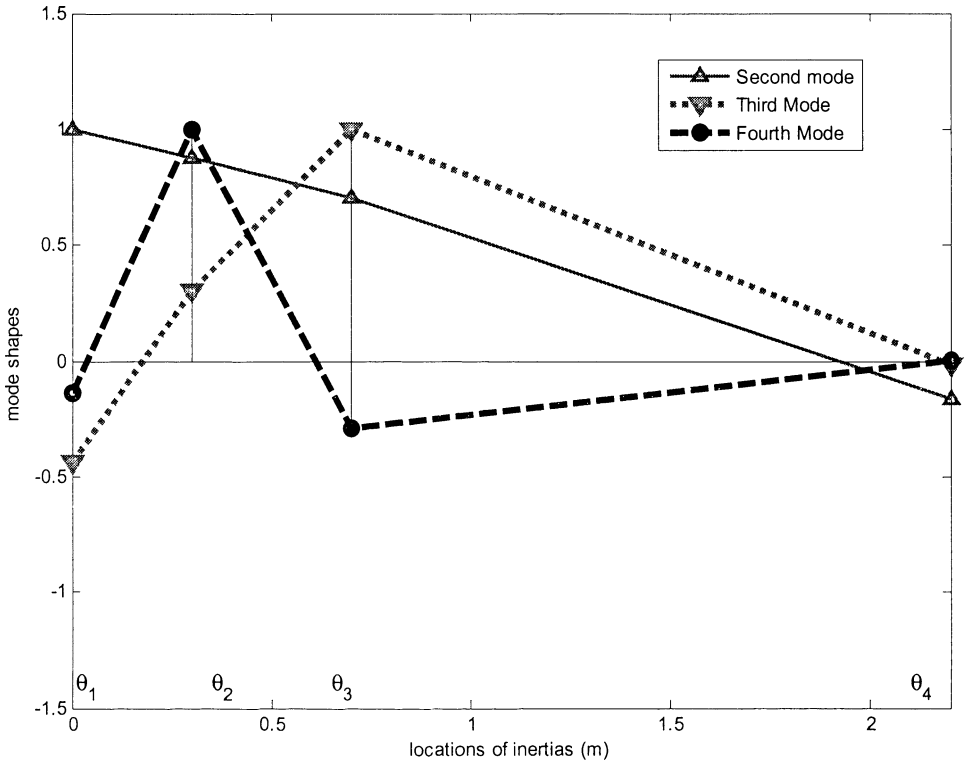

Figure 5.4. The second, third and fourth mode shapes of the first gear of the gear box

5.3.2 *Structure of the proposed ATVA*

The ATVA schematic diagram is shown in Figure 5.5, in which the inner cylinder with lugs is fixed on the rotating shaft. The MRE specimen operates as a torsional spring and the specimen is located between the inner and outer cylinder. Like the inner cylinder, there are lugs on the outer cylinder. These lugs cause tangent elastic forces as well as elastic torques between these cylinders (or rings). Therefore, the outer cylinder can vibrate relative to the inner cylinder.

The MRE is operated under a magnetic field, which is produced by a DC current. It should be noted that there are two solutions for supplying a DC current to the magnetic circuits of the ATVA. The first solution is that the magnetic circuit is fixed on the outer

cylinder, hence, a carbon brush can be used as the turning contact to supply the DC current to the magnetic circuit. The second solution, which is chosen in this thesis, is that the magnetic circuit is stationary while the outer cylinder rotates about the shaft. Because the influence of the imbalance and gyroscopic effect on the torsional vibration of the powertrain is a complicated problem and this is not included in this study and will be discussed in a further study. It is assumed that the ATVA imbalance and gyroscopic effect can be ignored in this application.

It can be seen in Figure 5.5, that the flux, which is produced by the magnetic circuit including the electromagnetic coil and mild steel core, goes through the MRE specimen. Because the inner and outer cylinders are made of brass, the flux will mainly go through the MRE sample. The detailed design of this ATVA will be described in Chapter 8.

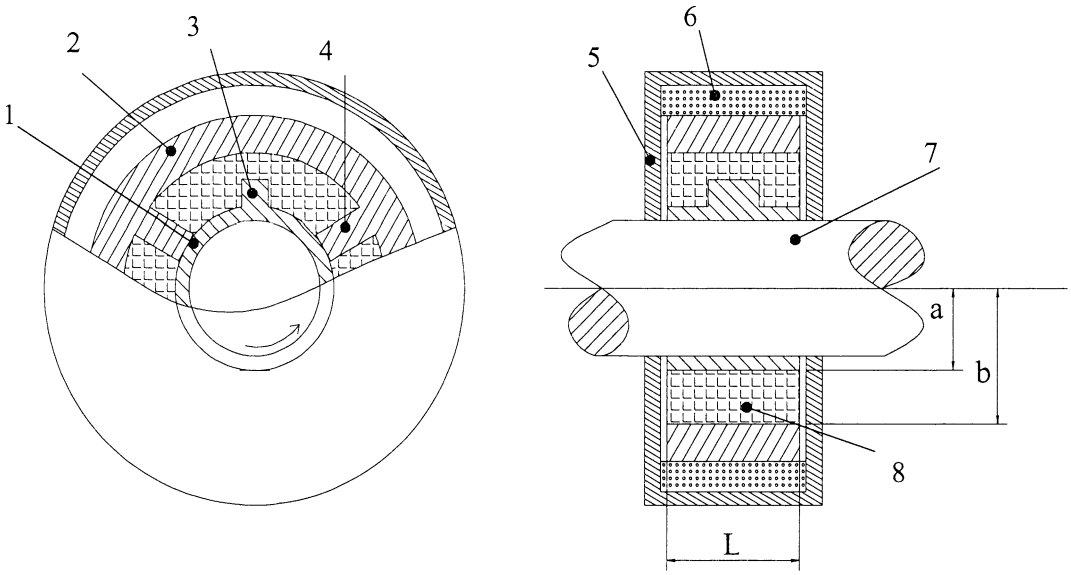

Figure 5.5. ATVA proposed design, 1, 2: inner and outer brass cylinder; 3, 4: lugs in inner and outer cylinder; 5: steel core; 6: coil; 7: shaft; 8: MRE specimen

If the MRE plays a role as a torsional spring and is modelled as a rubber cylinder with inner, outer radius and length as a, b and L respectively, as shown in Figure 5.5, the torsional stiffness coefficient of MRE can be calculated as [82]:

$$k_A = \frac{4\pi L a^2 b^2 G}{b^2 - a^2} \tag{5.4}$$

It is noted that equation (5.4) is a particular case of equation (3.19) in Chapter 3. In the equation (5.4) the shear modulus G is static and it is a real quantity.

Let J_A be ATVA's effective inertia moment and it can be calculated by:

$$J_A = \int r^2 dm = \sum mr^2 \tag{5.5}$$

Where r and dm are the moment arm and element of mass, respectively.

It is noted that the mass of the MRE material can be neglected as it is much smaller than that of the outer ring.

For more convenience, the outer ring can be assumed to be a cylinder with inner and outer radius b and b_1 respectively. Thus, the ATVA's effective inertia moment could be calculated as follows [see Appendix B for more detail]:

$$J_A = J_{outter\ ring} = \frac{1}{2} m(b_1^2 + b^2) = mR_0^2 \tag{5.6}$$

m is the mass of the outer ring; R_0 is the effective radius of gyration of the outer ring and it can be calculated by:

$$R_0^2 = \frac{1}{2}(b_1^2 + b^2) \tag{5.7}$$

Because parameters m, b, b_1 and R_0 are relatively independent, unknown parameters can be obtained easily from the others. For example, if R_0=0.15m is chosen, J_A=0.04kgm^2 and μ_A=0.1 will be calculated. In this chapter, for more convenience, the inertia ratio $\mu_A = J_A / J_3$ can be varied to investigate the ATVA's effectiveness in the design stage. ATVA natural frequency and damped frequency are calculated by:

$$f_A = \frac{1}{2\pi}\sqrt{\frac{k_A}{J_A}} \tag{5.8}$$

$$f_d = f_A\sqrt{1-\varsigma_A^2} \tag{5.9}$$

ς_A is the damping ratio of the MRE material.

In general, the damping property of MREs depends on several factors [8, 10, 85]. Chen et al [85] tested MRE samples under various magnetic fields, polymer matrices and dynamic strain regimes and reported that, when the magnetic field increases, the damping ratio slightly increases at first until it reaches a maximum value and then

decreases slightly. Results indicate that the damping ratio is always less than 0.35. This study seems to be the most comprehensive study about the MRE damping property to date. However, there has been no MRE sample that is similar to the soft MRE used for our work. Zhou [10] tested a MRE with 27% ferrous powders by volume embedded in a silicone rubber matrix and shows that the damping ratio is a slightly decreasing line (about 10%) when the magnetic field increases. The zero-field damping ratio ς_{A0}=0.24 was measured. As the MRE damping property used in this work was not determined, the damping model reported by Zhou [10] will be used. That means the damping ratio can be expressed as $\varsigma_A = \varsigma_A(I) = \varsigma_{A0} - \beta I$, β is the coefficient. If a decline of the damping ratio 10%, i.e., $\frac{\varsigma_{A\min}}{\varsigma_{A\max}} = 9/10$ was set, $\beta = \frac{\varsigma_{A0}}{10 I_{\max}}$ will be calculated and the damping ratio can be expressed as:

$$\varsigma_A = \varsigma_{A0} - \frac{\varsigma_{A0}}{10 I_{\max}} I = \varsigma_{A0}\left(1 - \frac{I}{10 I_{\max}}\right) \tag{5.10}$$

In this chapter, four zero-field damping ratios ς_{A0}=0.05, 0.10, 0.25 and 0.35 are used to investigate the ATVA's effectiveness. The characteristics of the four kinds of damping ratios are shown in Figure 5.6.

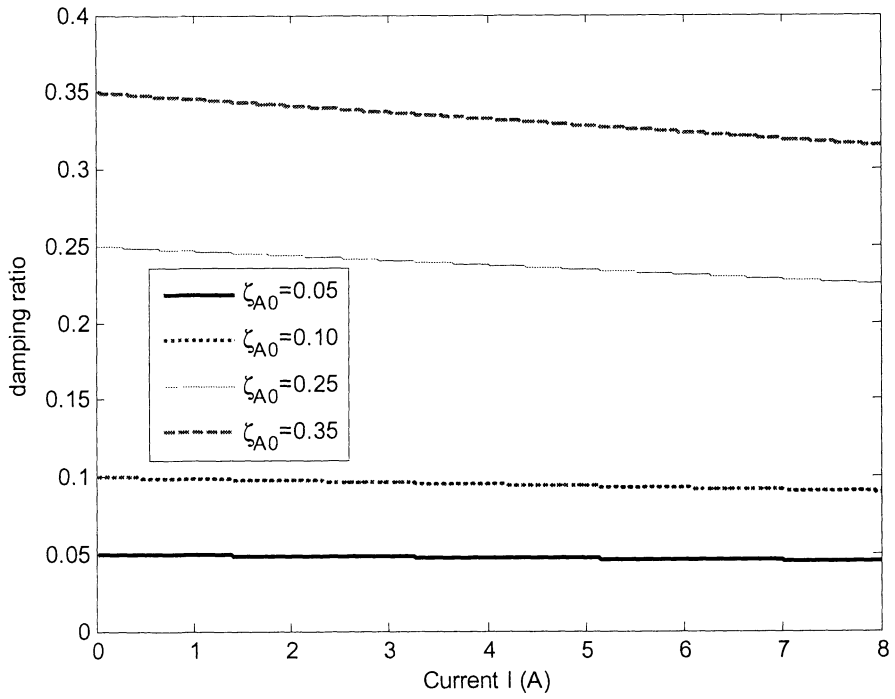

Figure 5.6. ATVA damping ratios for ς_{A0}=0.05, 0.10, 0.25 and 0.35

If a damping ratio ς_A is selected, the ATVA damping coefficient can be calculated:

$$c_A = \varsigma_A C_c \tag{5.11}$$

$C_c = 4\pi f_A J_A$ is the critical damping coefficient.

When the ATVA is added to the powertrain, J_A is fixed and current I is tuned for controlling ATVA damped frequency f_d (both k_A, c_A are tuned by I at the same time). The conversion among ATVA main parameters such as k_A, G, f_A, f_d, I, ς_A and c_A is calculated through equations (5.4), (5.8), (5.9), (5.10) and (5.11). It is noted that the powertrain modal frequency range is from f_{min}=7.5299Hz to f_{max}=68.4972Hz as shown in Table 5.1.

In this chapter, ATVA's main parameters are shown in Table 5.2.

Table 5.2. ATVA's main parameters

Inertial moment and geometry	MRE material	Magnetic field
μ_A=J_A/J_3=1/4, 1/5, 1/10, 1/20	G_0=3.50kPa	α=12500/m
a=0.085m	G_{max}=350kPa	I_{max}=8A
b=0.100m	ς_{A0}=0.05, 0.10, 0.25, 0.35	H_{max}=100kA/m
L=0.075m		

Figure 5.7 shows the ATVA's designed frequencies that depend on the input current I for the four damping ratio characteristics and the inertia ratio μ_A=1/10 was set.

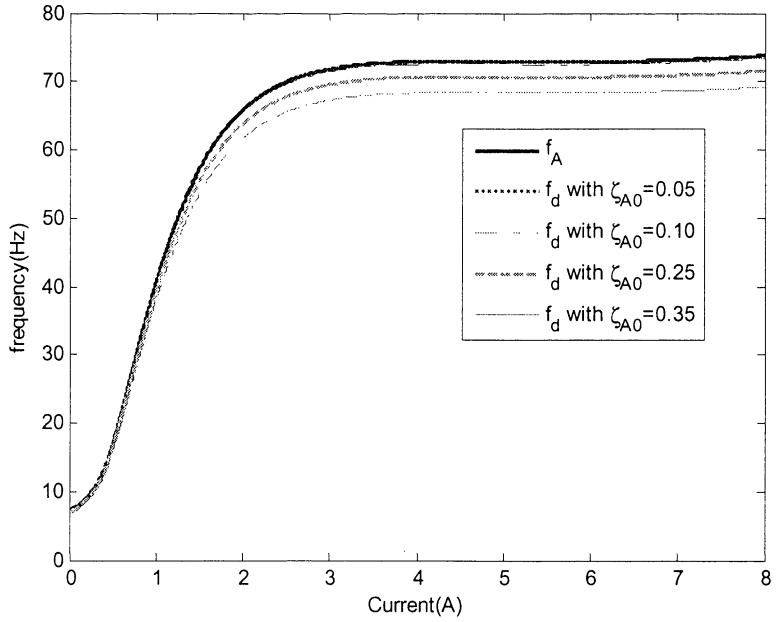

Figure 5.7. ATVA's frequency range for four damping ratio and for μ_A=1/10

It can be seen in Figure 5.7 that the ranges of f_A and f_d for ς_{A0}=0.05 and 0.10 are [7.3756 73.7475], [7.3664 73.6728] and [7.3387 73.4482] (Hz) respectively. For such zero-field damping ratios the difference between f_A and f_d is very slight, while the frequency ranges for ς_{A0}=0.25 and 0.35 are [7.1415 71.8565], [6.9094 69.9931] (Hz) and the difference is significant. Obviously, with the parameters as designed, the ATVA frequency range covers that of the powertrain (with $[f_{min}\ f_{max}]$=[7.5299 68.4972] Hz) as shown in Table 5.1.

5.4 Numerical simulations

5.4.1 Parameter influence on ATVA's effectiveness, a case study for the first gear

According to Wang et al [84], engine torque could be given as:

$$T = T_m + T_0 \sin(\Omega t) \tag{5.12}$$

Where T_m is the constant mean torque; T_0 and Ω are the amplitude and frequency of fluctuation torque, respectively. In this chapter, only fluctuation torque is considered and T_m is neglected. The forcing frequency Ω depends on the number of cylinders and engine speed. It is assumed that Ω is a half of engine rotational frequency for a single cylinder four stroke engine. If the engine is at idle speed (about 900rpm) it gives $\Omega = 2\pi \times 7.5$ (rad/s). When the first gear of the gearbox is operated, the resonance occurs to the second frequency f_2=7.5299Hz of the first gear as shown and noted in Table 5.1. To remove this resonance, an ATVA is attached to the third inertia J_3 of the powertrain as shown in Figure 5.8. In this configuration, the ATVA is mounted on the propeller shaft of the powertrain. This implementation of the ATVA to the powertrain will be showed more detail in experimental validation section in chapter 9. It should be noted that the ATVA has inertia moment J_A, stiffness and damping coefficients k_A and c_A respectively and θ_A is the rotational displacement of the ATVA.

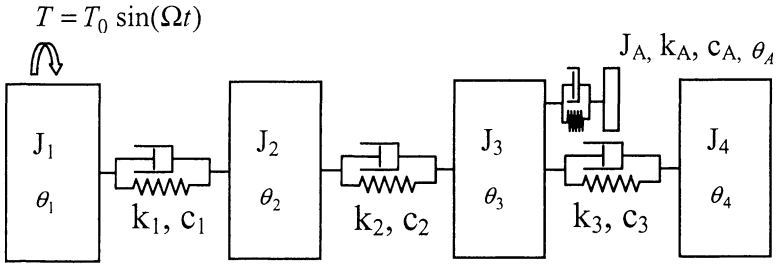

Figure 5.8. A powertrain model with an ATVA

With the ATVA, the system has five degrees of freedom and the equation of motion has the same form as equation (5.1) with $\boldsymbol{\theta} = [\theta_1 \ \theta_2 \ \theta_3 \ \theta_4 \ \theta_A]^T$ and the inertia matrix is expressed in the following form:

$$\mathbf{J} = \begin{bmatrix} J_1 & 0 & 0 & 0 & 0 \\ 0 & J_2 & 0 & 0 & 0 \\ 0 & 0 & J_3 & 0 & 0 \\ 0 & 0 & 0 & J_4 & 0 \\ 0 & 0 & 0 & 0 & J_A \end{bmatrix} \tag{5.13}$$

and the stiffness matrix has form as:

$$\mathbf{K} = \begin{bmatrix} k_1 & -k_1 & 0 & 0 & 0 \\ -k_1 & k_1 + k_2 & -k_2 & 0 & 0 \\ 0 & -k_2 & k_2 + k_3 + k_A & -k_3 & -k_A \\ 0 & 0 & -k_3 & k_3 & 0 \\ 0 & 0 & -k_A & 0 & k_A \end{bmatrix} \tag{5.14}$$

$$\mathbf{C} = \begin{bmatrix} c_1 & -c_1 & 0 & 0 & 0 \\ -c_1 & c_1 + c_2 & -c_2 & 0 & 0 \\ 0 & -c_2 & c_2 + c_3 + c_A & -c_3 & -c_A \\ 0 & 0 & -c_3 & c_3 & 0 \\ 0 & 0 & -c_A & 0 & c_A \end{bmatrix} \tag{5.15}$$

Please see Appendix A2 for more detail.

For the powertrain modal frequency f_2=7.5299Hz as shown and noted in Table 5.1, let ς_{A0}=0.1, μ_A=1/4 so that the current is converted as I=0.072A. In practice, I=0.05A or I= 0.1A is chosen, and f_d=7.433Hz or f_d=7.7139Hz is obtained. For instance, I=0.05A (f_d=7.433Hz) is tuned and the vector of powertrain natural frequencies **f** = [0.0 6.8639 8.1554 28.2069 62.3467]^T are re-calculated. Compared to those in Table 5.1, the powertrain frequencies have been shifted away from the resonant peak f=7.5299Hz by introducing two new frequencies 6.8639 and 8.1554(Hz).

The powertrain modal frequency after adding ATVA has been shifted, which means that the ATVA works effectively. To show more clearly the ATVA's effectiveness, the

forced vibration of the powertrain will be presented in the following section.

With $\Omega = 2\pi \times 7.5$ (rad/s) and let T_0=3Nm, the forced vibration problem of powertrain can be determined. In the steady state of powertrain, the excitation toque is only harmonics; thus, the forced vibration responses of powertrain can be obtained by a using complex magnitude method. As a result, the powertrain steady state vibration responses, before and after adding the ATVA, are solved and they are shown in Figure 5.9 (more detail of solving the equation of motion of the powertrain under harmonics excitation can be seen in Appendix A6).

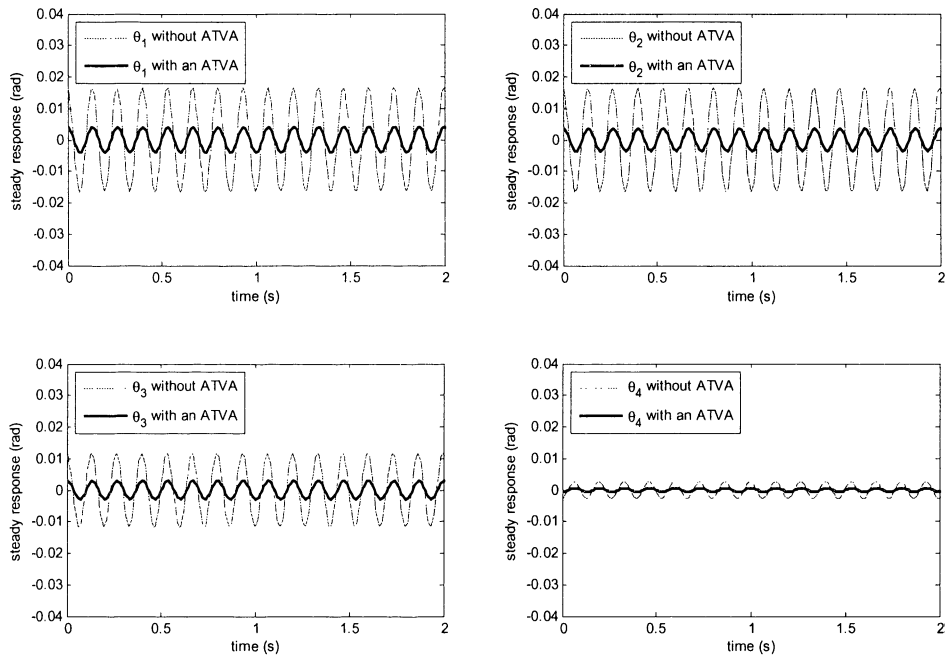

Figure 5.9. Steady state responses at current I =0.05A, ς_{A0}=0.1, μ_A=1/4

It can be seen that the vibration of the four inertias, $\theta_1, \theta_2, \theta_3$ and θ_4 is reduced significantly after adding ATVA. This also confirms that the ATVA works effectively.

It is noted that Figure 5.9 shows the ATVA's effectiveness for the vibration control of powertrain at only one specific excitation frequency $\Omega = 2\pi \times 7.5$ (rad/s). It is useful for designing an ATVA to demonstrate its effectiveness over an excitation frequency range. To illustrate the effectiveness of ATVA over a forcing frequency range, the powertrain vibration frequency response is shown in Figure 5.10. It is noted that in Figure 5.10, the

forcing frequency ratio Ω / ω_d is set from 0.6 to 1.4. In other words the forcing frequency range is [0.6 1.4]f_d= [4.4598 10.4062] (Hz).

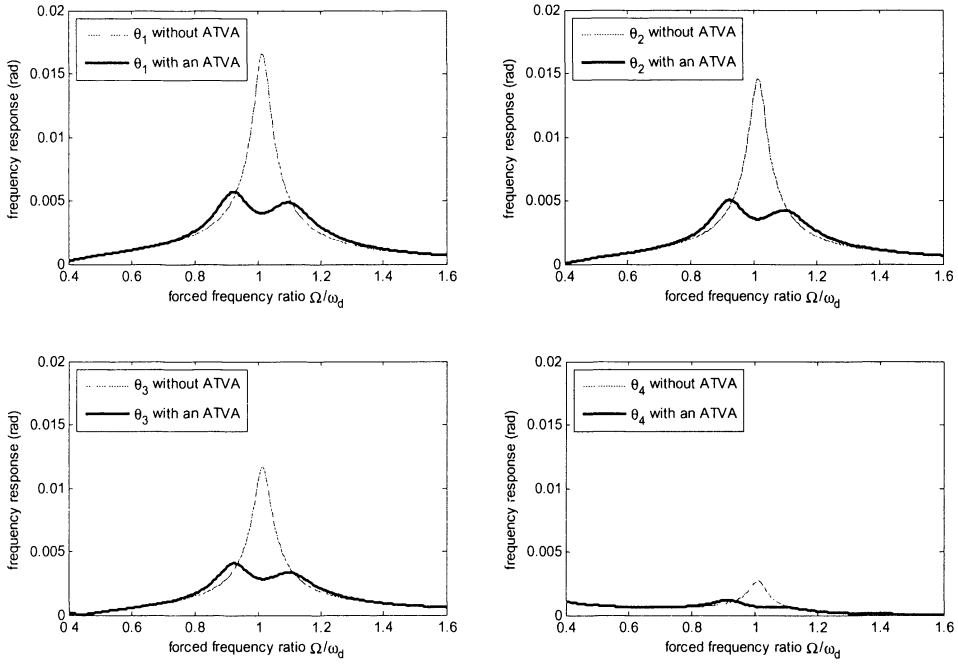

Figure 5.10. Frequency responses when ς_{A0}=0.1, μ_A=1/4

It is obvious that powertrain vibration steady state responses are reduced significantly at and around the resonant frequency f_d (at the forcing frequency ratio, Ω / ω_d, is equal to 1) when ATVA is added to the powertrain. It can be seen that after adding the ATVA the powertrain vibration can be reduced about three times. This confirms the ATVA works effectively for reducing the vibration of the powertrain.

It can also be seen from the Figure 5.10 that the powertrain modal frequency at the resonance was shifted far away from the excitation frequency by introducing two new peaks. In other words, the ATVA has worked as designed. Figure 5.10 provides more information of the ATVA's effectiveness for powertrain vibration control. In particular, the Figure 5.10 shows that at resonant frequency, the ATVA works effectively but in the non-resonant area, the vibration responses of the powertrain after and before adding the ATVA are almost the same. That means the MRE-based ATVA does not affect to the powertrain vibration in the non-resonant area.

In the following sections, the effect of altering ATVA parameters on its effectiveness will be discussed. The parameters discussed in this chapter, include ATVA inertia

moment, the input current of the magnetic field circuit and the damping ratio.
To show how the inertial moment J_A affects the effectiveness of the ATVA, the inertia ratio μ_A=1/4, 1/5, 1/10 and 1/20 was varied to compare the ATVA's effectiveness.

For the zero-field damping ratio ς_{A0}=0.1 was chosen; the responses of the second inertia, for example, are shown in Figure 5.11.

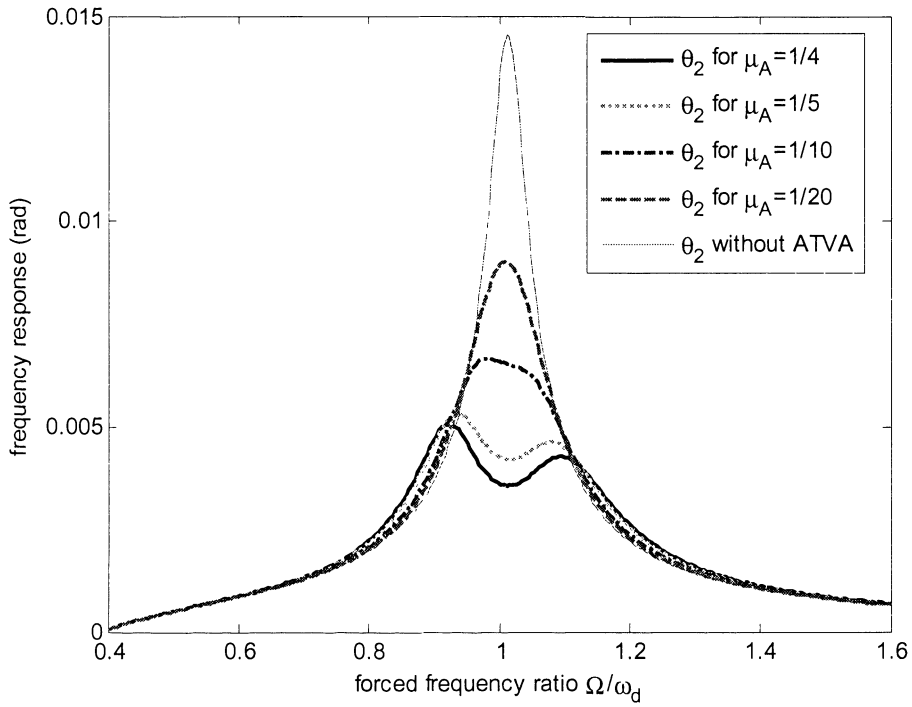

Figure 5.11. Frequency responses of the second inertia θ_2 for several inertia ratios μ_A

It can be seen that the larger the inertia ratio, the better vibration reduction effect of the ATVA can be. For large inertia ratios such as μ_A=1/4 and μ_A=1/5 the resonant peak is shifted far away by introducing two new invariant peaks; thus, the vibration responses are suppressed significantly. While for low inertia ratios μ_A=1/10 or 1/20 it is not so, the frequency is shifted to a lesser extent, as can be seen in Figure 5.11. Obviously, if μ_A is too small, the ATVA may not work.

To show how the input current, I, affects the powertrain responses, the responses with several input current values are calculated and compared. It is noted that if the input current varies, both the stiffness and damping coefficients will be changed. Figure 5.12 shows the responses of the second inertia (θ_2) for I=0.05, 0.10, 0.20 and 0.30A (f_d

=7.4331, 7.7725, 8.97 and 10.6178 Hz) respectively, and μ_A=1/4 was set.

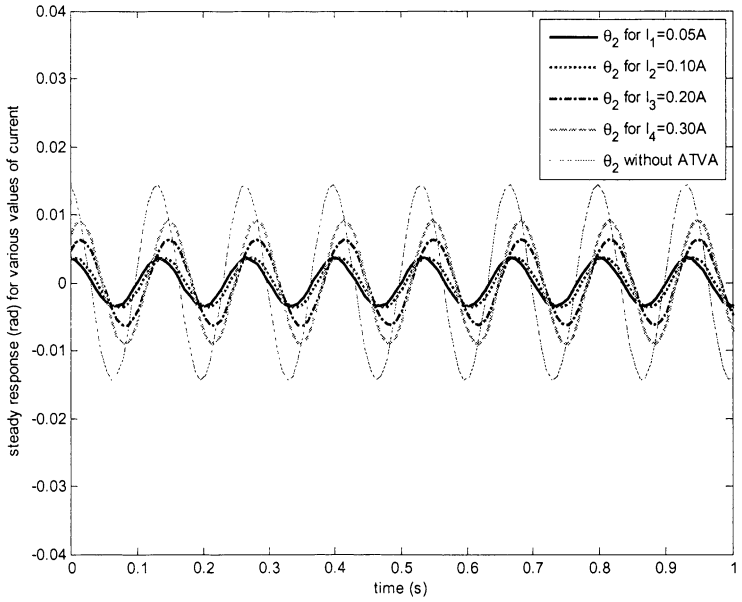

Figure 5.12. Forced vibration of θ_2 for several current values I for μ_A=1/4.

It can be seen that for I=0.05A and I=0.1A, the vibrations are small compared to the others as the current was tuned closer to the exactly current (I=0.072A), while for I=0.2A and 0.3A the vibrations are large. Therefore, the input current is sensitive to the ATVA's effectiveness in this case.

Figure 5.13 shows the effect of the damping ratio to ATVA's effectiveness for μ_A=1/4.

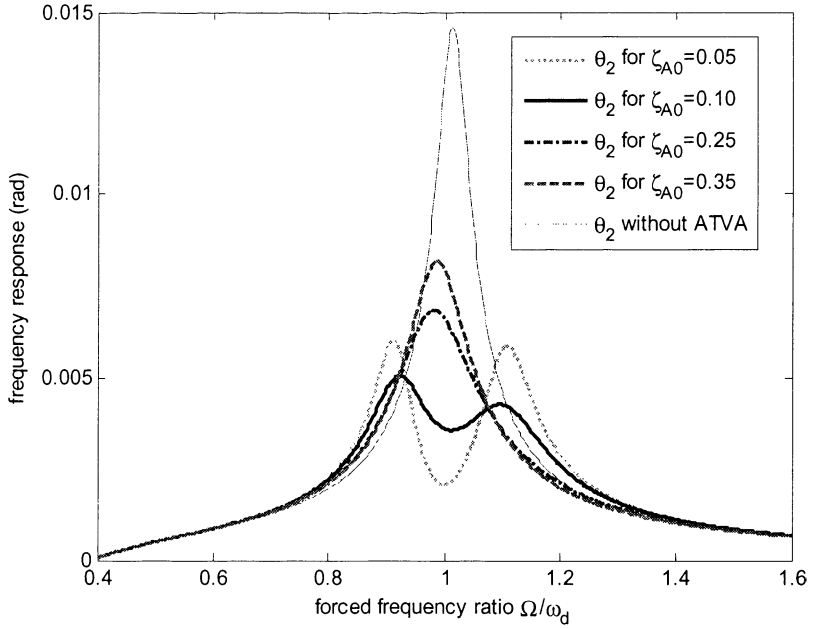

Figure 5.13. Vibration of the second inertia for several damping ratios

The less the damping ratio is, the lower the response at the resonant frequency can be. This is in agreement with the study reported by Sun et al [86]. These authors used a theoretical approach to study a dynamic absorber and show that the lower the damping ratio is, the better absorber effectiveness can be. However, a low damping ratio may result in a high vibration response at the two new invariant frequencies. For instance, for ς_{A0}=0.05 the frequency response is the smallest at ratio Ω/ω_d=1, but at two invariant peaks, the responses are higher than those when ς_{A0}=0.1. Thus, the damping ratio can be optimised to increase the ATVA's effectiveness and this will be discussed in a future study.

5.4.2 *The influence of ATVA location on its effectiveness*

In this section, the ATVA will be used when resonances happen to the third frequency of the second gear (f_3=28.7146Hz) and the fourth frequency of the fourth gear (f_4=68.4972Hz), as shown and noted in Table 5.1. At these frequencies, the ATVA location is very important and is the most essential difference between applications of ATVA for SDOF and MDOF systems. To show this more clearly, the ATVA's effectiveness is compared between two locations of ATVA, in which location A is one where the ATVA is added to the third inertia (θ_3) as shown in Figure 5.8, and location B is one where the ATVA is added to the second inertia (θ_2), as shown in Figure 5.14.

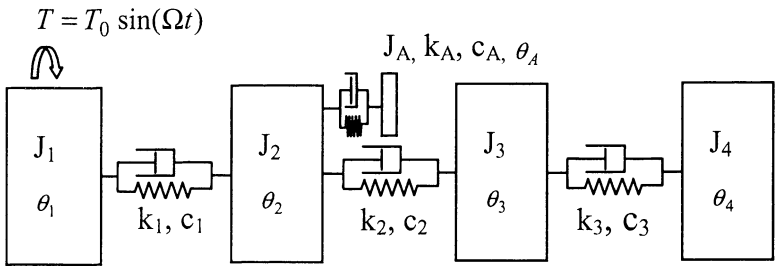

Figure 5.14. Location B of ATVA

If the ATVA is attached to location B, the equation of motion of the system keeps the same form as equation (5.1) with $\boldsymbol{\theta} = [\theta_1 \ \theta_2 \ \theta_3 \ \theta_4 \ \theta_A]^T$ and the inertia matrix $\mathbf{J}$=diag(J_1, J_2, J_3, J_4, J_A). The stiffness and damping matrix are expressed as:

$$\mathbf{K}=\begin{bmatrix} k_1 & -k_1 & 0 & 0 & 0 \\ -k_1 & k_1+k_2+k_A & -k_2 & 0 & -k_A \\ 0 & -k_2 & k_2+k_3 & -k_3 & 0 \\ 0 & 0 & -k_3 & k_3 & 0 \\ 0 & -k_A & 0 & 0 & k_A \end{bmatrix} \tag{5.16}$$

$$\mathbf{C}=\begin{bmatrix} c_1 & -c_1 & 0 & 0 & 0 \\ -c_1 & c_1+c_2+c_A & -c_2 & 0 & -c_A \\ 0 & -c_2 & c_2+c_3 & -c_3 & 0 \\ 0 & 0 & -c_3 & c_3 & 0 \\ 0 & -c_A & 0 & 0 & c_A \end{bmatrix} \tag{5.17}$$

Please see Appendix A3 for more detail.

The influence of ATVA's location on its effectiveness will be presented in flowing sections. In which, both locations A and B are examined to compare the ATVA's effectiveness. For both of the following cases, the inertia ratio μ_A=1/5 is set.

a) A case study for the second gear of the gear box

In this case the engine speed is assumed to operate at 3420 rpm. The forcing frequency of fluctuation torque $T=T_0\sin(\Omega t)$ is assumed as a half of rotational frequency of the engine. In other words, the excitation frequency $\Omega=2\pi\times28.5$ (rad/s) is obtained. It can be seen from Table 5.1 that the resonance occurs with the third frequency of the second gear of the powertrain f_3=28.7146 Hz. To deal with the resonance f_3=28.7146 Hz, the input current I=0.75A (f_d=28.6847Hz) is tuned. As a result, the forced vibration of the powertrain is calculated.

Figure 5.15 shows the frequency responses for ς_{A0}=0.1 and T_0=30Nm. It is noted that the ratio range is [0.6 1.4] (forcing frequency range is [17.2108 40.1586] Hz).

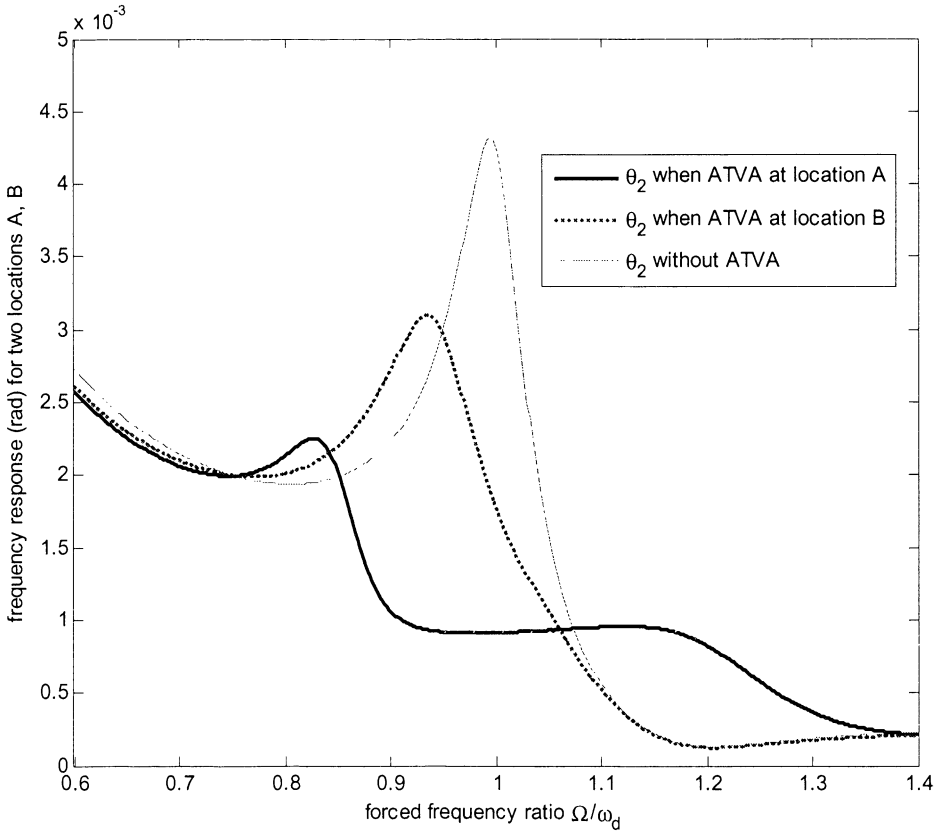

Figure 5.15. The frequency responses of the second gear

It can be seen that the response θ_2 when the ATVA is at location A is much smaller than the others. This response, when ATVA is located at location B, is partially reduced around the resonant frequency because the resonant frequency is not shifted away. It is confirmed that in spite of the same parameters, the ATVA works effectively when it is located at location A only in this case.

b) A case study for the fourth gear of the gear box

In this study, Ω is assumed to be 68Hz as a half of the frequency of the engine speed of 8160 rpm. For this speed, the fourth gear of the gear box is operated. The resonance occurs at the fourth frequency f_4=68.4972Hz of the fourth gear, as shown in Table 5.1. For this frequency, the ATVA current I=2.4A (f_d=68.5337Hz) is tuned. The frequency response, when the ATVA is located to either location A or B, is shown in Figure 5.16 for ς_{A0}=0.25, T_0=30Nm and the ratio range is [0.6 1.4] (forcing frequency range is [41.1202 95.9472](Hz)).

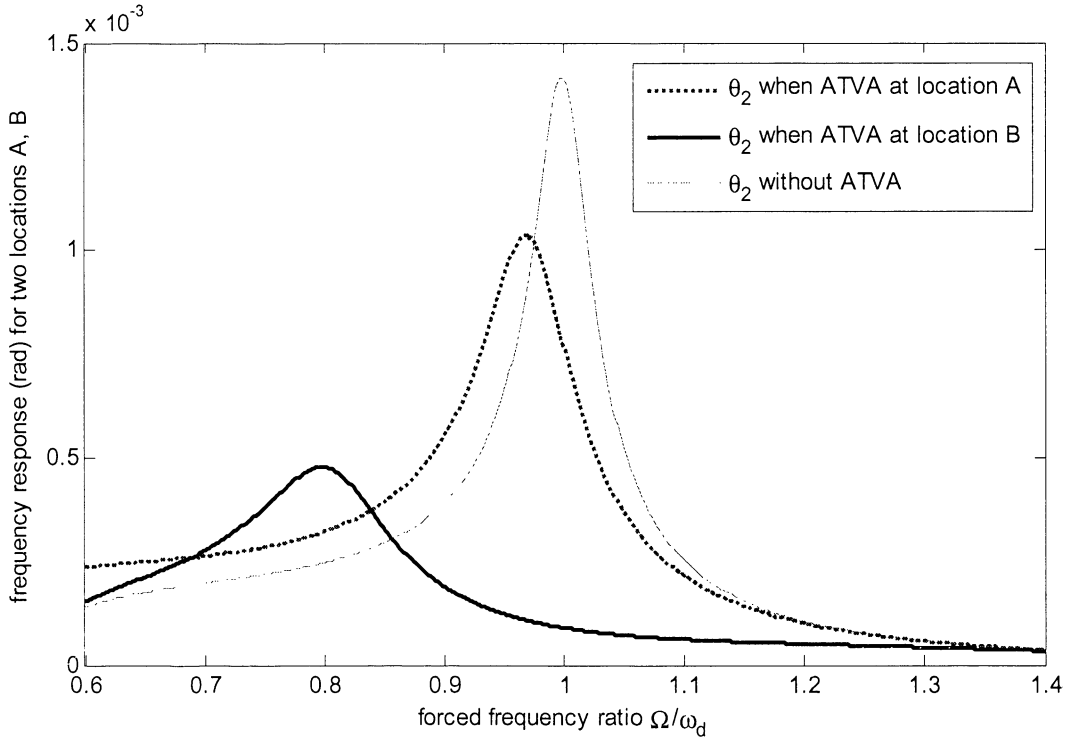

Figure 5.16. The frequency responses for the fourth gear

In this case, the ATVA has worked effectively when it is attached to the location B only because the powertrain's natural frequencies are shifted away from the resonant peaks 68.4972 Hz. Meanwhile if ATVA is added to location A, it does not work because powertrain's natural frequencies are not shifted and the powertrain response is not reduced significantly at the resonant frequency.

5.4.3 Vibration of ATVA

It is noted that the purpose of the dynamic absorber (and ATVA) is to absorb the vibration of the primary system. In this study, although the vibration of powertrain was reduced significantly and the MRE-based ATVA works effectively, the vibration of the ATVA should be investigated because if the amplitude of the ATVA is too big, the implementation of the ATVA to the powertrain could be prevented. Figure 5.17 shows the vibration of the ATVA and the vibration of the transmission J_3, which was shown in Figure 5.9.

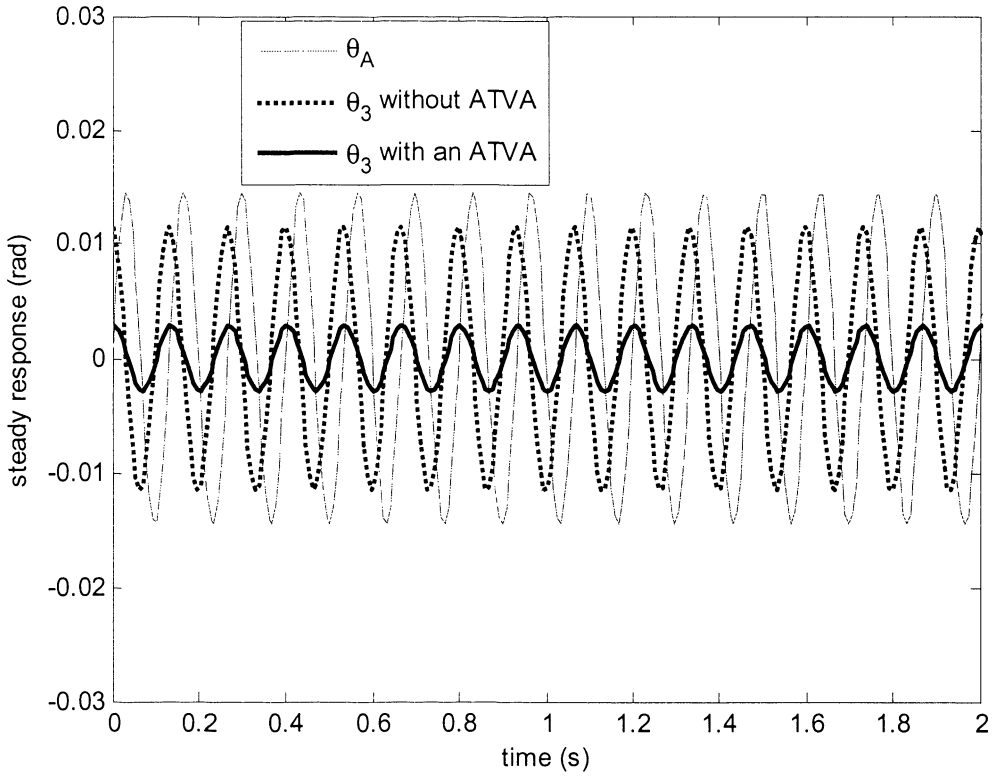

Figure 5.17.ATVA frequency

It can be seen that with the ATVA, the vibration of the powertrain is reduced significantly while the vibration of ATVA is large. In other words, after adding the ATVA to the powertrain system, the ATVA absorbs the vibration from the powertrain. It is also noted that the ATVA inertia is small compared to the inertia of the transmission. In practice, the ATVA is manufactured to experience a high vibration. Thus, in following chapters, the ATVA's effectiveness is investigated for reducing the powertrain vibration but the vibration of ATVA will be not investigated.

5.5 Discussion

This chapter used a soft MRE for constructing an ATVA for torsional vibration suppression of a powertrain, which is a MDOF system. The development of a torsional MRE-based ATVA for a MDOF application has not been so far reported.

Using the soft MRE, whose increase in elastic modulus is significant, a new concept design of an ATVA was proposed in which the ATVA consists of two main

components: the stationary part and the rotating part. The stationary part consists of the magnetic circuit and frame support. The magnetic field is produced by an electromagnetic coil, and the magnetic flux of the magnetic field goes through MRE specimens, which are located between the outer ring and inner ring of the rotating part. Since the MRE specimens work as a torsional spring whose stiffness can be controlled by the magnetic field, the MRE-based ATVA frequency can be tuned magnetically. With the concept design, numerical simulations were conducted to show the ATVA's effectiveness for vibration reduction of a simplified powertrain model. It was found that with the significant increase in elastic modulus of the soft MRE, the ATVA can work over a wide range of frequencies. To be specific, with the soft MRE material the ATVA can effectively work in a frequency range from around 7 to 70Hz (ten times increase in relative frequency range). With such a frequency range, this proposed MRE-based ATVA overcomes the limitation of traditional TVAs, which are effective for mechanical vibration control only in a narrow bandwidth.

Based on such a wide working frequency range, the ATVA can be properly tuned for shifting natural frequencies of powertrain for four gears of gearbox of powertrain transmission. When ATVA works effectively, the natural frequencies of the powertrain are shifted away from the resonant area, thus, powertrain steady vibration is reduced significantly.

It was confirmed that the MRE-based ATVA's effectiveness is affected not only by the elastic modulus (stiffness coefficient) but also by the inertia and the damping ratio of the ATVA. The simulation results also show that although the damping and stiffness of MRE-based ATVA are correctly tuned, the ATVA can still not work effectively if it is not attached in a suitable location of the powertrain. This is the main difference between the application of ATVA for MDOF and SDOF systems.

5.5.1 Limitations

In this chapter, the proposed vibration model of the powertrain is a simplified one, although the model parameters were only chosen to be close to a real powertrain model. In other words, these parameters do not belong to a specific vehicle. In fact, the parameters were chosen with the purpose that the powertrain frequencies were close to

those of a real vehicle powertrain. For example, inertia moment J_1=0.82 kgm^2 for engine, J_2=0.22 kgm^2 for clutch, J_3=0.6 kgm^2 for transmisstion, J_4=60kgm^2 for driveline components are realistic values. Damping and stiffness parameters were then assumed so that the powertrain frequencies were close to those of a real vehicle powertrain system. It would be useful for validating the ATVA's effectiveness if a equivalent model of a real powertrain is used, in which the modal testing method is used to validate the accurateness of the model and the error of the model can be examined. This should be conducted in futher work.

To model the gear changes of the powertrain, it is assmued that only the stiffness coefficient k_2 is changed. In fact, for powertrain system, although the mass of trasmissmiision gear box is constant, the inertia moment may change. Thus, the the inertia moment J_3 and the damping coefficient c_2 would be considered as non-constant parametrs. This consideration should be investigated in a futher study.

Although the elastic model of MRE was numerically reported, it is not very convenient to use the numerical data of the soft MRE for deriving parameters of ATVA such as shear modulus, stiffness or frequency as shown in equations (5.4) or (5.9). Therefore, it would be useful to approximate the shear modulus of MRE as an explicit function of magnetic flux density to facilitate the ATVA design process. This approximation of shear modulus of the soft MRE will be established in Chapter 6.

In addition, because the damping of the soft MRE was not reported, this chapter used the damping model by Zhou [10] for the numerical simulation instead. As a result, the damping model may not accurately represent the damping property of the soft MRE.

It is noted that the magnetic flux density 0.3Tesla is assumed in the MRE surface only. The magnetic field distribution in the MRE layer should be determined by using an electromagnetic finite element method; however, the objective of this chapter is to introduce a concept design of the ATVA using the new MRE to show the potential application of the MRE material for a vibration control of powertrain. The detailed design, such as the distribution of the magnetic field in the MRE layer, was not considered in this study. In other words, it is assumed that the magnetic flux density 0.3

Tesla can be provided sufficiently for the MRE layer. In practice, the magnetic flux density 0.3 Tesla can be supplied by changing some factors of the magnetic circuit such as the number of turns of coils. The use of FEM for investigating the magnetic field of MREs should be undertaken in further studies.

Although the numerical simulation show that the MRE-based works as designed (with the reduction of vibration response is about three times), this chapter was not defined exactly what is the criterion for reduction of powertrain vibration to make sure that the ATVA work effectively. This should be carried out in future research. Alternatively, the effectiveness of the MRE-based ATVA can be evaluated by integrating the energies over a frequency range to calculate how much reduction in vibration energy that the ATVA can do. Ii other words, the reduction of vibration energy can be used as a criterion for validating the MRE-based effectiveness.

In this study, the effect of ATVA imbalance and gyroscopic effect was ignored. In fact, the effect may affect to the vibration of the powertrain significantly and then to the ATVA's effectiveness. This consideration should be carried out in future work.

5.6 Summary

This chapter presented a concept design of an ATVA using a soft MRE for the vibration control of a simplified powertrain model. Numerical simulations were used to validate ATVA's effectiveness for powertrain vibration minimization. Numerical results show that, with the ATVA, the powertrain frequencies were shifted away from the resonant frequency. As a result, the forced vibration responses of the powertrain were significantly suppressed.

Chapter 6 A DUAL ATVA FOR POWERTRAIN STEADY VIBRATION REDUCTION

6.1 Introduction

The objective of this chapter is to present the application of a dual MRE-based ATVA for powertrain vibration control under either single or multi harmonic excitation. The MRE used in this chapter to develop the ATVA is also the soft MRE introduced in Chapter 5. Similar to Chapter 5, the dual ATVA is used in this chapter to reduce the steady state vibration of the powertrain.

After introducing and solving the free vibration of a powertrain model, a proposed dual ATVA for dealing with the two resonances at the same time is presented. To facilitate the ATVA design, a model for shear modulus of the MRE material is derived. This is followed by numerical simulations of powertrain fitted with the dual ATVA to show the ATVA's effectiveness. Three cases are conducted in the numerical simulations. The first case is the use of the dual ATVA to deal with a single resonance occurring in the first order multiple (also the fundamental) frequency of the powertrain system. Second, the two resonances occurring in both the first and third multiples of the fundamental frequency are examined. Last, the use of the dual ATVA for dealing with the resonances, which occur at the first and second multiples of the fundamental frequency, is conducted.

This chapter presents a dual MRE-based ATVA rather than a single ATVA for two main reasons. The first is that the effectiveness of a single ATVA for the primary MDOF powertrain system depends on not only the ATVA parameters such as the inertia

moment, stiffness and damping coefficients but also on the powertrain vibration mode shapes. In other words, if a single ATVA is installed at a fixed position in the powertrain, it may only work effectively with one or few powertrain frequencies. That means this single ATVA will not be able to deal with resonances at other powertrain frequencies, although these frequencies are within its working frequency range. The second reason is that a single ATVA cannot deal with more than one resonance at the same time, while the vehicle's engine fluctuation torque is a multi-frequency excitation because of the internal combustion engine characteristics. According to the engine speed, the dual ATVA frequency can be tuned to shift powertrain frequencies away from resonances, which occur in several powertrain vibration modes. This device will be an innovative device for powertrain vibration reduction.

Dual absorbers have been used widely in many applications [87, 88-91]. Yamashita et al [87] designed dual dynamic absorbers for reduction of vibration of piping system. In line with these authors, Yan and Lin [88] developed a dual dynamic absorber for suppressing the computer hard disk driver vibration. Burdisso and Heilmann [89] used a dual dynamic absorber for vibration reduction of a structure. Iwanami and Seto [90] optimised the design parameters of a dual dynamic absorber for a SDOF system. Al-Bedoor and Moustafa [91] used a dual dynamic absorber for the reduction of start-up vibration of synchronous motor-driven compressors, modelled as a MDOF system. Even though these studies show that there are several advantages to using dual ATVAs over single ones, the role of vibration mode shapes of the primary MDOF system has not been fully addressed. In particular, the application of dual MRE-based ATVA for two resonances at the same time has not been investigated.

6.2 A powertrain simplified vibration model

Similar to Chapter 5, the powertrain vibration model that is described in Figure 5.1 is used to validate the dual ATVA for the steady state vibration reduction of the powertrain. In this chapter, let J_1=0.8, J_2=0.25, J_3=0.5, J_4=8kgm^2; c_1=5.0, c_2=10.0, c_3=15.0Nms/rad; k_1=20000, k_3=10000Nm/rad. Also, it is assumed that there are four transmission gears of gear box of powertrain system. Accordingly, k_2=13000, 15000, 16000 and 18000 Nm/rad are set for the first, second, third and fourth gear, respectively. With these parameters, the free vibration problem of the powertrain can be

solved. Thus, the powertrain frequencies and damping ratio ζ for four gear ratios of the gear box are shown in Table 6.1.

Table 6.1. Powertrain natural frequencies and damping ratio ζ for four gear ratios

	first gear		second gear		third gear		fourth gear	
index	f (Hz)	ζ (%)	f (Hz)	ζ (%)	f (Hz)	ζ (%)	f (Hz)	ζ (%)
f_1	0[a]		0[a]		0[a]		0[a]	
f_2	11.0494[b]	3.91	11.2758	3.96	11.3708	3.99	11.5329	4.06
f_3	31.9372[b]	9.24	32.6012[b]	8.67	32.8924	8.42	33.4069	8.01
f_4	63.0397	9.48	65.0439[b]	9.36	66.0436	9.30	68.0324	9.15

[a] the first natural frequency is zero due to the rigid body rotation of the whole system

[b] powertrain natural frequencies are used to validate the ATVA's effectiveness in this chapter

The powertrain vibration mode shapes of the first gear are shown in Figure 6.1.

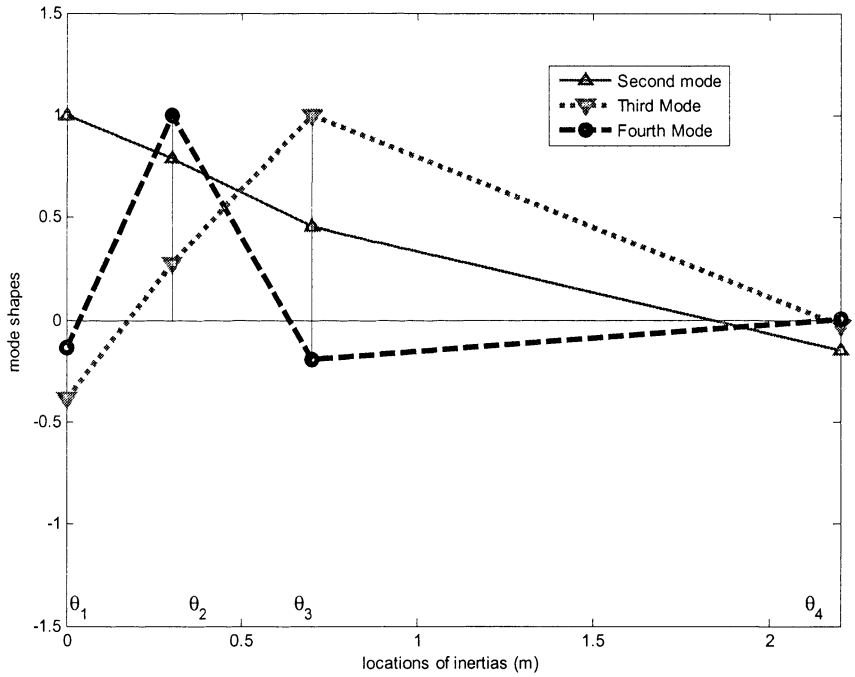

Figure 6.1. The second, third and fourth mode shapes of the first gear of gearbox

It can be seen that the second mode is sensitive to either the first, second or third inertia. In other words, the second frequency of the powertrain can be shifted away if an ATVA is added to these three inertias. Meanwhile, the third and fourth modes seem to be only sensitive to the third and second inertia, respectively. If only a single ATVA is installed at a fixed position in the powertrain, it will not be able to deal with resonances happening to all the three vibration mode shapes.

6.3 A proposed dual ATVA

From the powertrain mode shapes shown in Figure 6.1, the dual ATVA location is proposed as in Figure 6.2. Here, single ATVAs 1, 2 are installed on the side of transmission box (third inertia-J_2) and clutch (second inertia-J_3), respectively.

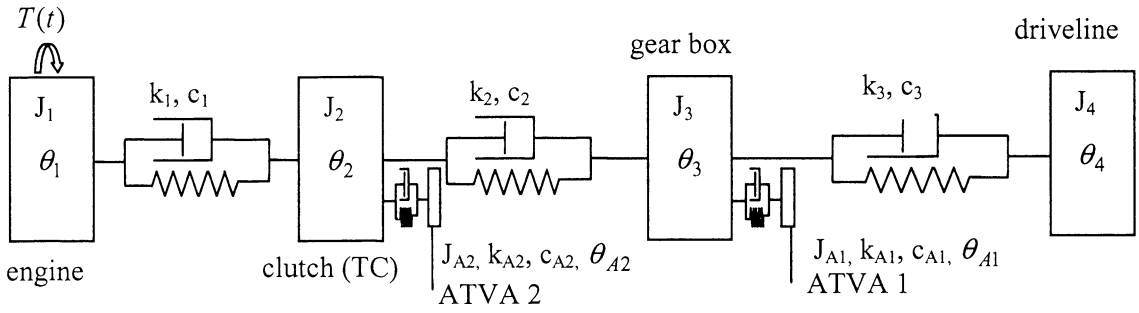

Figure 6.2. Powertrain with dual ATVA

This combination of the two single ATVAs is the best option because ATVA 1 can deal with the resonances, which occur to the second and third powertrain vibration modes, and ATVA 2 can work effectively for dealing with the resonances happening to the second and fourth modes. Thus, resonances occurring in all three powertrain vibration frequencies as shown in Table 6.1 can be managed.

It is noted that after the dual ATVA is attached to the powertrain, as in Figure 6.2, the system now has 6 DOFs and its equation of motion keeps the same form as equation (5.1) in Chapter 5 but vectors of the generalized coordinates and external torque are $\boldsymbol{\theta} = [\theta_1\ \theta_2\ \theta_3\ \theta_4\ \theta_{A1}\ \theta_{A2}]^T$ and $\mathbf{T} = [T(t)\ 0\ 0\ 0\ 0\ 0]^T$ respectively. In addition, the inertia matrix is expressed as:

$$\mathbf{J} = \begin{bmatrix} J_1 & 0 & 0 & 0 & 0 & 0 \\ 0 & J_2 & 0 & 0 & 0 & 0 \\ 0 & 0 & J_3 & 0 & 0 & 0 \\ 0 & 0 & 0 & J_4 & 0 & 0 \\ 0 & 0 & 0 & 0 & J_{A1} & 0 \\ 0 & 0 & 0 & 0 & 0 & J_{A2} \end{bmatrix} \tag{6.1}$$

The stiffness matrix has the following form:

$$\mathbf{K}=\begin{bmatrix} k_1 & -k_1 & 0 & 0 & 0 & 0 \\ -k_1 & k_1+k_2+k_{A2} & -k_2 & 0 & 0 & -k_{A2} \\ 0 & -k_2 & k_2+k_3+k_{A1} & -k_3 & -k_{A1} & 0 \\ 0 & 0 & -k_3 & k_3 & 0 & 0 \\ 0 & 0 & -k_{A1} & 0 & k_{A1} & 0 \\ 0 & -k_{A2} & 0 & 0 & 0 & k_{A2} \end{bmatrix} \tag{6.2}$$

and the damping matrix **C**

$$\mathbf{C}=\begin{bmatrix} c_1 & -c_1 & 0 & 0 & 0 & 0 \\ -c_1 & c_1+c_2+c_{A2} & -c_2 & 0 & 0 & -c_{A2} \\ 0 & -c_2 & c_2+c_3+c_{A1} & -c_3 & -c_{A1} & 0 \\ 0 & 0 & -c_3 & c_3 & 0 & 0 \\ 0 & 0 & -c_{A1} & 0 & c_{A1} & 0 \\ 0 & -c_{A2} & 0 & 0 & 0 & c_{A2} \end{bmatrix} \tag{6.3}$$

Please see Appendix A4 for more detail.

6.4 A proposed model of soft magnetorheological elastomer

In this chapter, the soft MRE, which was used in Chapter 5, is used to numerically validate the ATVA's effectiveness. Although the numerical data of the MRE shear modulus was used in Chapter 5 for designing the ATVA, it is not convenient to convert among ATVA parameters. As a result, there is a need to approximate the numerical data of the MRE by an explicit function of magnetic flux density or magnetic field intensity H. In this section, a model of shear modulus is proposed as a symbolic function of magnetic flux density B.

It is noted that Stepanov et al. [69] tested several MRE samples, which have similar components to the soft MRE in this chapter, and reported that the dependence of the elastic modulus on magnetic flux density B is a curve that looks like S-shaped. In addition, according to Abramchuk et al [70], at B=0 and at $B=B_S$=0.3-0.4Tesla (saturated point), shear modulus G reaches minimum and maximum values, G_0 and G_{max} (3.5kPa and 350kPa), respectively.

In this chapter, the shear modulus of the soft MRE can thus be modelled as a cubic polynomial of magnetic flux density B as below:

$$G = G(B) = \begin{cases} G_0 & B \le 0 \\ G_0 + \sum_0^3 p_i B^i & 0 < B < B_S \\ G_{\max} & B \ge B_S \end{cases} \tag{6.4}$$

Where p_i, i=0..3, are coefficients.

The coefficients c_i can be determined from four conditions such that $G(0) = G_0$, $G(B_S) = G_{\max}$, $G'(0) = 0$, $G'(B_S) = 0$.

With few calculations, it is straightforward to obtain coefficients: $p_0 = 0$, $p_1 = 0$, $p_2 = \frac{3(G_{\max} - G_0)}{B_S^2}$ and $p_3 = \frac{-2(G_{\max} - G_0)}{B_S^3}$, respectively. Substituting the coefficients p_i to equation (6.4), the shear modulus G of the soft MRE can be represented in the following form:

$$G = \begin{cases} G_0 & B \le 0 \\ G_0 + (G_{\max} - G_0)\frac{B^2}{B_S^2}(3 - 2\frac{B}{B_S}) & 0 < B < B_S \\ G_{\max} & B \ge B_S \end{cases} \tag{6.5}$$

It is clear that the proposed model of shear modulus G of the soft MRE as shown in equation (6.5) can be effectively used for designing ATVA. With the proposed model, ATVA parameters such as stiffness and damping coefficients or frequency can be easily converted to one another.

To validate the proposed model as shown in equation (6.5), it is compared with the experimental data, as shown in Figure 6.3, in which the data is expressed in terms of a logarithm of the relative change (G/G_0) relative to the magnetic field intensity H. Abramchuk et al [70] reported that before the saturated point B_S=0.35T, the relationship between magnetic flux density B and magnetic intensity H is linear, $B = \mu H$ where μ is the permeability.

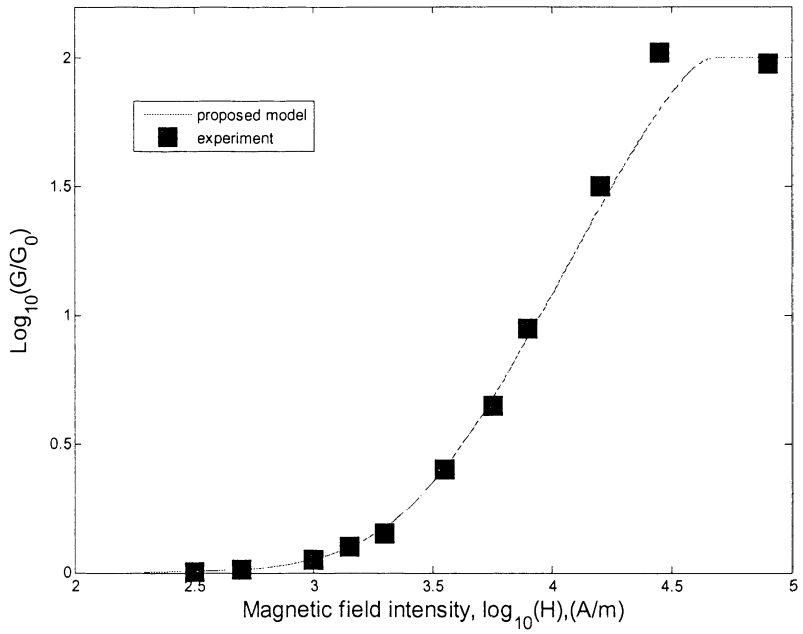

Figure 6.3. MRE shear modulus proposed model and experiment [70]

It can be seen that the proposed model and experiment data are in agreement. With the proposed model, the dual ATVA parameters such as stiffness and damping coefficients can be treated as explicit functions of magnetic flux density B. Thus, the ATVA frequency can be tuned properly so that the proposed model is effective for designing the dual ATVA.

6.5 Dual ATVA for suppression of powertrain vibration

6.5.1 The ATVA frequency

A proposed design of a single ATVA is the same as shown in Figure 5.5 (Chapter 5). If m=2kg, b=0.1m and R_0=0.2m are given, ATVA inertia J_A=0.08kgm^2 and inertia ratio $\mu_A = J_A / J_3$ =0.2 are calculated. This is similar to Chapter 5; the inertia ratio μ_A can be varied to investigate the ATVA's effectiveness in this chapter.

It is noted that since the damping of the soft MRE has not been reported yet, a damping model proposed by Zhou [10] is used. According to this author, the damping ratio is a slightly decreasing line (about 10%). Thus, in this chapter, this damping model can be represented as below:

$$\varsigma_A = \varsigma_A(B) = \varsigma_0 - \frac{\varsigma_0 - \varsigma(B_{\max})}{B_{\max}} B = \varsigma_0 (1 - \frac{B}{10 B_{\max}}) \tag{6.6}$$

Here $\varsigma(B_{\max}) = 0.9\varsigma_0$ was set and four zero-field damping ratios ς_0 = 0.05, 0.10, 0.25

and 0.35 were set to examine the dual ATVA's effectiveness. The ATVA main parameters and MRE properties are shown in Table 6.2.

Table 6.2. ATVA and the soft MRE material parameters

ATVA	MRE
a=0.095m	G_0=3.50kPa
b=0.1m	G_{max}=350kPa
L=0.045m	B_{max}=0.5T, B_S=0.35T
μ_A=0.05, 0.1, 0.2 and 0.25	ς_0 = 0.05, 0.10, 0.25 and 0.35

With ATVA parameters as in Table 6.2, the shear modulus is calculated as in equation (6.5), and the ATVA stiffness is then calculated from equation (5.4) in Chapter 5. As a result, ATVA natural frequency f_n and damped frequency f_d are calculated from equations (5.8) and (5.9) in Chapter 5, with the damping ratio is calculated from equation (6.6). These frequencies of the ATVA, f_n and f_d, with four damping ratios ς_0 = 0.05, 0.10, 0.25 and 0.35 are shown in Figure 6.4.

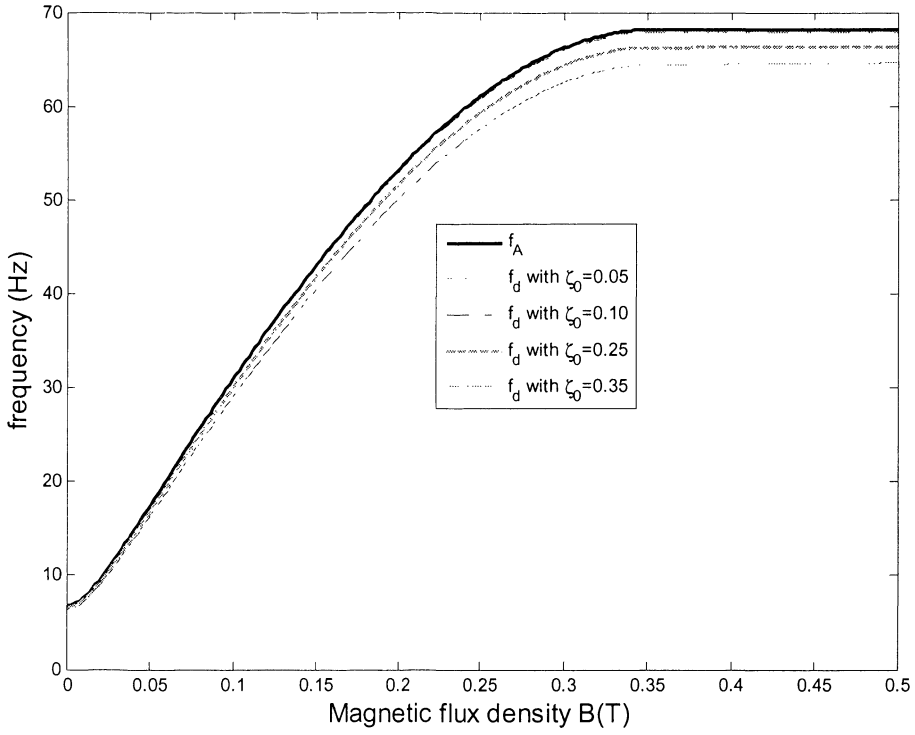

Figure 6.4. ATVA natural and damped frequencies with four damping ratios (μ_A=0.2)

It can be seen that the ATVA frequency range covers all powertrain natural frequencies, as shown in Table 6.1.

6.5.2 Application of dual ATVA for dealing with a single resonance of powertrain

According to Citron and O'Higgins [92], the dynamic engine torque can be expressed in terms of Fourier series, as below

$$T(t) = T_m + \sum_{i=1}^{N} T_i \sin(i\Omega t + \varphi_i) \tag{6.7}$$

In which N is the number of harmonics. T_i and φ_i (i=1..N) are amplitude and phase angle of i^{th} harmonic. Ω is the fundamental frequency and it depends on the number of cylinders of the engine and the engine speed. In this study, it is supposed that Ω is the same as that of engine speed. That means there are two cylinders in this engine. Here, only the vibration problem is considered and the mean torque T_m is neglected.

In this chapter, it is assumed that the resonance can occur in two cases: one resonance and two resonances at the same time will be discussed in section 6.5.3.

If only the first harmonic is considered, from equation (6.7), the excitation fluctuation torque can be re-written as below:

$$T = T_1 \sin(\Omega t + \varphi_1) \tag{6.8}$$

If the speed of the engine is 660rpm, this gives $\Omega = 2\pi \times 11$ (rad/s), and it is assumed that at engine idle speed, the first gear of the gearbox is operated. As a result, the resonance occurs to the second frequency of the first gear of the powertrain f_2=11.0494Hz as shown and noted in Table 6.1. If the target frequencies of each of the dual ATVA f_d=11 Hz are tuned, with zero-field damping ratio ς_0=0.1 and inertia ratio μ_A=1/5, by solving equation (5.9) in Chapter 5, the magnetic flux density B=0.0293(T) is obtained. After that, from equations (5.4) and (5.11) ATVA stiffness and damping coefficients, k_A and c_A, are computed. Then, the stiffness and damping matrix can be re-calculated by equations (6.2) and (6.3).

Let T_1=5Nm, φ_1=0. By solving the equation of the motion of the powertrain with the dual ATVA, the powertrain vibration frequency responses are shown in Figure 6.5.

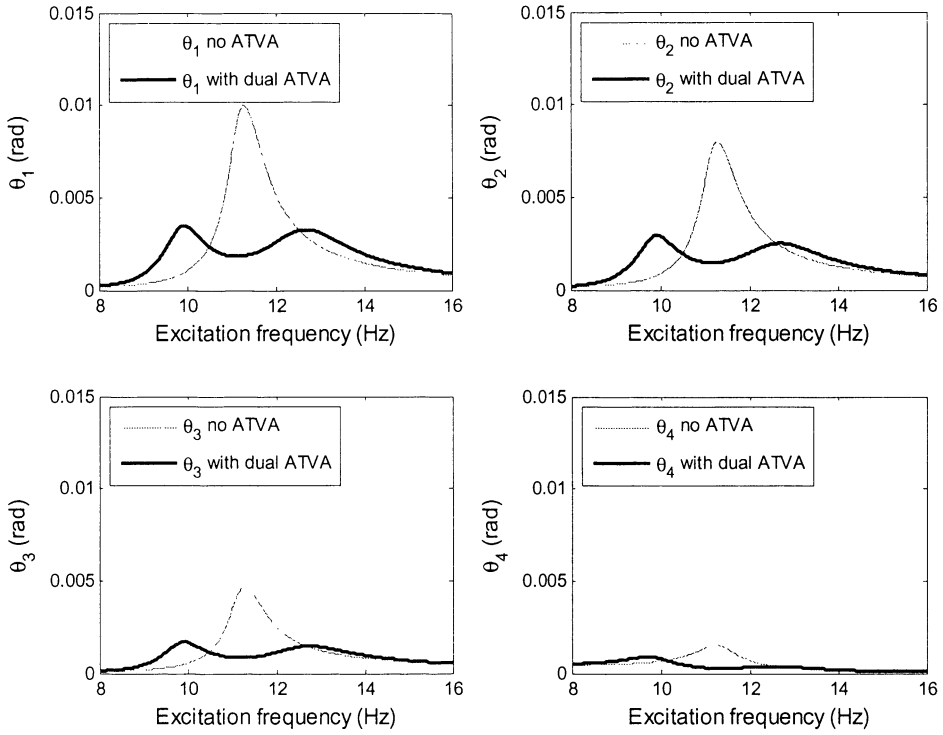

Figure 6.5. Powertrain vibration before and after adding dual ATVA

The vibration of the four inertias, $\theta_1, \theta_2, \theta_3$ and θ_4 is reduced significantly after adding ATVA.

It can be seen that powertrain vibration frequency responses, which include four responses $\theta_1, \theta_2, \theta_3$ and θ_4, are reduced significantly at and around the resonant frequency f_2=11Hz. For each of them, the resonant peak has been shifted to two new locations, as in Figure 6.5. In other words, the dual ATVA has worked effectively as the powertrain natural frequencies are shifted away from the resonant frequency. As a result, the powertrain's steady responses are reduced significantly. In addition, responses at two invariant peaks, which are introduced after adding the dual ATVA, as shown in Figure 6.5, are small as well.

It is noted that the dual ATVA parameters such as inertia ratio, stiffness and damping coefficients can be varied to choose optimal values. ATVA parameters are optimal if the powertrain vibration response at resonant peak is small. Responses at the two invariant peaks are also small. The effect of the dual ATVA parameters (inertia, damping and stiffness) on its effectiveness will be discussed in following sections.

To show how the dual ATVA damped frequency f_d (ATVA stiffness as well) affects to its effectiveness, its several values such as f_d=10.5, 10.7, 11 and 11.5 Hz are varied to compare. With these values, the vibration frequency responses of the second inertia, θ_2, are compared in Figure 6.6.

It is noted that the ATVA frequency value f_d is considered as the optimal value if at the resonant frequency the powertrain response is small. Also, at the two invariant peaks, as shown in Figure 6.6, the frequency responses are small. It can be seen that the optimal frequency value of f_d is between 10.7 and 11Hz in this case.

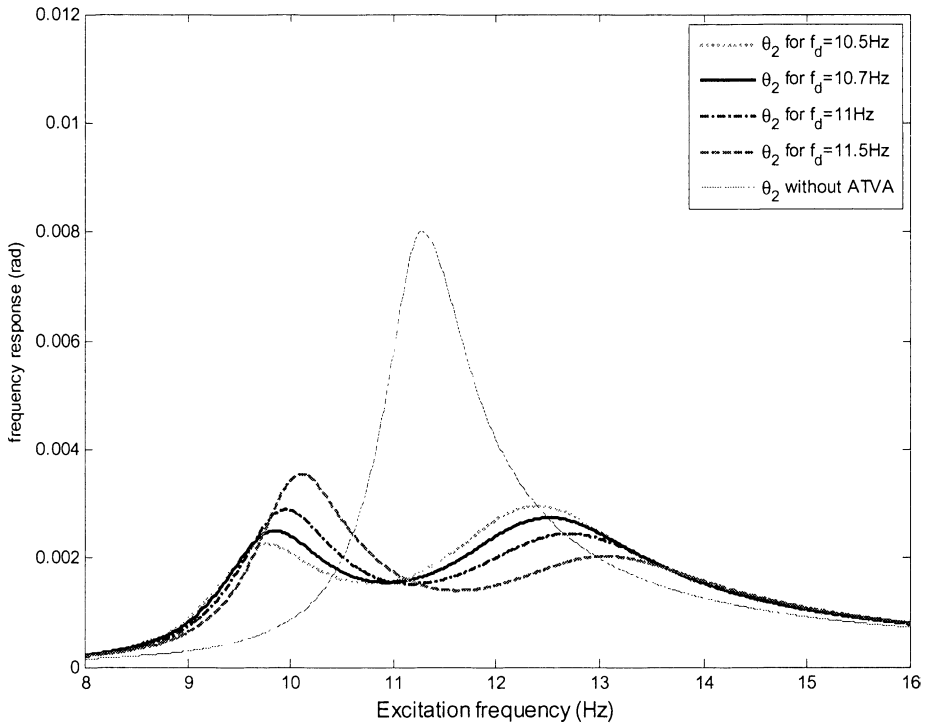

Figure 6.6. Vibration of second inertia θ_2 with several dual ATVA frequencies

Similarly, to show how the inertial moment J_A and the damping affect the dual ATVA's effectiveness, several values of inertial moment J_A and zero-field damping ratios are chosen and the steady state vibration responses of the powertrain are calculated and compared. For example, Figure 6.7 shows the responses of the second inertia θ_2 of the powertrain with four values of the inertia ratios μ_A=1/4, 1/5, 1/10, 1/20, respectively.

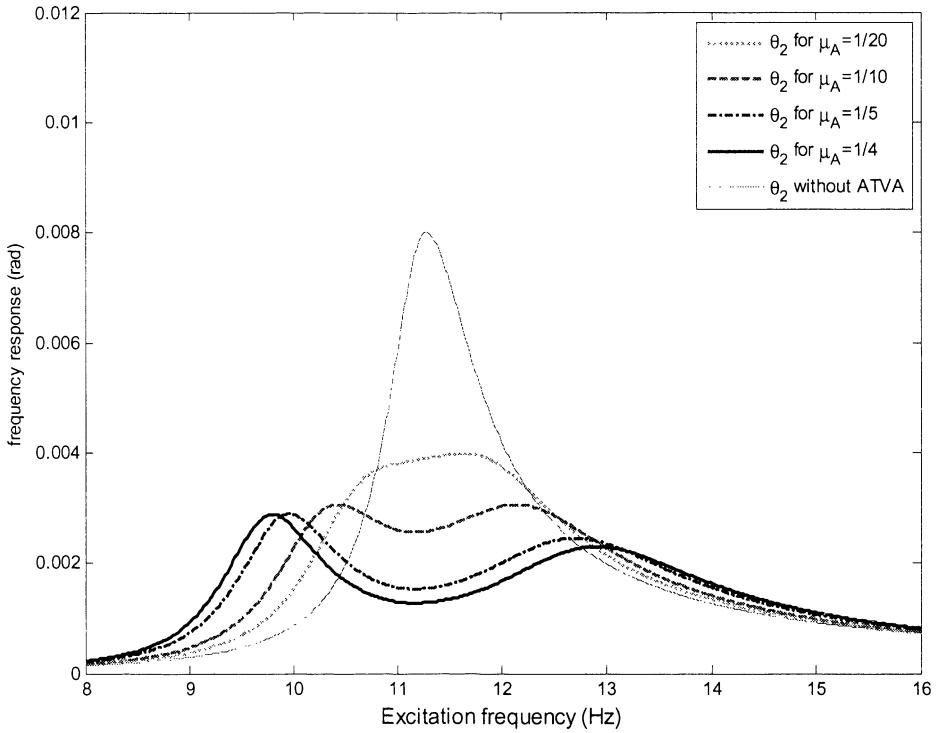

Figure 6.7. Vibration of second inertia θ_2 with several values of inertia ratio μ_A

It can be seen that the larger inertia ratio is, the better vibration reduction effect of the ATVA can be. For large inertia ratios μ_A=1/4, μ_A=1/5 the resonant peak is shifted far away by introducing two new invariant peaks. In contrast, for low inertia ratios μ_A=1/10 or 1/20, two new invariant frequencies have not been shifted significantly from the resonant frequency. In other words, if the inertia ratio is too small, the dual ATVA is not effective.

Figure 6.8 shows the effect of damping on the ATVA's effectiveness. It can be seen that the lower the damping ratio is, the smaller the response at the resonant frequency can be. However, a small damping ratio may result in high responses at the two invariant frequencies. For instance, for ς_0=0.05 the response of the second inertia θ_2 after adding the ATVA is the smallest at the resonant frequency, but at two invariant peaks the response is higher than those when ς_0=0.1. It can be seen that the damping ς_0=0.1 seems to be the optimal value compared to other values, as seen in Figure 6.8.

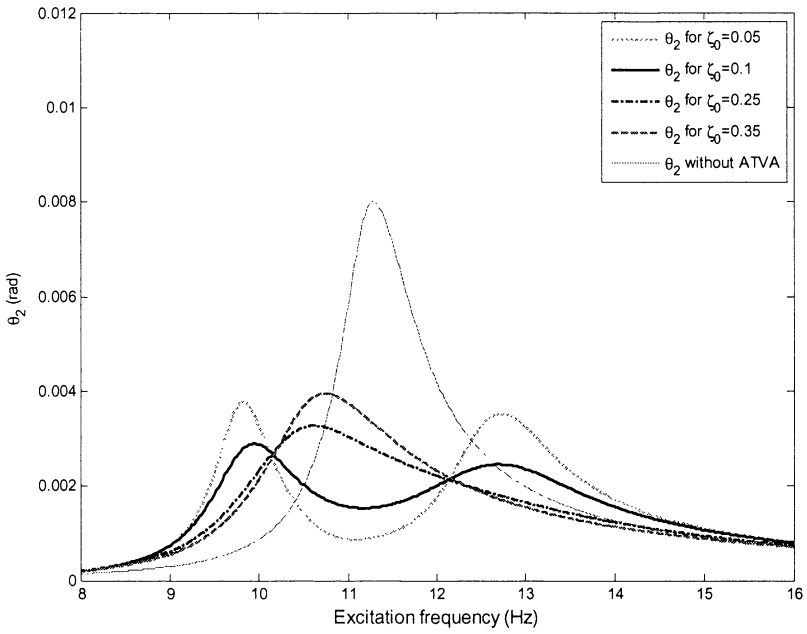

Figure 6.8 Vibration of second inertia θ_2 with four values damping ratio

If the excitation frequency $\Omega = 2\pi \times 32.5$(rad/s) (the engine speed is 1950rpm) and the second gear of the gearbox is used. As a result, the resonance happens to the third frequency of the second gear f_3=32.6012Hz as noted in Table 6.1. If each single ATVA frequency f_d=30 Hz is tuned; let ς_0=0.25, μ_A=1/4, T_1=50Nm, φ_1=0, the frequency response of the second inertia before and after adding ATVA is shown in Figure 6.9.

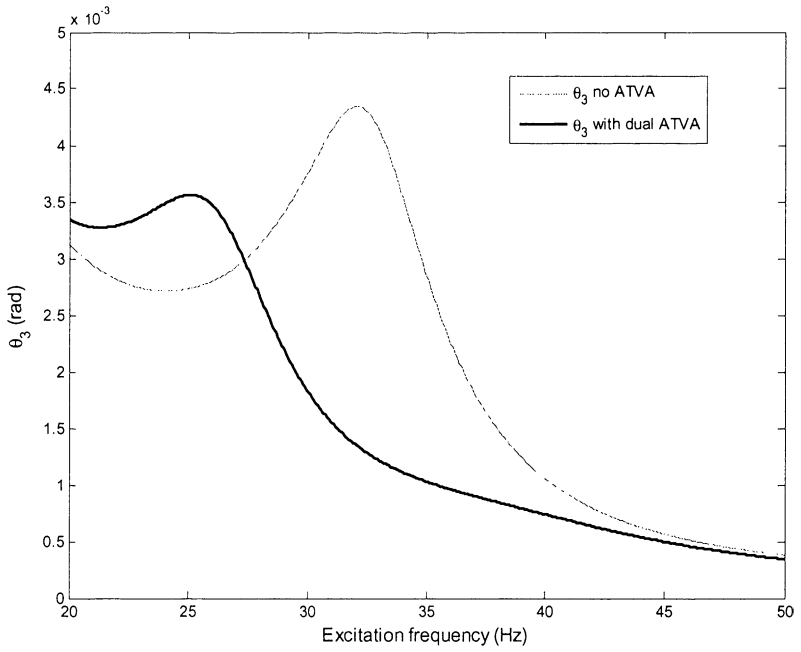

Figure 6.9. The effectiveness of dual ATVA for resonance at frequency f_3=32.6012Hz

Similarly, the ATVA can deal with the resonance happening to the fourth frequency f_4=65.0439Hz of the second gear, as noted in Table 6.1, when $\Omega = 2\pi \times 65$ rad (at which engine speed is 3900rpm).

Clearly, with the dual ATVA, the resonances occurring in all three modes of powertrain as shown in Table 6.1 have been dealt with. This can not be done if a single ATVA is used. In particular, the dual ATVA is more effective for the case in which there are two or more than two resonances occurring at the same time. The application for dealing with the two resonances at the same time will be discussed in the following sections.

6.5.3 Application of dual ATVA for dealing with two resonances of powertrain

If $\Omega = 2\pi \times 11$(rad/s) and the first and third harmonics of engine torque are dominant, the second harmonics can be neglected and the engine fluctuation torque can be re-written as:

$$T = T_1 \sin(\Omega t + \varphi_1) + T_3 \sin(3\Omega t + \varphi_3) \tag{6.9}$$

With the powertrain modal frequency of the first gear as shown and noted in Table 6.1, there are two resonances at the same time, in this case f_2=11.0494 and f_3=31.9372Hz. To do this, frequencies of ATVA 1 and ATVA 2 will be tuned at f_{d1}=32Hz (to deal with the resonance of the third mode) and f_{A2}=11Hz (to deal with the resonance of the second mode). It is noted that these mode shapes were shown in Figure 6.1.

To numerically validate the ATVA's effectiveness for dealing with the two resonances at the same time, parameters φ_1=0, $\varphi_3 = \pi/2$ and ς_0=0.25 are chosen, T_1=5Nm, T_3=35Nm are set. As a result, the steady state vibration response of powertrain is calculated.

Figure 6.10 shows the vibrations of the second and third inertias, θ_2 and θ_3 before and after adding the dual ATVA. It can be seen that the vibration has been reduced significantly after adding the dual MRE-based ATVA. This confirms that the dual ATVA works effectively.

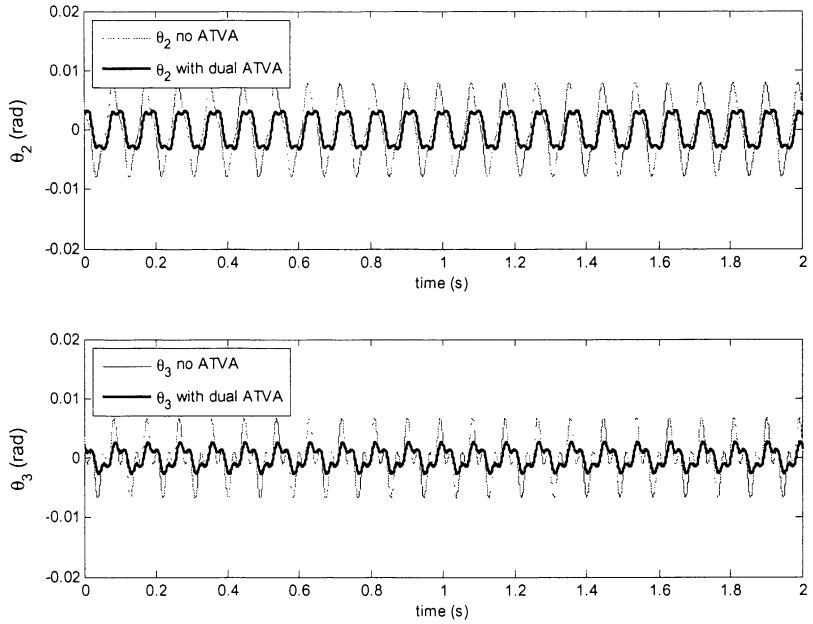

Figure 6.10. The effectiveness of dual ATVA at two resonances ($\Omega = 2\pi \times 11$ rad)

To show the effect of the location of each ATVA, the time response θ_3 is shown in Figure 6.11 for three cases: before adding the ATVA; after adding the ATVA as shown in Figure 6.2; and after adding the dual ATVA with the locations of the two single ATVAs are reversed.

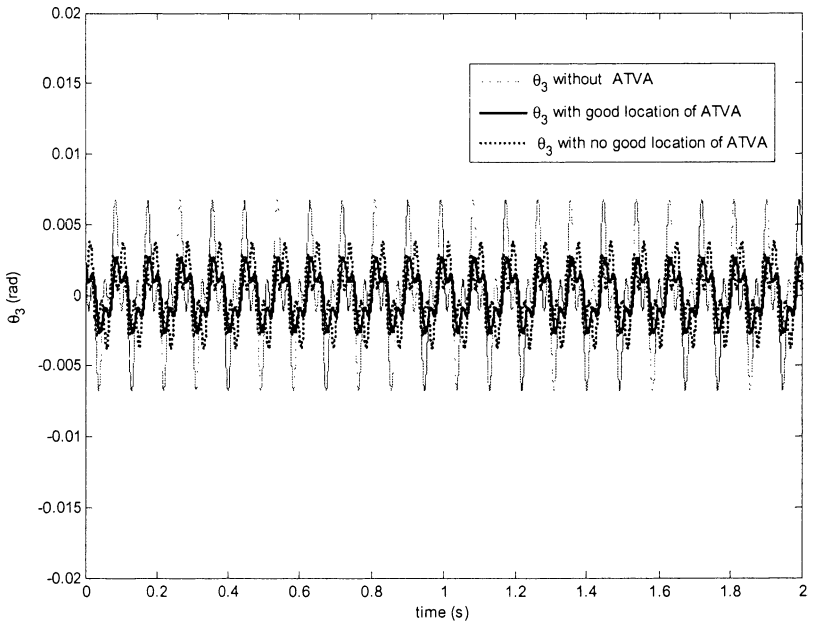

Figure 6.11. Effect of the dual ATVA location on its effectiveness

It can be seen that after the locations of the single ATVAs are swapped, the dual ATVA's effectiveness is changed significantly. Once more, it can be seen that the location of the dual ATVA is sensitive to its effectiveness.

Similarly, if $\Omega = 2\pi \times 32.5$(rad/s) (the engine speed is 1950rpm). In this case it is assumed that the first and second harmonics are dominant, the third harmonics can be neglected and the engine fluctuation torque is re-written as:

$$T = T_1 \sin(\Omega t + \varphi_1) + T_2 \sin(2\Omega t + \varphi_2) \tag{6.10}$$

At this engine speed, the second gear of the gearbox is used. This can be seen from Table 6.1 with f_3=32.6012Hz and f_4=65.0439Hz. Once again, there are two resonances occurring at the same time. To compensate for this, the frequencies of ATVA 1 and ATVA 2 will be tuned as f_{d1}=32Hz (to eliminate the third mode) and f_{A2}=65Hz (to eliminate the fourth mode). Let phase angles φ_1=0, $\varphi_2 = \pi/2$; zero-field damping ratio ς_0=0.35 is chosen. T_1=5Nm, T_2=35Nm are set. The response of the powertrain is shown in Figure 6.12.

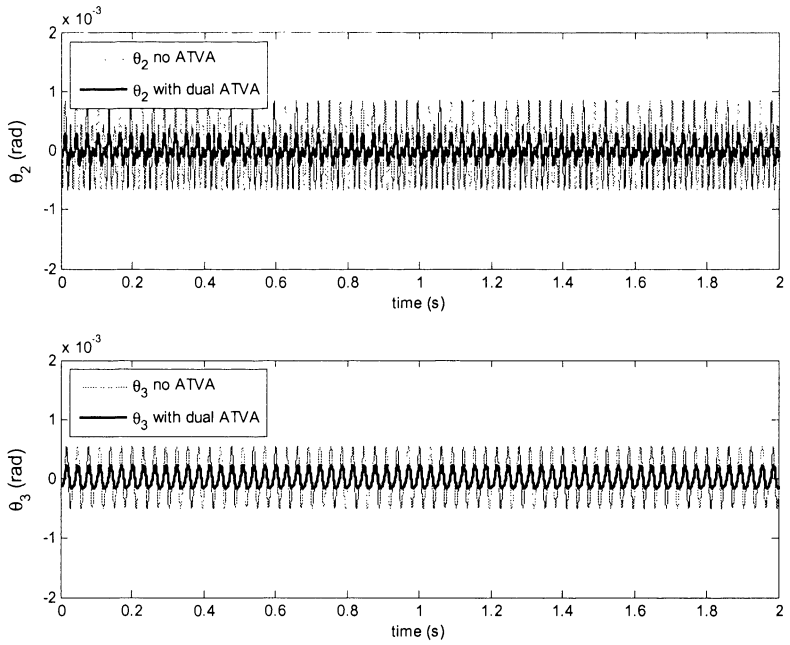

Figure 6.12. The effectiveness of dual ATVA at two resonances ($\Omega = 2\pi \times 32.5$ rad)

Obviously, the dual ATVA works effectively because the vibration responses have been reduced significantly. It is noted that both resonances cannot be attenuated if a single ATVA is used.

6.6 Discussion

In this chapter, three resonances, which occur for three vibration modes of a powertrain, can be dealt with by using the dual ATVA. By tuning the frequency of the dual ATVA, powertrain resonant frequencies are shifted away from the excitation frequencies, thus, steady state vibration response of the powertrain is significantly suppressed. It was found that the dual ATVA can deal with not only single resonance but also two resonances of powertrain at the same time. These resonances can not be dealt with if a single ATVA is used.

In addition, a model of MRE shear modulus has been proposed in this chapter, in which the shear modulus is derived as a function of magnetic flux density B. The proposed model is in good agreement with the experimental data. With the proposed model, the ATVA frequency can be tuned effectively.

6.6.1 Limitations

Similar to Chapter 5, the set of powertrain parameters do not belong to a real powertrain system. The powertrain parameters were only chosen to ensure that powertrain system has natural frequencies which are (or are close to) multiples of the fundamental excitation frequency of the powertrain. Also, is also assumed that the powertrain's multiple resonances occur at the same time. This would be useful if an actual model of a real powertrain is used to investigate the dual MRE-based ATVA's effectiveness.

6.7 Summary

A dual dynamic absorber using a soft MRE is presented in this chapter for powertrain vibration reduction. With the dual MRE-based ATVA, the vibrations of powertrain resonances for all vibration modes were reduced significantly. To facilitate the ATVA design, an effective formula for shear modulus of the soft MRE was proposed. The proposed model is in a good agreement with the experimental data and it is used effectively for tuning ATVA parameters according to the engine speed.

The influence of dual ATVA parameters such as inertia moment, stiffness and damping coefficients was also examined. Furthermore, based on powertrain vibration mode shapes, the best location option of dual ATVA was proposed. Thus, resonances happening for all powertrain vibration modes can be dealt with.

Chapter 7 ATVA FOR POWERTRAIN TRANSIENT VIBRATION REDUCTION

7.1 Introduction

This chapter presents the ATVA's effectiveness for powertrain vibration reduction during the transient state. In the chapter, the excitation frequency of the fluctuation torque varies with time instead of being constant, as in the steady state. Following the background, a powertrain model is presented in which the torque model is proposed. This is followed by the application of the ATVA, which uses a new MRE material for reduction of powertrain transient vibration. The MRE used to develop the ATVA has a significant increase in shear modulus and a small loss factor (or damping as well). After that, according to the excitation frequency, a method of turning ATVA frequency is presented for conducting numerical simulations to examine the ATVA's effectiveness. Finally, the effect of ATVA parameter modification is investigated to find optimal values.

7.2 Background

Transient vibration of a powertrain is an important consideration and it is necessary to minimise this vibration. One of the most frequent transient vibrations, which can be seen while vehicles are travelling, occurs when the vehicle engine speed accelerates from 600-900 rpm (idle speeds) to 5000-6000 rpm (top working speeds). During the acceleration, the engine speed will pass through one or several powertrain frequencies so that powertrain vibrations will be significantly increased. This phenomenon seems to

have been inevitable so far and methods to deal with it have not been fully addressed.

Walsh and Lamancusa [45] developed an ATVA, which has variable stiffness, by introducing a compound leaf spring for minimizing the transient vibration for a single degree of freedom (SDOF) application with time-varying excitation frequency. By using the compound leaf spring, the ATVA increase in relative stiffness is up to 45 times. However, there were two main shortcomings in this study. Firstly, the frequencies of the combined system, which includes both the primary system and the ATVA, were not examined to show how the frequency of the primary system had been shifted to make sure whether or not the resonance had been dealt with. Secondly, the ATVA was used for a SDOF application only and it may not be applied for powertrains, which are MDOF systems.

The objective of this chapter is to use a new MR elastomer of the third generation of MRE material to develop an ATVA for powertrain transient vibration in the acceleration of vehicles. This new MR elastomer has two advantages compared to other MREs. Firstly, it has a significant increase in stiffness but the damping is small. Secondly, the magnetic field needed to reach the MRE maximum stiffness is only 0.3T. These advantages are essential for developing MRE-based ATVAs to solve engineering problems in practice.

7.3 Powertrain torsional vibration model for transient state

As mentioned in Chapter 5, the powertrain has a number of gear ratios. For each gear ratio the gearbox has a different stiffness coefficient and this is characterized by a varying stiffness coefficient k_2. In this chapter, it is assumed that during engine speed acceleration the second gear of the gearbox is used. To investigate the effectiveness of the MRE-based ATVA for the powertrain transient state, the powertrain vibration parameters are chosen. Firstly, J_1=0.82, J_2=0.22, J_3=0.6, J_4=60kgm^2, which are realistic values, are set for the inertia of engine, clutch and driveline, respectively. Then, damping and stiffness coefficients c_1=8, c_2=2, c_3=10Nms/rad; k_1=14000, k_2=15000, k_3=10350Nm/rad were assumed to make sure that the powertrain frequencies are close

to those of a real vehicle powertrain system. With these parameters, powertrain natural frequencies and damping ratios ζ are shown in Table 7.1.

Table 7.1. Natural frequencies of a simplified powertrain model

index	damped frequency (rad)	damping ratio ζ (%)
ω_1 [a]	0[a]	-
ω_2	$2\pi \times 10.2138$	2.24
ω_3	$2\pi \times 28.5814$ [b]	5.75
ω_4	$2\pi \times 62.4686$	6.59

[a] ω_1 is zero due to the rigid body rotation of whole system

[b] used to validate the ATVA's effectiveness in this chapter.

The vibration mode shapes are shown in Figure 7.1.

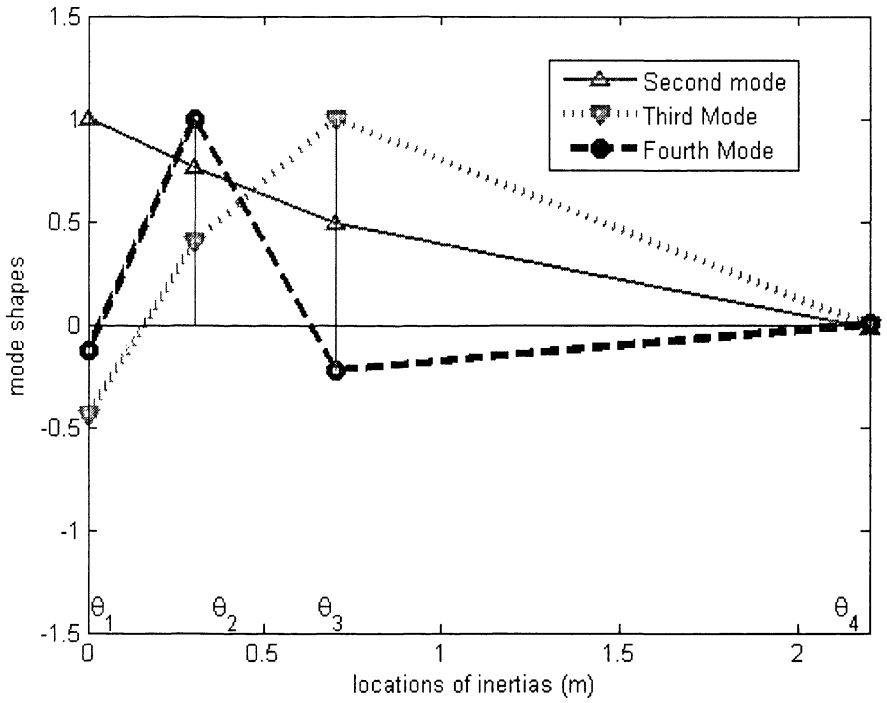

Figure 7.1. Powertrain vibration mode shapes

7.3.1 *Transient excitation torque model*

Wang et al [84], proposed an input torque model for powertrain systems. According to these authors, the engine torque consists of a constant mean and a harmonic fluctuation torque. Similar to Chapter 5, in this chapter the mean torque is ignored and the excitation frequency of fluctuation torque is assumed as a constant. During the transient

state the excitation frequency varies with the time, the excitation of the fluctuation torque could be modelled by Brennan [93] as follows:

$$\begin{cases} T(t) = T_0 \sin(\Omega_1 t) & t \le T_1 \\ T(t) = T_0 \sin[a(t-T_1)^2 + b(t-T_1)] & T_1 < t < T_2 \\ T(t) = T_0 \sin(\Omega_2 t) & t \ge T_2 \end{cases} \tag{7.1}$$

Here $a = \dfrac{\Omega_2 - \Omega_1}{2(T_2 - T_1)}$, $b = \Omega_1$.

In this study, the transient state starts at T_1=2s and finishes at T_2=6s; with $\Omega_1 = 2\pi \times 20$ rad/s (engine speed is 1200rpm), $\Omega_2 = 2\pi \times 40$ rad/s (engine speed is 2400rpm) and T_0 =20Nm was set.

During the transient state [T_1 T_2], the conversion between arbitrary time t^* and time-dependent excitation frequency Ω^* can be expressed as follows; see White and Pinnington [94] for more detail:

$$\Omega^* = 2a(t^* - T_1) + b\,,\ t^* = \frac{\Omega^* - b}{2a} + T_1 \tag{7.2}$$

The excitation frequency during the transient state in this study is shown in Figure.7.2.

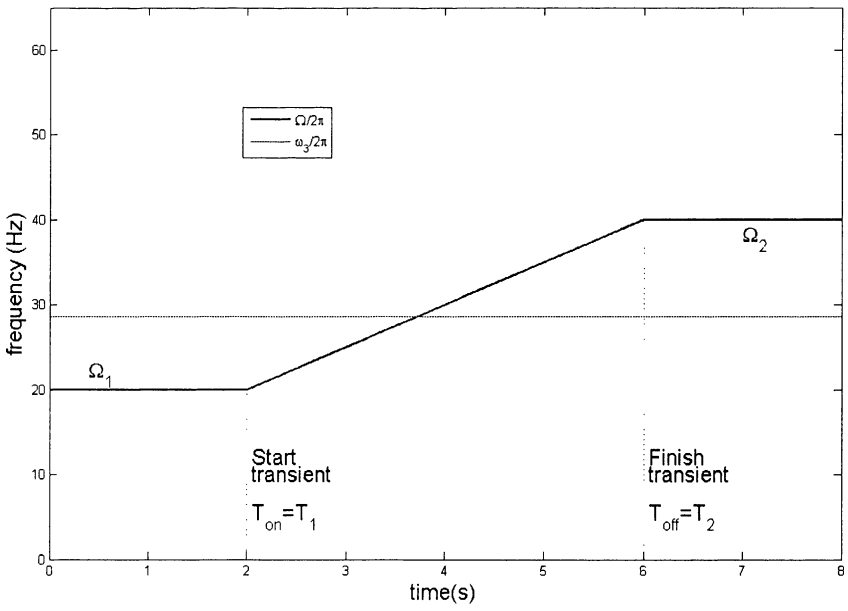

Figure 7.2. Transient excitation frequency Ω

It can be seen in Figure 7.2 that when the excitation frequency Ω increases from

$2\pi\times20$ to $2\pi\times40$Hz it will pass through the third natural frequency of powertrain $\omega_3=2\pi\times28.5814$ as shown and noted in Table 1. Thus, the resonance occurs and powertrain vibration will be increased significantly.

For the transient torque model as shown in equation (7.1) the equation of motion of the powertrain, which was derived in equation (5.1), Chapter 5, must be solved by integration methods. In this chapter, the *ode45 solver* based on Runge-Kutta formula in Matlab software version 7.5 (R2007b) is used to obtain powertrain transient responses (see Appendix A7 for more detail).

7.4 ATVA for powertrain transient vibration control

7.4.1 A new magnetorheological elastomer and its proposed viscoelastic model

Chertovich et al [71] developed two MRE samples, the soft and the hard MRE, as reported in Chapter 3 (section 3.4), and the hard sample will be used in this chapter. The hard MRE sample is used for developing the MRE-based ATVA rather than the soft one for two main reasons. Firstly, the hard MRE can provide more stiffness than the other. Secondly, the damping of the hard MRE sample is smaller than that of the soft MRE sample as shown in Figure 3.10 in Chapter 3. In this chapter, the hard MRE is subsequently called as the new MRE.

The new MRE viscoelatic property was characterised by the complex shear modulus as follows:

$$G=G^{'}+iG^{''}=G^{'}(1+\eta i) \tag{7.3}$$

In which $G^{'}$ and $G^{''}$ are the storage modulus and loss modulus. These moduli represent the ability of MRE for stiffness and internal damping respectively, η is the loss factor of MRE and is calculated by:

$$\eta=\frac{G^{''}}{G^{'}} \tag{7.4}$$

The storage modulus, loss modulus and the loss factor of the MRE under a magnetic

field 0.3T were measured by the dynamic test method and shown in Figure 7.3 a, b.

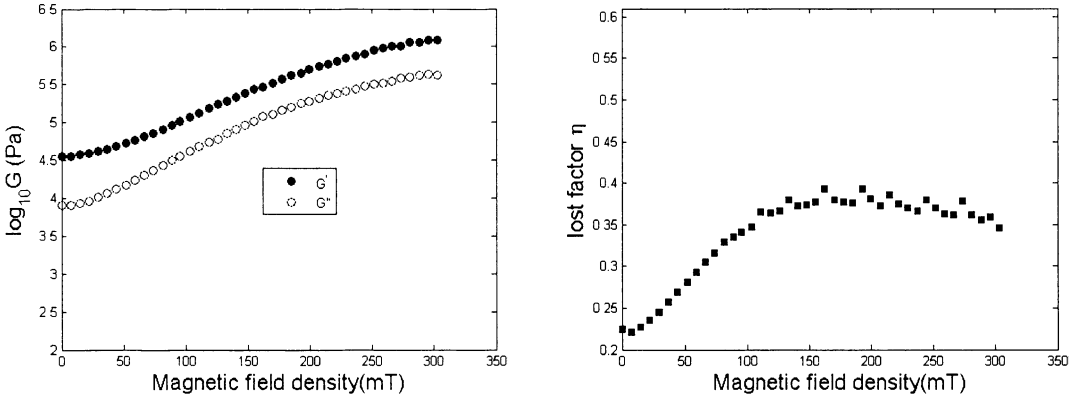

a) Storage and loss moduli b) Loss factor

Figure 7.3. MRE storage and loss shear modulus by Chertovich et al [71]

Obviously, the increase in the moduli is significant and the loss factor is small. Thus, this new MRE is suggested for developing a new generation of MRE-based ATVAs. For more detail see Chertovich et al [71].

Similar to Chapter 6, for the new MRE in this study the storage shear modulus G' can be expressed as a cubic function of magnetic field density as in the following form:

$$G' = G'(B) = \begin{cases} G'_0 & B \le 0 \\ G'_0 + (G'_{\max} - G'_0)\dfrac{B^2}{B_{\max}^2}(3 - 2\dfrac{B}{B_{\max}}) & 0 < B < B_{\max} \\ G'_{\max} & B \ge B_{\max} \end{cases} \tag{7.5}$$

According to Chertovich et al, [71], it was reported that the loss factor increases from η_0=0.22 to maximum $\eta_{\max}$=0.38 at critical value B_C=0.15T and then it slows slightly to η_{end}=0.34 at $B_{\max}$ =0.3T. Thus, the loss factor η is approximated as:

$$\eta = \eta(B) = \begin{cases} q(B) = \sum_0^3 q_j B^j & 0 \le B < B_C \\ p(B) = \sum_0^2 p_k B^k & B_C \le B \le B_{\max} \end{cases} \tag{7.6}$$

By using conditions which are similar to those that were applied for the proposed model

of storage modulus $G^{'}$, coefficients q_j and p_k in equation (7.6) can be determined. As a result, the loss factor η can be expressed:

$$\eta = \begin{cases} 0.22 + 21.3333B^2 - 94.8148B^3 & 0 \le B < B_C \\ 0.34 + 0.5333\mathrm{B} - 1.7778\mathrm{B}^2 & B_C \le B \le B_{\max} \end{cases} \tag{7.7}$$

The validation of the proposed models for storage modulus, the loss modulus and loss factor are shown in Figure 7.4 a) and b) Here, the loss modulus can be calculated as $G^{"} = \eta G^{'}$.

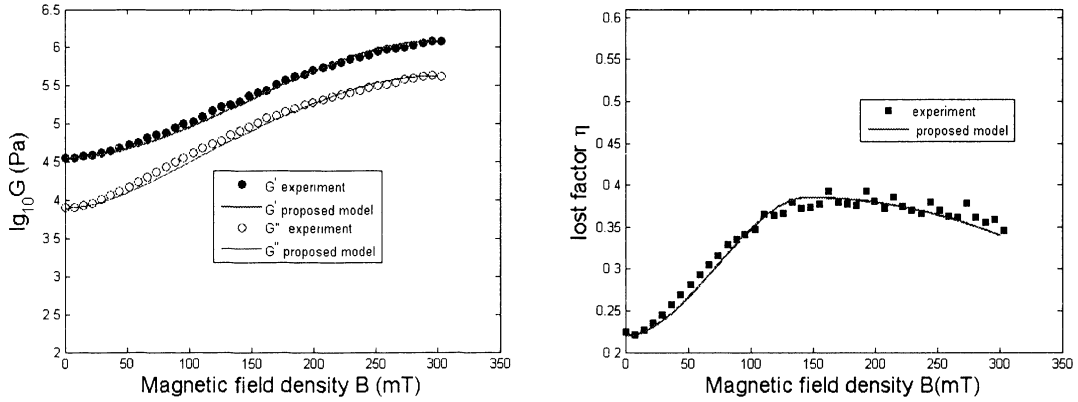

a) Storage and loss moduli b) Loss factor

Figure 7.4. Proposed models of storage and loss modulus of new MRE

It can be seen from Figure 7.4 that the proposed models as in equations (7.5) and (7.6) are in good agreement with the experimental results. These models will be used for tuning the ATVA frequency for shifting powertrain frequencies, which will be presented in following sections.

7.4.2 Frequency of the proposed ATVA design

The proposed design of the ATVA can be seen in Figure 5.5 in Chapter 5. With the proposed design, the MRE plays a role as a torsional spring and it is modelled as a rubber cylinder with inner, outer radius and length as a, b and L, respectively.

It is noted that the complex torsional stiffness coefficient $\hat{k}$ of the MRE layer can be calculated as in equation (3.19) in Chapter 3. Alternatively, for the ATVA, a SDOF

mechanical vibration system, three regular parameters (k_A, c_A and J_A) are used. In which the stiffness coefficients k_A is expressed as:

$$k_A = \text{Real}(\hat{k}) = \frac{4\pi L a^2 b^2 G'}{b^2 - a^2} \tag{7.8}$$

and damping coefficient c_A can be calculated as:

$$c_A = 2\omega_A J_A \varsigma_A = 4\pi f_n J_A \varsigma_A \tag{7.9}$$

Here ς_A is the damping ratio and it is determined from the relationship with the loss factor, as reported by Kaliko [4] (section 10.1) as:

$$\varsigma_A = \frac{\eta}{2} \tag{7.10}$$

It is similar to Chapter 5 and Chapter 6: the mass ratio μ_A can be varied to investigate the ATVA's effecivness. For example, let μ_A= J_A / J_3 =1/5 then J_A=0.12kgm^2 is calculated.

The ATVA main parameters and MRE properties are chosen and summarised in Table 7.2.

Table 7.2. ATVA and MRE parameters

ATVA parameter	MRE
a=0.085m	G_0=36kPa
b=0.1m	G_{max}=1222kPa
L=0.035m	B_{max}=0.3T, B_C=0.15T
(μ_A= 1/12, 1/5, 1/4)	η_0=0.22, η_{max}=0.38, η_{end}=0.34

With the ATVA parameters as shown in Table 7.2, the ATVA stiffness and damping coefficients will be calculated from equations (7.8) and (7.9). It is noted that the storage modulus G' in equation (7.8) is calculated from equation (7.5) and the damping ratio ς_A is calculated from equation (7.10) with loss factor η is proposed in equation (7.7). As a results, with inertia ratio μ_A=1/5, ATVA natural frequency f_n and damped frequency f_d are calculated as in equation (5.8) and equation (5.9) in Chapter 5, as shown in Figure 7.5.

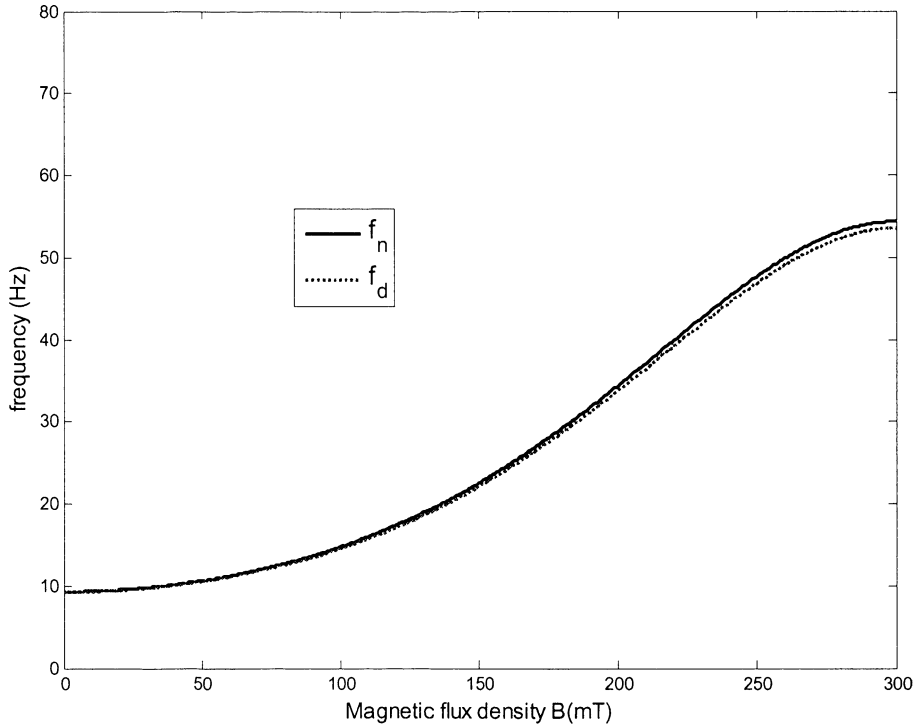

Figure 7.5. ATVA natural and damped frequencies

7.4.3 Application of the ATVA for powertrain vibration reduction

As discussed in section 7.3.1, because the excitation frequency varies from 20 to 40Hz, the ATVA frequency, which was shown in Figure 7.5, covers the frequency range of [20 40]Hz so that the ATVA frequency required for the transient state can be tuned.

To deal with the resonance occurring in the third frequency $\omega_3 = 2\pi \times 28.5814$ as shown in Table 7.1, from the vibration mode shapes as in Figure 7.2, the ATVA location is chosen as shown in Figure 7.6.

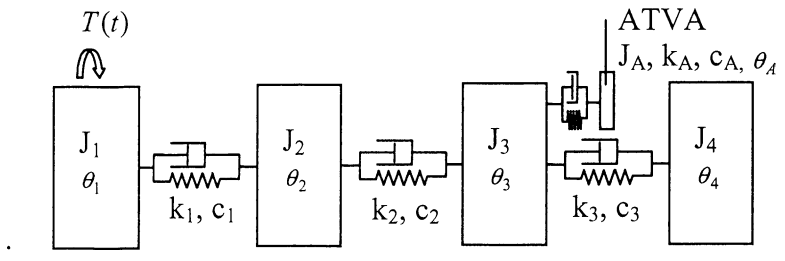

Figure 7.6. A powertrain model with an ATVA

It is noted that there is a difference between Figure 7.6 and Figure 5.8 in Chapter 5. In Figure 7.6, the excitation torque $T(t)$ is not a harmonics and it is determined by equation (7.1) instead.

It is also noted that with the location of ATVA in the powertrain as in shown Figure 7.6, the equation of motion of the powertrain is the same form as equation (5.1) and the inertia, stiffness and damping matrices will be calculated from equations (5.13), (5.14) and (5.15) in Chapter 5. However, the transient response of the powertrain in this transient state has to be solved by numerical methods.

7.5 Tuning ATVA frequency and numerical simulations

7.5.1 Definition of resonance area

According to Wachel and Szenasi [4], the excitation frequency Ω in the steady state should be greater or less than 10 percent of any natural frequency of torsional vibration system ω_n. In other words, Ω and ω_n should satisfy the following condition:

$$\Omega > 1.1\omega_n \text{ or } \Omega < 0.9\omega_n \tag{7.11}$$

Obviously, in most engineering problems ω_n is a fixed value and the excitation frequency Ω will be tuned accordingly. By contrast, in this chapter ω_n will be tuned instead. Thus, equation (7.11) can be rewritten as:

$$\omega_n \leq \Omega/1.1 \text{ or } \omega_n \geq \Omega/0.9 \tag{7.12}$$

Equation (7.12) is also considered as the criteria for ATVA design in this work. When excitation frequency Ω varies with time as in equation (7.1) (also in Figure 7.2), $\Omega/1.1$ and $\Omega/0.9$ will be the lower and upper limit lines, as shown in Figure 7.7. The area, which is limited by the upper and lower limit lines, is the so-called 'resonance area' over the transient state [T_1 T_2]. In other words, the ATVA will be considered to work effectively if powertrain frequencies after adding the ATVA are shifted away from this resonance area, as shown in Figure 7.7.

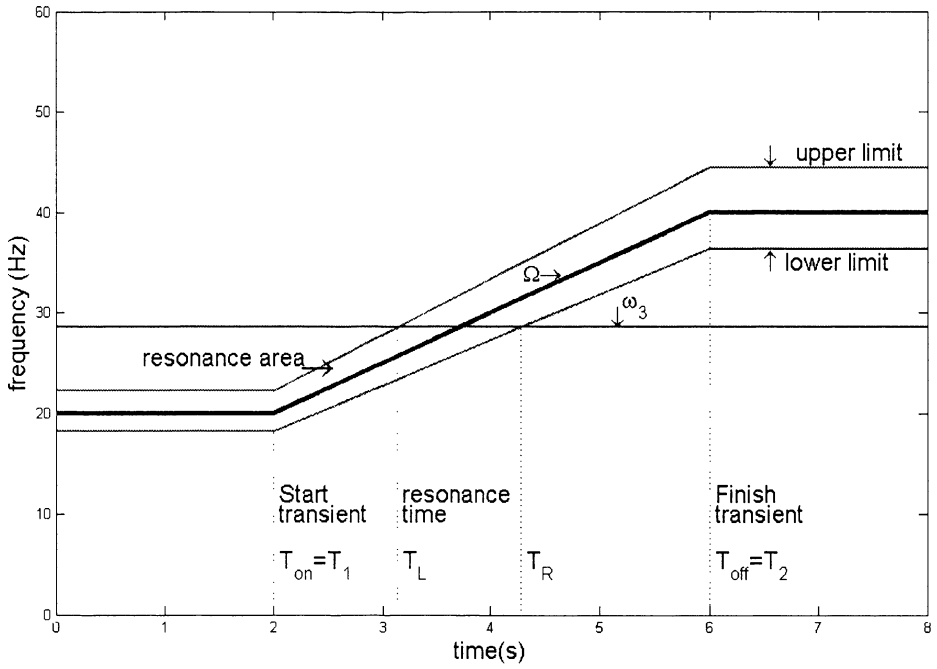

Figure 7.7. Powertrain resonance area

Let T_L and T_R be instant times, at which $\Omega = 0.9\omega_3$ =26.1rad/s and $\Omega = 1.1\omega_3$ =31.9rad/s, respectively, as shown in Figure 7.7. From equation (7.2) T_L=3.2s and T_R =4.3s will be calculated. According to equation (7.12) and as discussed in section 7.5.1, the primary powertrain system (without ATVA) will be in the resonance interval from T_L to T_R =[3.2 4.3s] so that powertrain vibration responses increase significantly. Thus, time range [T_L T_R] is called the 'resonance time', and the ATVA will be used to counteract this resonance.

7.5.2 Tuning ATVA frequency

To deal with the resonance occurring during the transient state, an ATVA damped frequency ω_d is proposed that is similar but not exactly the same as the excitation frequency Ω to make sure that the powertrain frequencies after adding ATVA are always above the upper or under the lower limit values as shown in Figure 7.7.

That means ω_d can be determined from equations (7.1) and (7.2) but the initial and end values are ω_{on} and ω_{off} instead of Ω_1 and Ω_2. Clearly, ω_{on} and ω_{off} are not unique

values. For example, the values can be chosen by adding 5% greater and less than the upper and lower values respectively in equation (7.12) during the design process, as recommended by Wachel and Szenasi [4]. That means $\omega_{on} = \Omega_1 / 1.15 = 2\pi \times 17.4\,(\text{Hz})$ and $\omega_{off} = \Omega_2 / 0.85 = 2\pi \times 47\,(\text{Hz})$ are calculated and the ATVA proposed frequency variation for dealing with the resonance occurring in the transient state is shown in Figure.7.8.

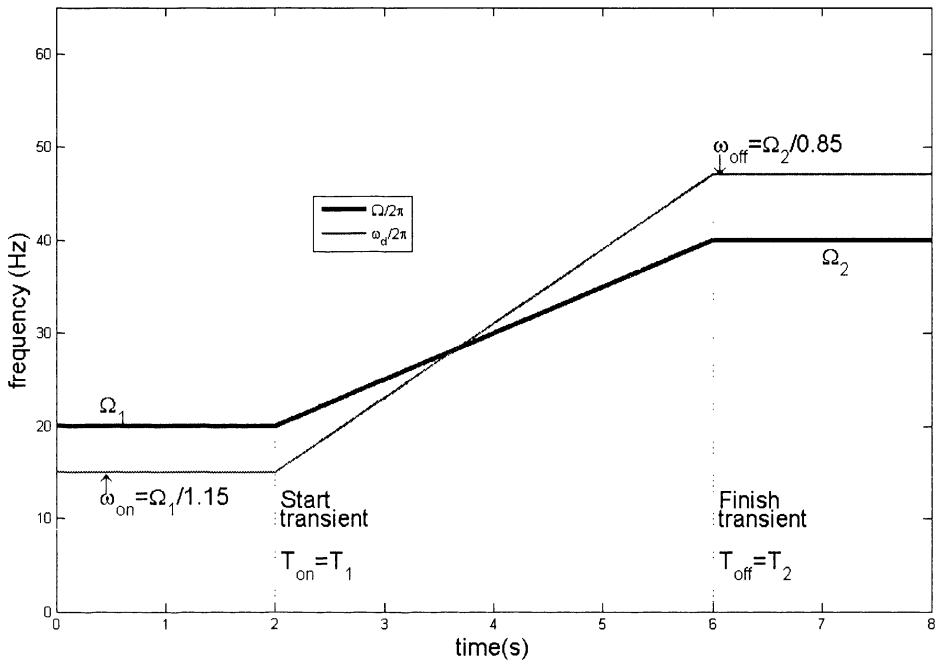

Figure 7.8. Proposed ATVA frequency ω_d and excitation frequency Ω

It is noted that when the ATVA is installed in the powertrain, inertia matrix **J** (as in equation (5.13) in Chapter 5) is fixed but the stiffness and damping matrix **K, C** in equation (5.14) and (5.15) change. Because k_A, c_A are functions of magnetic field density B, the right side of equation (5.9) is a function of magnetic field density B as well. Thus, at an arbitrary time instant t*, if a value of ATVA damped frequency $f_d^* = \omega_d^* / 2\pi$ is tuned, from equation (5.9) the magnetic field density B* can be obtained by solving this nonlinear equation (use *fzero* function in Matlab for example), [95]. Then, storage modulus G'^* and loss factor η^* are calculated by equations (7.5) and (7.7). From equation (7.10), damping ratio ς_A^* is determined. After that, stiffness coefficient k^*_A and damping coefficient c^*_A are calculated by equations (7.8) and (7.9).

Thus, matrices **K**, **C** can be re-calculated so that the vibration features of the powertrain fitted with the MRE-based ATVA can be obtained.

As a result, with the proposed ATVA frequency as shown in Figure 7.8, the magnetic field density B is calculated and shown in Figure 7.9.

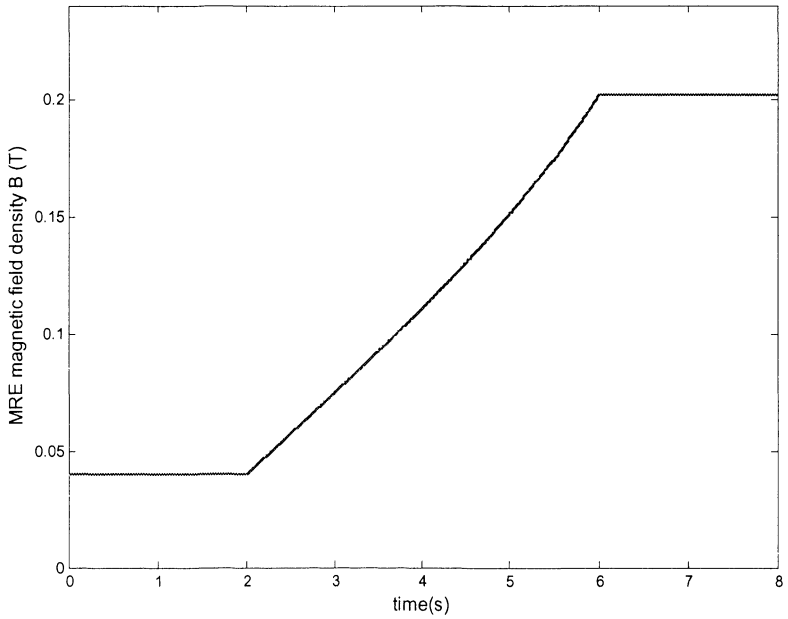

Figure 7.9. Magnetic field density of MRE required during transient state

ATVA stiffness and damping coefficients k_A, c_A, which are calculated by equation (7.8) and (7.9) respectively, are shown in Figures 12 a) and b).

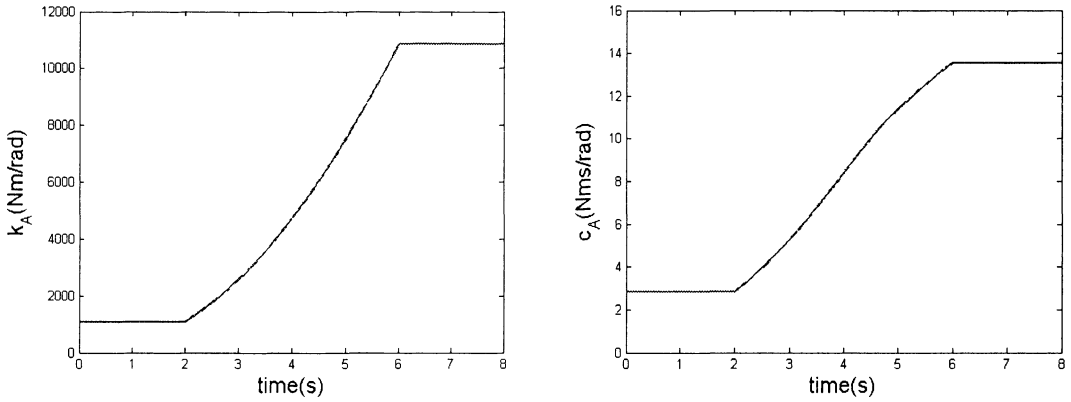

a) stiffness coefficient k_A b) damping coefficient c_A

Figure 7.10. ATVA stiffness and damping coefficients

With the stiffness and damping coefficients k_A, c_A as shown in Figure 7.10, the stiffness

and damping matrix **K, C** as in equation (5.16) and (5.17) are determined. Thus, powertrain frequencies and the transient response after adding the ATVA can be obtained.

For the ATVA stiffness and damping as shown in Figure 7.10, the powertrain frequencies after adding ATVA are shown in Figure 7.11.

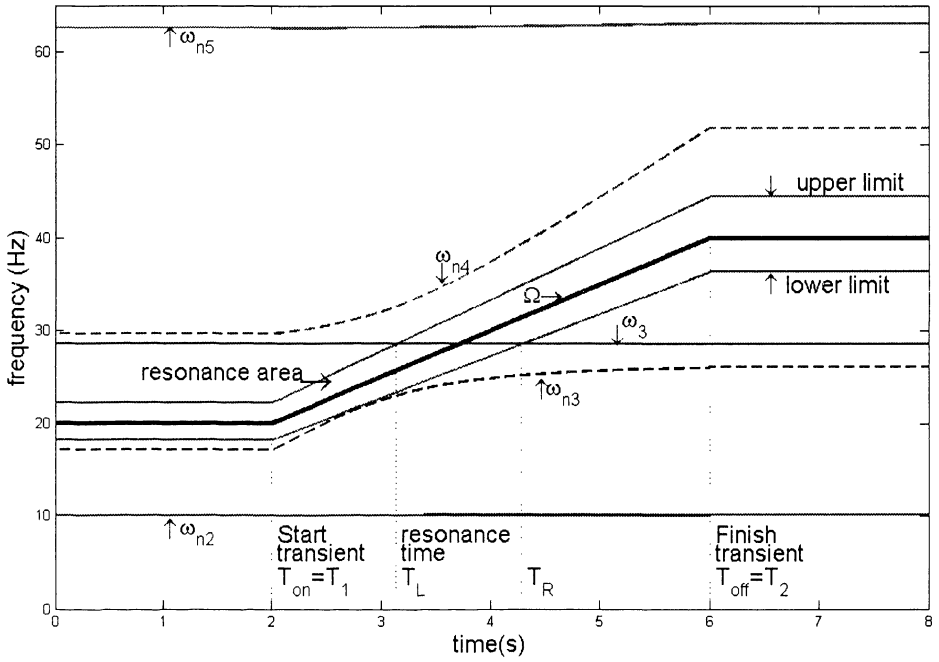

Figure 7.11. Powertrain frequencies after adding ATVA

It should be noted that before adding ATVA the vector of powertrain modal frequency is $\boldsymbol{\omega} = [\omega_2\ \omega_3\ \omega_4\ ]^T$ as shown in Table 7.1. After adding the ATVA, the vector will be $\boldsymbol{\omega} = [\omega_{n2}\ \omega_{n3}\ \omega_{n4}\ \omega_{n5}\ ]^T$ as shown in Figure 7.11. It can be observed in Figure 7.11 that there is no powertrain natural frequency in resonant time [T_L T_R] or in the resonance area over the transient stage [T_1 T_2]. While ω_{n2} and ω_{n5} seem to be constant, ω_{n3} and ω_{n4} look like two hyperbolic curves. It is obvious after adding the ATVA that the frequency ω_3 of the original powertrain system was shifted to ω_{n3} and ω_{n4} which are two new frequencies introduced after adding the ATVA to the powertrain, as shown in Figure 7.11. In other words, the ATVA has worked well because all of the elements of vector $\boldsymbol{\omega} = [\omega_{n2}\ \omega_{n3}\ \omega_{n4}\ \omega_{n5}\ ]^T$ are not in the resonance area.

It is interesting to see that in the time range [0 T_1] before the transient stage as in Figure 7.11, when ATVA frequency ω_d is far away the third frequency $\omega_3 = 2\pi \times 28.5814$, ω_{n3} is almost the same as the initial frequency of ATVA (ω_{on}) and ω_{n4} are close to ω_3. That means that powertrain frequencies were shifted insignificantly during this time and is reason why ω_{on} and ω_{off} should be set under lower and above upper limits, respectively, as shown in Figure 7.8. In this case, if the ATVA frequency is set exactly the same as excitation frequency Ω as suggested by Walsh and Lamancusa [45], ω_{n3} will be in the resonant area during the time [0 T_1] so that the resonance will not be dealt with completely. The time-history of powertrain modal frequency as shown in Figure 7.11 is a good reference for examining the ATVA's effectiveness.

The powertrain transient response such as the relative angular displacement between clutch and engine, and between transmission and clutch are shown in Figure 7.12 and Figure 7.13 to verify the ATVA's effectiveness. More detail of solving the transient response of the powertrain under general excitation torque is reported in Appendix A7.

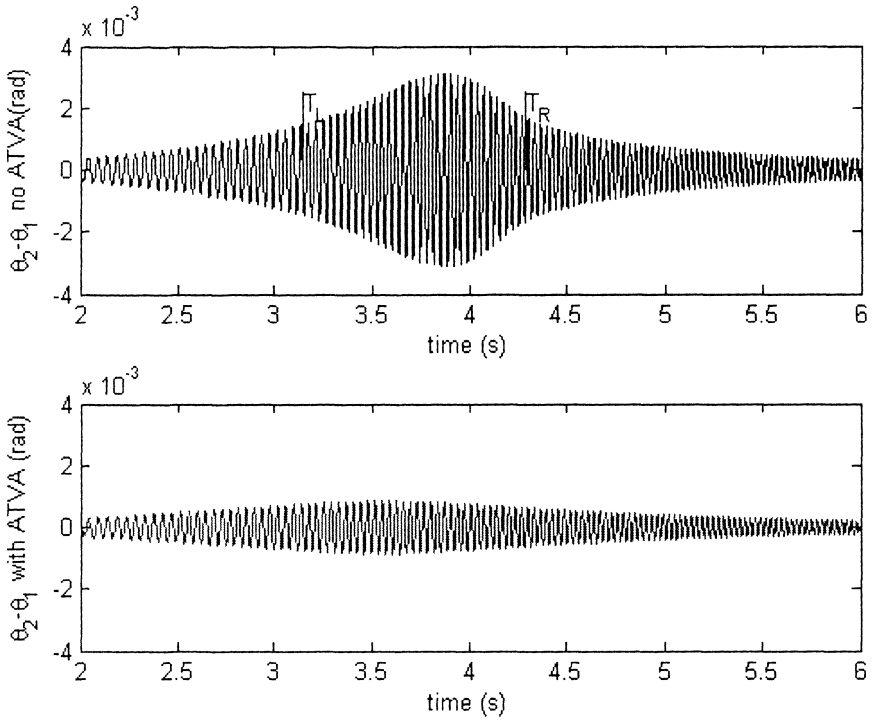

Figure 7.12. Relative vibration between clutch and engine

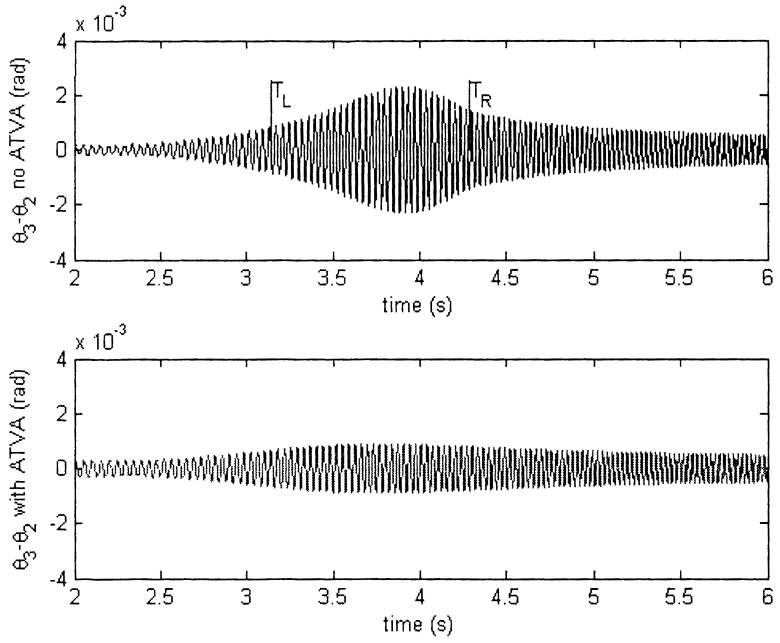

Figure 7.13. Relative vibration between transmission and clutch

It can be observed in Figures 7.12 and 7.13 that after adding ATVA the powertrain transient vibration is reduced significantly. This is in agreement with the results shown in Figure 7.11 because there is no powertrain modal frequency in the resonant area. That means the resonance has been removed. In other words, the ATVA is confirmed to work effectively.

It is noted that although the ATVA has worked already as observed in Figure 7.11, ATVA parameters are not optimal because it can be seen in the figure that although ω_{n4} was far away the upper limit, ω_{n3} is still too close to the lower limit. As a result, ATVA parameters such as μ_A, ω_{on} or ω_{off} should be investigated for optimisation.

To show the effect of ATVA parameters such as ATVA frequency or ATVA inertia moment on ATVA's effectiveness, these parameters will be varied and compared. It should be emphasised that for the MRE-based ATVA when k_A is tuned, c_A will be tuned automatically.

The effect of ATVA inertia moment J_A, is investigated as shown in Figure 7.14. In this figure, three values of inertia μ_A=1/4, 1/5, 1/12 were compared. Obviously, the more μ_A is, the further ω_{n3} and ω_{n4} are shifted away the resonance area. However, if μ_A is too small (1/12 in this case) as seen in Figure 7.14, the ATVA does not work effectively because the frequency ω_{n3} is still in the resonance area.

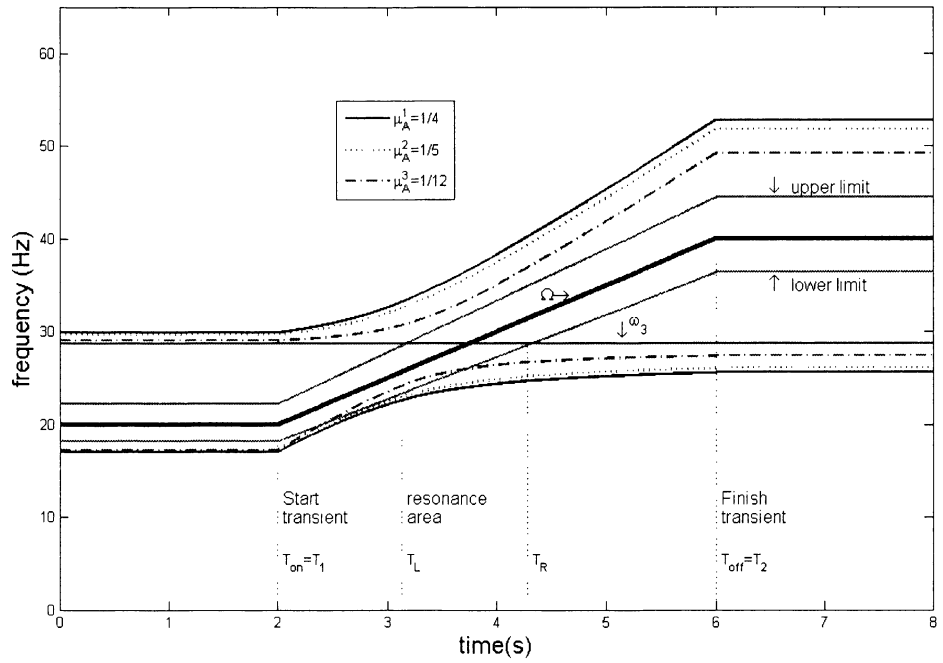

Figure 7.14. Frequencies ω_{n3} and ω_{n4} for three values of ATVA inertia moment μ_A

If $\omega_{off} = \Omega_2 / 0.85 = 2\pi \times 47.06$ (Hz) is fixed, four values of ATVA initial frequency ω_{on} were varied and the powertrain frequencies ω_{n3} and ω_{n4} are shown in Figure 7.15.

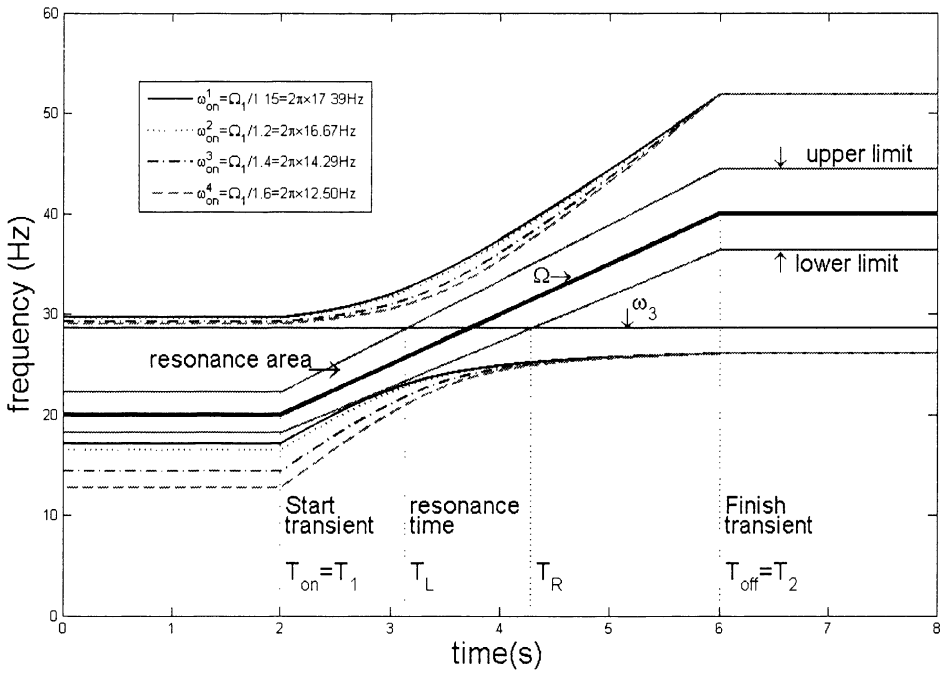

Figure 7.15. Frequencies ω_{n3} and ω_{n4} for four values of ATVA initial frequency ω_{on}

It is obvious that in this case ω_{on} seems to be optimal in a value between $\Omega_1/1.6$ and $\Omega_1/1.4$ (between 12.50 and 14.29 Hz) because both ω_{n3} and ω_{n4} are far away from the resonance area.

Similarly, if $\omega_{on} = \Omega_1/1.15 = 2\pi \times 17.4$ (Hz) is fixed, several values of ATVA maximum frequency ω_{off} are varied and the powertrain frequencies ω_{n3} and ω_{n4} are shown in Figure 7.16.

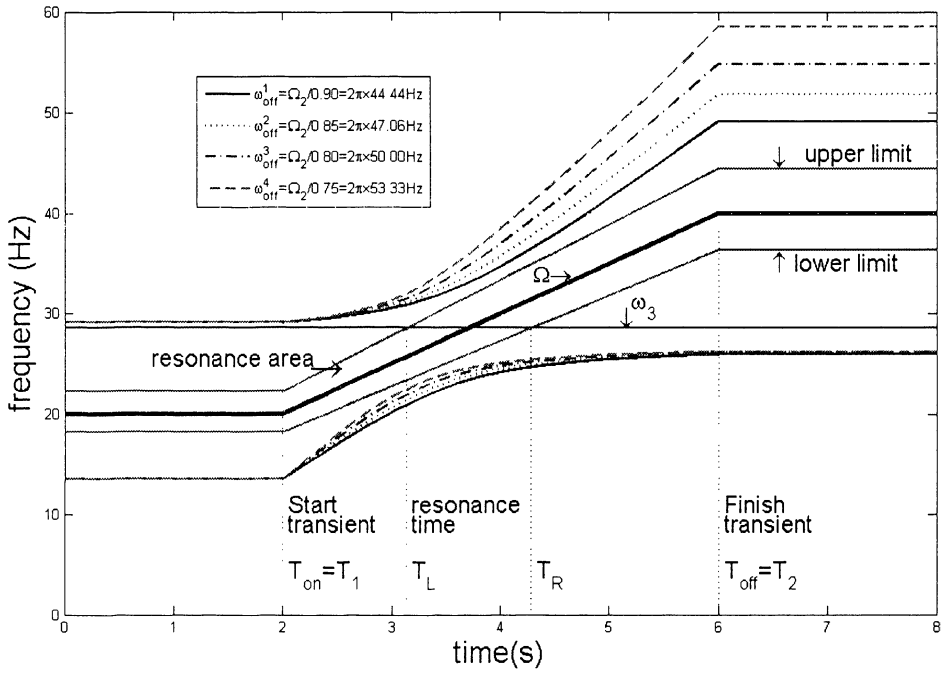

Figure 7.16. Frequencies ω_{n3} and ω_{n4} for four values of ATVA frequency ω_{off}

It can be seen in Figure 7.16 that ω_{off} seems to be optimal in a value between $\Omega_2/0.9$ and $\Omega_2/0.85$ (between 44.44 and 47.06 Hz). Clearly, the time history of the powertrain modal frequency is useful to determine the optimal parameters of the MRE-based ATVA.

With the ATVA proposed design, the resonance, which happens to powertrain vibration during the transient state, has been completely removed, as shown in Figure 7.11. Thus, the powertrain transient response has been reduced significantly as shown in Figures 7.12 and 7.13. This confirms that the MRE-based ATVA works effectively as designed.

7.6 Discussion

With a new MRE, which has a significant increase in elastic modulus and low damping, a MRE-based ATVA was proposed for transient vibration reduction of powertrain when powertrain accelerates from 1200 to 2400rpm. With the new MRE, the ATVA can work in a frequency range of 10-55Hz. Thus, the ATVA can be tuned to deal with the resonance for the whole powertrain transient process with excitation frequency Ω from 20 to 40Hz.

It was found that by using the ATVA, the powertrain modal frequency was actively shifted away from the excitation frequency. This finding was numerically validated in both the frequency and time domains. By using the MRE-based ATVA, the resonance, which occurs in powertrain modal frequency in the transient state, was completely removed. As a result, the powertrain transient response was reduced significantly.

It was also found that there is a different method of tuning ATVA frequency between the steady state and transient state for dealing with the resonance. In the steady state the ATVA frequency is tuned exactly the same or closely around the excitation frequency (to obtain an optimal parameter because of damping). By contrast, in the transient process, to make sure the powertrain modal frequency is shifted out of the resonant area, the ATVA frequency might be chosen quite differently from the excitation frequency. This finding is shown in Figure 7.8. The ATVA frequency can be chosen, for example, 15% lower or higher than the excitation frequency when the excitation frequency is far away from the modal frequency of powertrain. In other words, tuning ATVA frequency exactly the same the excitation frequency is only effective if the excitation frequency coincides with or is close to the modal frequency of the powertrain. When the excitation frequency is far from the modal frequency of the powertrain, tuning the ATVA frequency exactly to be the same as the excitation frequency may increase rather than reduce the powertrain transient vibration responses.

This chapter has derived effective formulas for elastic modulus and damping ratio of the new MRE as explicit functions of magnetic flux density. The derived formulas are in a good agreement with the experiment data. With these formulas, stiffness and damping

coefficients are converted effectively from the magnetic flux density.
In addition, the influence of ATVA parameters on ATVA's effectiveness was investigated, in which the initial and end values of ATVA frequency ω_{on} and ω_{off} were examined. Furthermore, the impact of the ATVA inertia on its effectiveness was investigated. From the effect of such parameters, a set of optimal values for ATVA parameters for dealing with the resonance in the transient state can be obtained.

7.6.1 Limitations

Firstly, this chapter is based on an assumption that the shear modulus of the new MRE could be tuned continuously to provide sufficient stiffness. As a result, the frequency of MRE-based ATVA can be tuned as seen in Figure 7.8. Actually, the MRE may need more time to provide the stiffness and damping, as shown in Figure 7.9 or 7.10. In other words, the time delay was ignored in this chapter.

Secondly, similar to Chapter 5 and Chapter 6, the parameters of a simplified powertrain model were choosen but they did not belong to a real powertrain. In this chapter, a set of powertrain parameters such as inertia stiffness and damping were chosen. As a result, there are four frequenies of powertrain, in which the first frequency is zero due to the rigid body rotation of the system. The second, third and fourth frequency of the powertrain are 10.2138Hz, 28.5814 and 62.4686 Hz respecively. Thus, with the set of powertrain parameters, the excitation frequency range 20-40Hz will pass through the third frequency of powertrain f_3 =28.5814Hz.

Thirdly, the transient state (the acceleration of engine speed) is assumed as a ramp function, in which the angular acceleration of the engine is assumed as a constant for the process. It would be useful if the powertrain engine torque during the transient process can be measured to validate in this case.

Lastly, this work is based on the assumption that the magnetic field produced by electromagnetic coil is sufficient for MRE samples, which are located between the inner and outer rings. In fact, using FEM for analysing the magnetic field in MRE layers of the ATVA should be conducted. This topic should be carried out in further study.

7.7 Summary

This chapter used a MRE-based ATVA for transient vibration reduction of the powertrain. The transient process investigated in this chapter is the acceleration of the engine from 1200rpm to 2400rpm. The new MRE used to for developing the ATVA has a significant increase shear modulus and low damping. By using the MRE, the ATVA can work in a frequency range from 10-55Hz. Numerical simulations were conducted to show the ATVA's effectiveness. The numerical simulation results show that with the MRE-based ATVA, the frequency of the powertrain can be shifted far away from the resonant area. As a result, the transient vibration of the powertrain was reduced significantly.

Chapter 8 A DESIGN OF ATVA FOR VIBRATION CONTROL OF UTS POWERTRAIN TEST RIG

8.1 Introduction

The objective of this chapter is to present the detailed design of a MRE-based ATVA, which will be used for shifting the frequency of the UTS powertrain test rig. Before designing the ATVA, a MRE is fabricated and experimentally investigated in the Dynamic and Solid Mechanics Laboratory, UTS. As a result, the Young's modulus and damping ratio of the MRE are measured in this chapter. With the measured properties of the MRE and specification of the UTS powertrain test rig, an ATVA design is proposed. As a result, mechanical and magnetic parameters of the MRE-based ATVA are presented.

8.2 Background

To validate the ATVA's effectiveness, a powertrain test rig was built for testing purposes. The UTS powertrain test rig is shown in Figure 8.1. This rig was designed as a copy of an AU Falcon, which is a common taxi in Sydney. To have equivalent inertia with a real car whose mass is 1500kg, a combination of small and large fly wheels as well as tires as shown in Figure 8.1, is used to provide the correct inertia. More detail of the UTS powertrain test rig can be found in Crowther [1].

In this application the MRE-based ATVA will be mounted on the propeller shaft of the test rig, which is used to transfer power from the transmission to the driveline components such as differential, tires and the flywheels of the test rig.

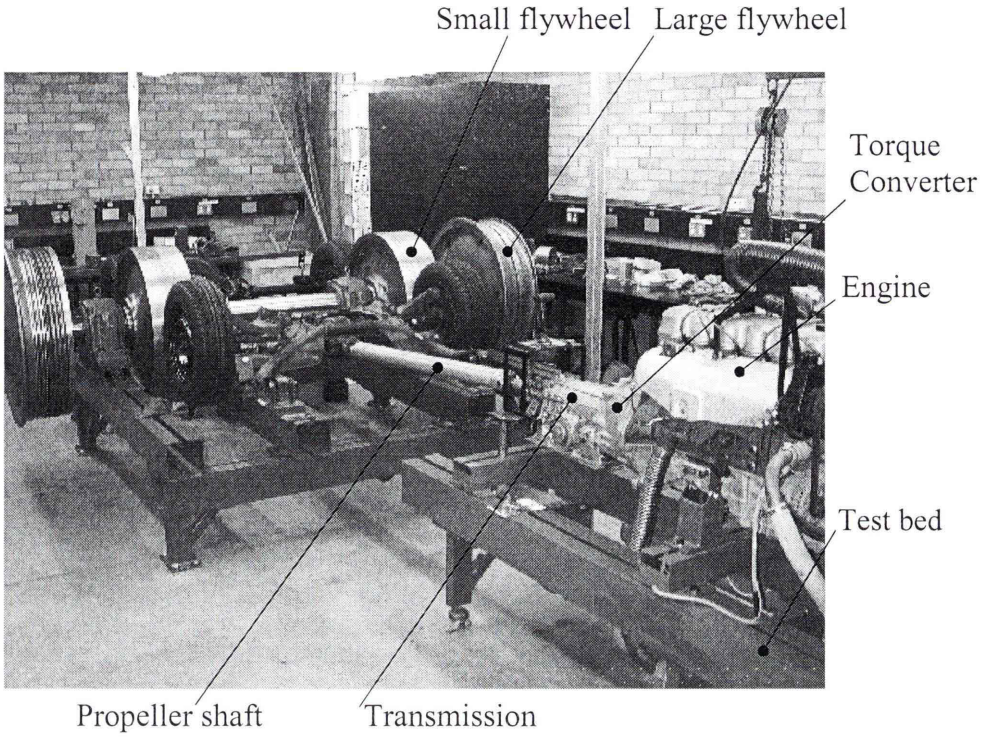

Figure 8.1. UTS powertrain test rig

The UTS Powertrain main specifications can be summarised in Table 8.1.

Table 8.1. UTS Powertrain test rig main specifications

Engine maximum torque	280Nm
Transmission maximum torque	360Nm
Transmission maximum power	160W
Engine speed operating range	1000-4000rpm
Flywheel speed operating range	190-570rpm
Torque converter diameter	280mm
Flywheel diameter	850mm
Tire diameter	625mm
Propeller shaft diameter	86mm
Engine oscillation the first order	15-70Hz
Engine oscillation the second order	30-140Hz
Engine oscillation the fourth order	60-280Hz

The purpose of this chapter is to design an MRE-based ATVA for vibration control of the UTS powertrain test rig. To be specific, the ATVA will be used for dealing with the

resonances, which happen to the first torsional fundamental frequency of the test rig. It is noted that the ATVA will be mounted on a propeller shaft, which has diameter of 86mm. Before the ATVA design is proposed, a MRE material is fabricated and the mechanical properties are measured.

8.3 A magnetorheological elastomer

8.3.1 MRE preparation

The MRE consists of a rubbery silicone polymer matrix, silicone oil which serves as a plasticiser and magnetic particles with weight fractions of 60%, 20%, 20% respectively. The size of the magnetic particles is 6-7 μm. To enhance the MR effect, the mixed material was placed in a strong magnetic field before being cut into rectangular prism samples 16×16×45mm for testing. This MRE material was fabricated at the University of Wollongong, Australia. In this experiment, a viscous model is used to measure MRE properties including Young's modulus and the damping ratio.

8.3.2 Measure Young's modulus

The test was conducted at the Dynamic and Solid Mechanics Laboratory, University of Technology, Sydney. The Young's modulus of MREs is measured by using the tensile and compression device INSTRON 1026. The schematic diagram and experimental set-up for measuring the Young's modulus are shown in Figures 8.2 and 8.3, respectively.

It can be seen in Figure 8.2 that by tuning the distance between two parallel identical permanent magnets, the magnetic flux density created by the two magnets can be varied. The closer the two magnets are, the stronger the MRE magnetic flux density will be. As a result, the MRE properties are measured at several values of magnetic flux density.

Cylindrical magnets D-D50H12.5-N45 (disc 50mm diameter×12.5mm high) are used and the MRE magnetic field density is measured by BELL 610 Gauss-meter, which is connected by a Hall probe to measure the magnetic field on the MRE sample surface, as shown in Figure 8.3.

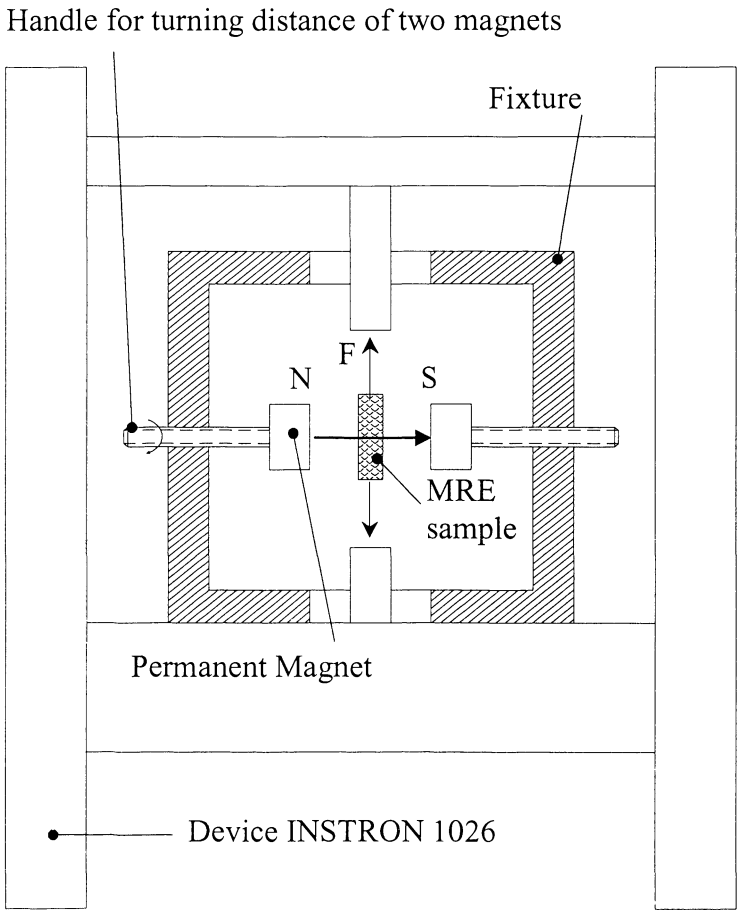

Figure 8.2. The schematic diagram for measuring MRE Young's modulus E

The MRE Young's modulus is measured using the equation.

$$E = \frac{\sigma}{\varepsilon} = \frac{F / A_0}{\Delta l / l_0} = \frac{F l_0}{A_0 \Delta l} \tag{8.1}$$

Where E is the Young's modulus, F is the applied force; A_0 is the original cross-sectional area through which the force is applied; Δl the length change of the MR specimen; l_0 is the original specimen length.

It can be seen in Figures 8.2 and 8.3 that the MRE sample is fixed at both ends to the INSTRON device. Thus, the force F applied to the MRE sample and length change, Δl, are provided by the Device INSTRON 1026. This device is connected to the National Instrument module (model NI SCXI-1125) to transfer data to the PC, in which the data acquisition is conducted by Labview software version 8.6. As a result, Young's modulus can be calculated as equation (8.1).

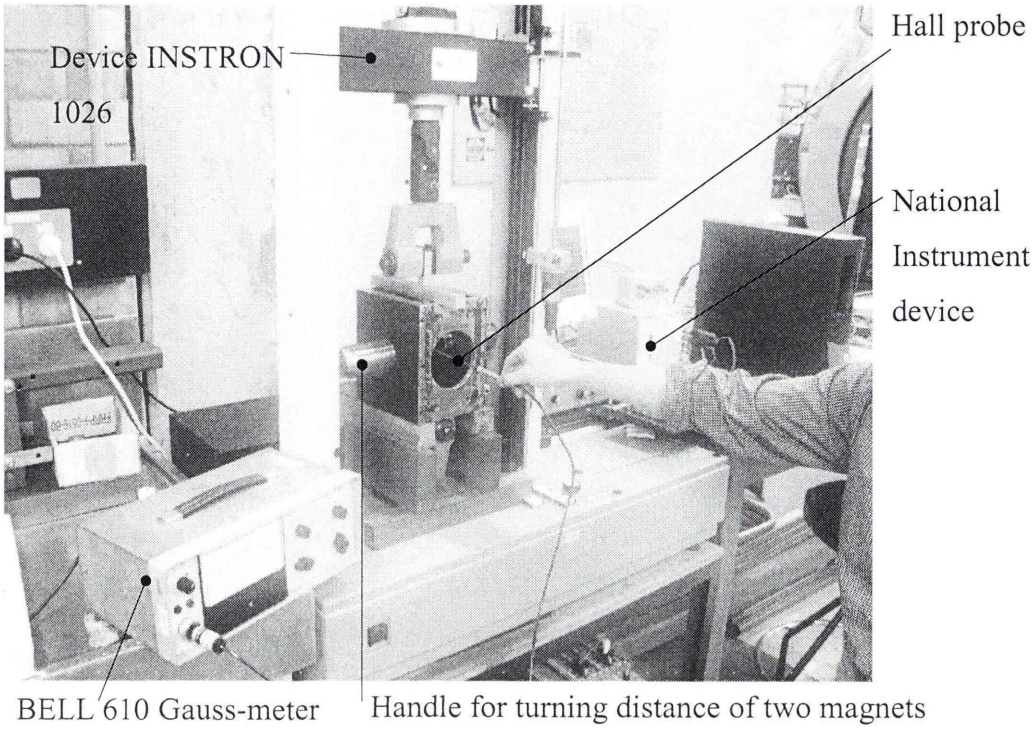

Figure 8.3. Experimental set-up for measuring the Young's modulus of MRE

8.3.3 Measure damping ratio

The experimental set-up for measuring the damping ratio is the same as shown in Figure 8.3. It is noted that to measure the MRE damping ratio, the viscous model, which was presented in section 3.3 in Chapter 3, is used. The procedure of this experiment is described as follows: by measuring the free vibration of a weight, which is attached to a MRE rectangular prism sample as the model shown in Figure 3.2. Thus, the damping ratio can be obtained by using the equation (3.7). To pick up the signal of vibration of the weight, an accelerometer, namely, Crossbow CXL01LF1 is used.

In this experiment, there is only one different thing between measuring MRE damping ratio and measuring Young's modulus. For measuring the MRE damping, the free vibration of the weight is transferred from the accelerometer Crossbow CXL01LF1 to the National Instrument module, whereas it is transferred from the Device INSTRON 1026 for measuring the Young's modulus of the MRE.

It is noted that for the powertrain vibration problem, only a small deformation of the MRE strain is focused in this experiment.

8.3.4 Experimental results of Young's modulus and damping ratio

The results of the experimental testing of Young's modulus at strain 1% and the damping ratio compared to the proposed models are shown in Figures 8.4 and 8.5.

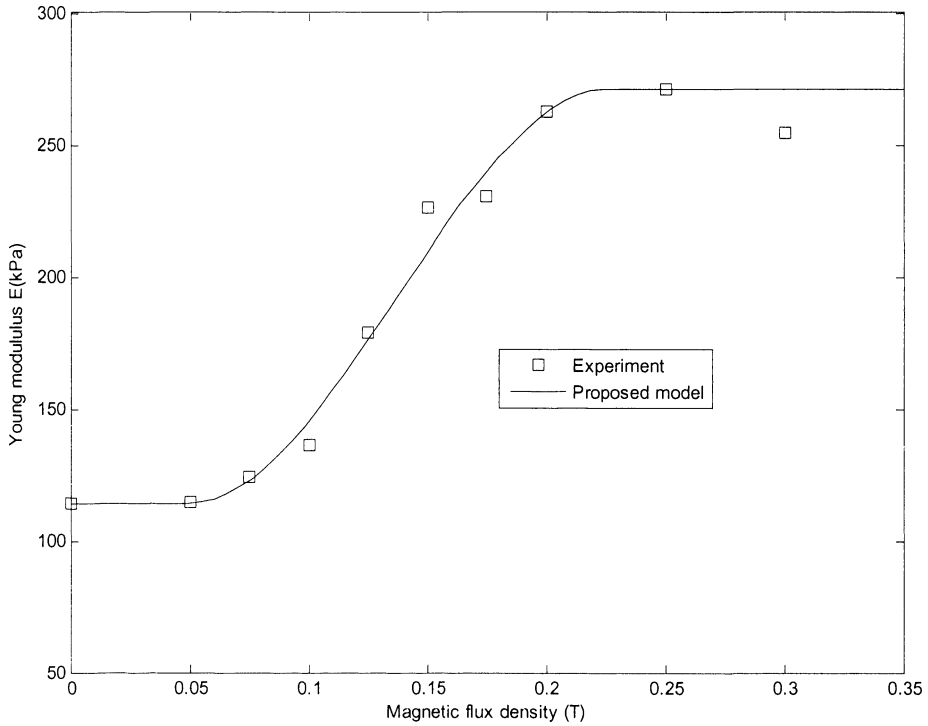

Figure 8.4. Young's modulus proposed model and experimental data

To facilitate the ATVA design, the Young's modulus is approximated by the following equation:

$$E = E(B) = \begin{cases} E_0 & B \le B_0 \\ E_0 + (E_{\max} - E_0)\dfrac{B^2}{B_S^2}(3 - 2\dfrac{B}{B_S}) & 0 < B < B_S \\ E_{\max} & B \ge B_S \end{cases} \tag{8.3}$$

Here B_0=0.05T is the value of magnetic flux density when the MRE material starts to increase Young's modulus; B_S=0.225T is the saturated point; E_0=114.2kPa and E_{max}=270.9kPa are the initial and maximum value respectively of Young's modulus.

It can be seen in Figure 8.4 that the Young's modulus of this MRE does not change if the magnetic flux density on the MRE surface is less than 0.05T. However, the Young's modulus increases significantly if the magnetic flux density B is from 0.1T to 0.2 Tesla. The MRE Young's modulus saturates at magnetic flux density B=0.225Tesla. Thus, the

interval of magnetic flux density [0.1 0.2]T will be effective to tune the stiffness of the MRE material.

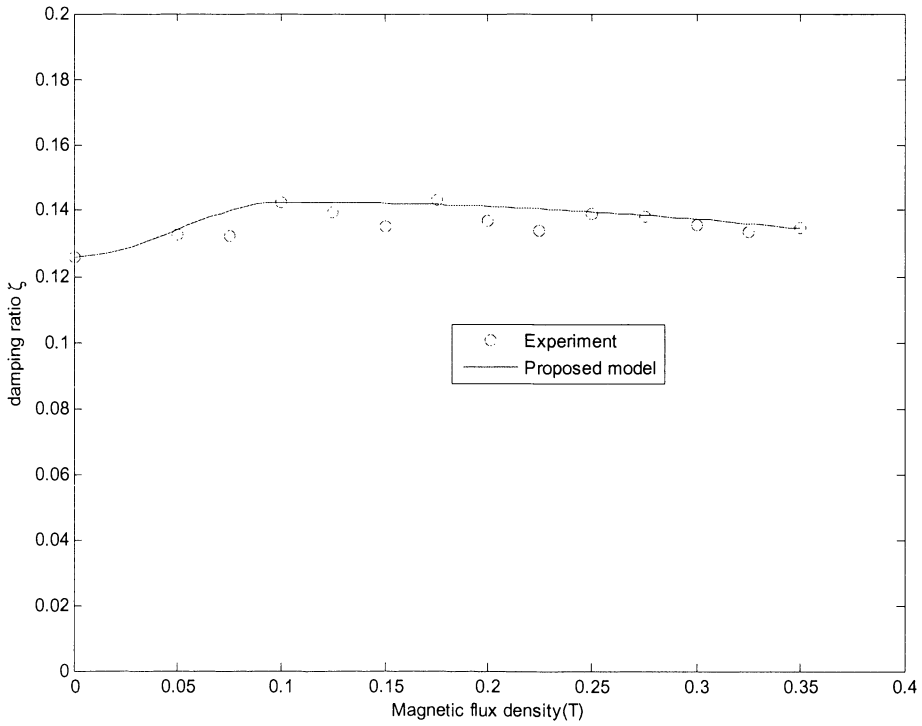

Figure 8.5. Proposed model of damping ratio and experimental data

It can be observed in Figure 8.5 that the damping ratio increases from 0.126 and reaches maximum value 0.14 at $B=B_C=0.1T$. After that the ratio decreases slightly until $B=B_{max}=0.35T$. Similar to Chapter 7, the damping ratio is proposed as:

$$\varsigma = \begin{cases} 0.126 + 4.9794B^2 - 33.1958B^3 & 0 \le B < B_C \\ 0.1412 + 0.0256\mathrm{B}^2 - 0.1281\mathrm{B}^2 & B_C \le B \le B_{\max} \end{cases} \tag{8.4}$$

Obviously, the experimental result and the proposed models are in good agreement. The model presented in equations (8.3) and (8.4) will be used for the ATVA design in following sections.

It can be seen from Figure 8.4 and Figure 8.5 that when the magnetic flux density from 0.1 to 0.225 Tesla the damping ratio of MRE is almost constant, while the Young's modulus is increased significantly. Thus, the interval [0.1-0.2T] will be effective for turning the MRE-based ATVA frequency.

8.4 Mechanical design

The exploded view of ATVA is shown in Figure 8.6 and the summary of ATVA mechanical parameters is shown in Tables 8.2 and 8.3.

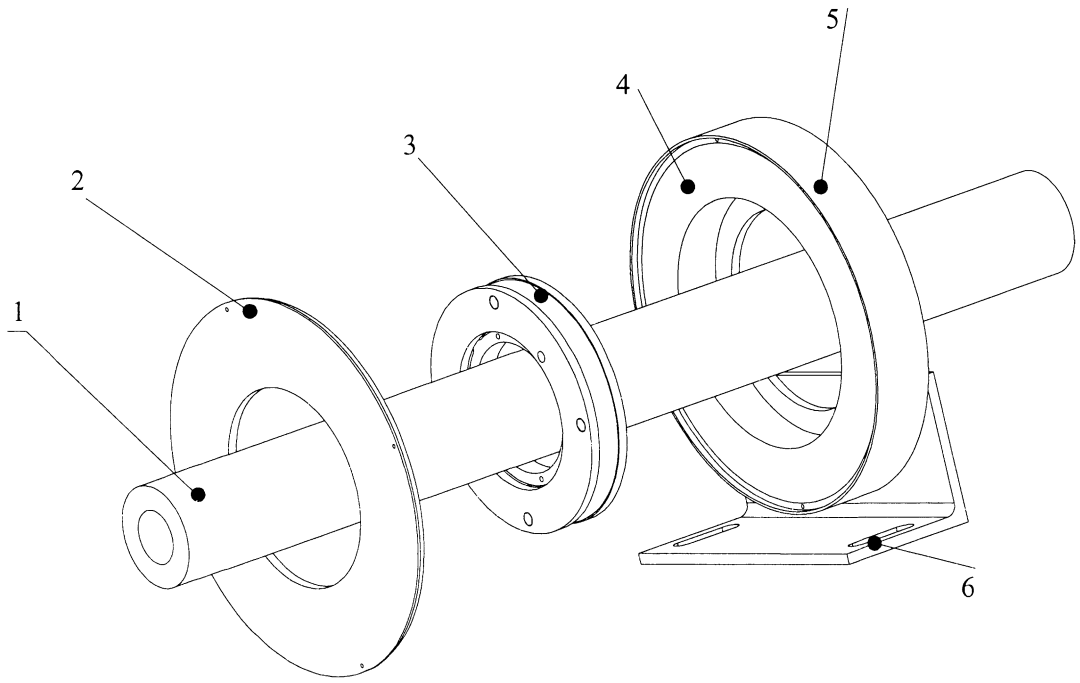

Figure 8.6. ATVA exploded view

1: Powertrain propeller shaft; 2: Mild steel core cover

3: Rotating part; 4: Copper coil; 5: Mild steel core; 6: Frame support

The rotating part, 3, which is the main part of ATVA, consists of an outer ring, inner ring and eight MRE specimens put in the gap between the rings. The MRE specimens act as springs to make sure that the rotating part is a torsional SDOF system and the rotating part is located on the powertrain propeller shaft, 1. The whole system is fixed on the frame support, 6, and this frame support with two slots is used to fix the ATVA on the UTS Powertrain test bed, which was shown in Figure 8.1.

A magnetic field is produced by a copper coil, 4, with mild steel cores, which are mild steel core, 5, and the mild steel cover, 2. The magnetic field is tuned by changing the electric current I supplied to the electromagnetic coil. The stiffness and damping of MRE specimen is controlled by this magnetic field.

The cross section of the ATVA is shown in Figure 8.7. It is noted that eight MRE specimens act as 8 translational springs. These specimens create elastic forces between outer and inner rings. Thus, the rotating part works as a torsional SDOF system.

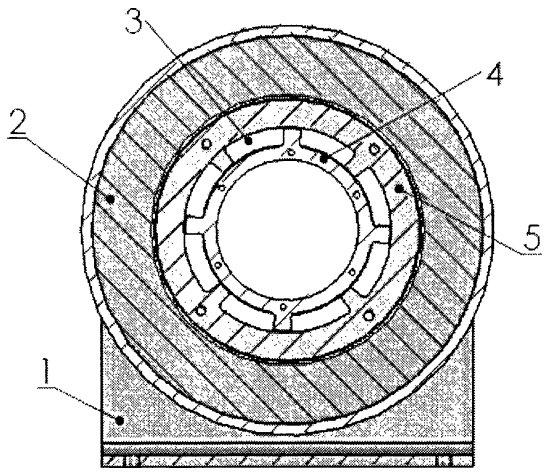

Figure 8.7. Cross section of ATVA design:1. Frame support; 2.Magnetic circuit; 3. MR elastomer specimen; 4. Inner ring; 5.Outer ring

Figure 8.8 shows the exploded view of the ATVA rotating part. This consists of inner and outer rings, MRE specimens and two overlap mild steel sheets and a tapered bushing. The tapered bushing, which is cut into two halves and bolted to the inner ring, is used to fasten the inner ring to the propeller rotating shaft of the UTS powertrain and the overlap mild steel sheets are bolted to the outer ring to make sure that the magnetic flux will direct mainly to the MRE specimens instead of going the outer ring, which is made of brass.

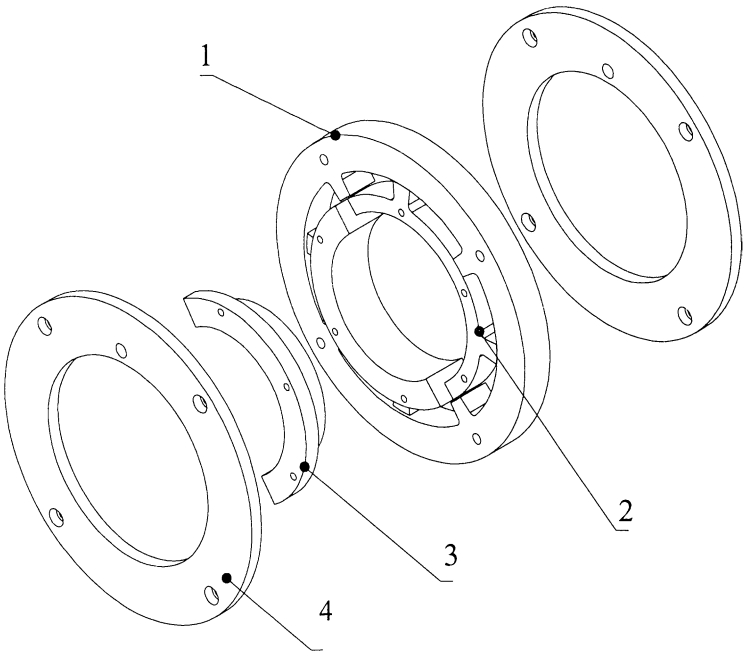

Figure 8.8. Exploded view of the rotating part

1. Outer ring ; 2. Inner ring; 3. A haft of tapered bushing; 4. Overlap mild steel sheet

The inner ring, outer ring and the overlap sheet are shown in Figures 8.9, 8.10 and 8.11.

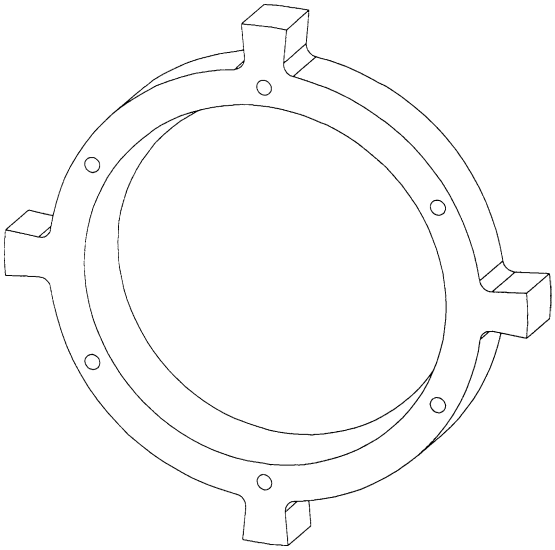

Figure 8.9. Brass inner ring

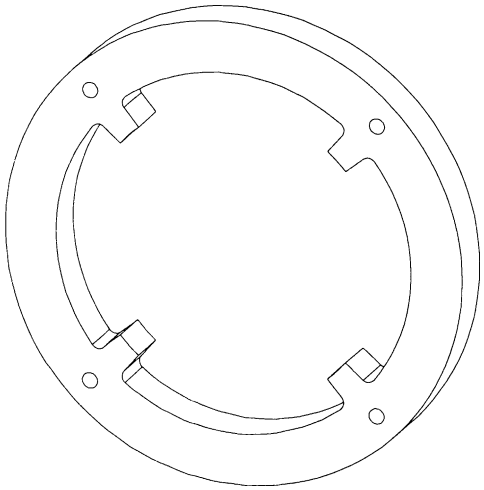

Figure 8.10. Brass outer ring

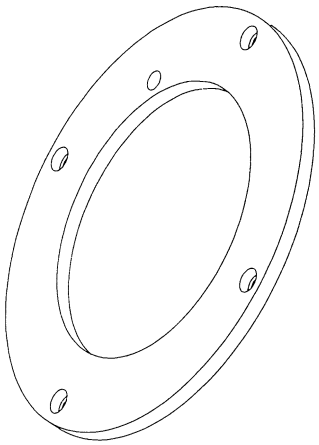

Figure 8.11. Mild steel overlap sheet

8.5 Magnetic circuit analysis

The magnetic flux path is shown in Figure 8.12. It is noted that to enhance the flux from the magnetic coil and direct mainly to MRE specimens rather than the brass outer ring, there are two mild steel overlap sheets which are bolted to both sides of the outer ring.

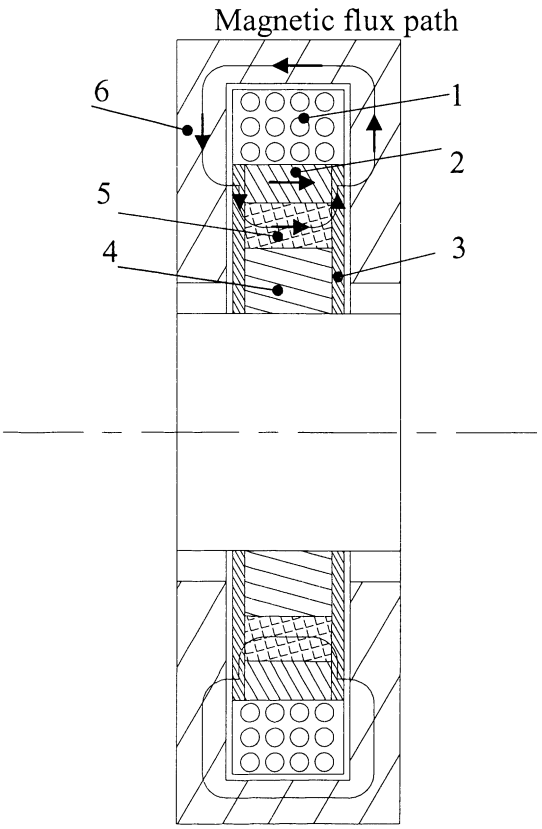

Figure 8.12. Magnetic flux path, 1: Coil; 2: Outer ring; 3: Mild steel overlap sheet; 4: Inner ring; 5: MRE specimen; 6: Mild steel core

By using Ohm's law for the magnetic circuit, the equivalent magnetic circuit of the ATVA is shown in Figure 8.13.

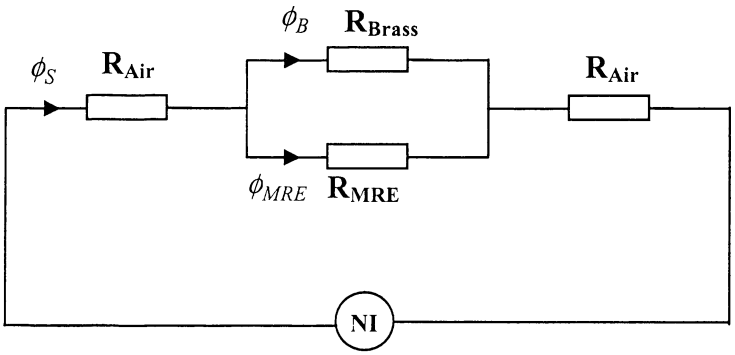

Figure 8.13. ATVA magnetic circuit

In Figure 8.13, ϕ_S, ϕ_B and ϕ_{MRE} are magnetic flux through steel, brass and MRE respectively. As the permeability of mild steel is much larger than that of air, brass or MRE, the magnetic reluctance of the steel path can be ignored. The magnetic reluctance for air, brass, MRE is calculated as follow:

$$R_{Air} = \frac{L_{Air}}{\mu_0 \mu_S A_{Air}} \tag{8.5}$$

$$R_B = \frac{L_B}{\mu_0 \mu_B A_B} \tag{8.6}$$

$$R_{MRE} = \frac{L_{MRE}}{\mu_0 \mu_{MRE} A_{MRE}} \tag{8.7}$$

Here $\mu_0 = 4\pi \times 10^{-7}$ (H/m) is the permeability of free space, μ_S=1000, μ_B=1, μ_{MRE}=4 are the relative magnetic permeability of the mild steel brass and MRE. A_{Air} A_B, A_{MRE} are the cross-sectional area of the circuit of air, brass and MRE, respectively. L_{Air}, L_B, L_{MRE} are the length of the circuit of air, brass and MRE, respectively.

The total magnetic reluctance of the circuit is calculated by:

$$R_{\Sigma} = 2R_{Air} + \frac{R_B R_{MRE}}{R_B + R_{MRE}} \tag{8.8}$$

The flux goes through the mild steel core can be calculated by:

$$\phi_S = \phi_B + \phi_{MRE} = \phi_B + B_{MRE} A_{MRE} \tag{8.9}$$

Here B_{MRE} is given according to the requirement of MRE. In this design, is assumed that the MRE is operated in the maximum of magnetic flux density B_{MRE} = 0.4T.

In addition, the flux goes through the brass branch ϕ_B can be calculated from the relationship $\phi_B R_B = \phi_{MRE} R_{MRE}$ or:

$$\phi_B = \frac{\phi_{MRE} R_{MRE}}{R_B} \tag{8.10}$$

If MRE's magnetic flux density B_{MRE} is given, the Ampere turns NI can be determined by:

$$NI = R_{\Sigma} \times \phi_S \tag{8.11}$$

In which N is the number of turns of the coil and I the DC input current supplied to the electric coil.

The summary of ATVA parameters and cost is shown in Table 8.2 and 8.3.

Table 8.2. ATVA's mechanical parameters

Items	Material	Mass	Dimensions(mm)	Cost (AU$)
Outer ring	Brass	1.6kg	Ri=70, Ro=90, W=18	100
Inner ring	Brass	0.8kg	Ri=48, Ro=57,W=16	50
Overlap sheet	Mild steel	2x0.8kg	Ri=58, Ro=90,W=7	50
Mild steel core	Mild steel	7kg	Ri=74, Ro=139,W=7	300
Electric coil	Copper	5.3kg	Ri=92, Ro=132 ,W=34	300
Adaptive element	MRE		35×8×7mm	400
				Total: 1200

R_o: outer radius; R_i: inner radius; W: Width;

Table 8.3. ATVA's magnetic circuit parameters

permeability of vacuum	$\mu_0 = 4\pi \times 10^{-7}$ (H/m)
relative permeability of the mild steel	μ_S =1000
relative permeability of brass	1
relative permeability of MRE	4 [81]
relative permeability of air	1
MRE specimen	35×8×7mm
cross-sectional area of air circuit A_{Air}	220 mm^2
cross-sectional area of brass circuit	10000mm^2
cross-sectional area of MRE circuit	2240 mm^2
length of the air circuit L_{Air}	1mm for each side
length of the brass circuit L_B	18mm
length of the MRE circuit L_{MRE}	8mm
Ampere turns NI	3000 Ampere turns
coil resistance	15 Ω
brass mass density	8730kg/m^3
mild steel density	7860kg/m^3

It can be seen that the ATVA is a SDOF system. Because the inner ring is fixed in the propeller shaft of the powertrain, the inertia of ATVA can be calculated by:

$$J_A = J_{Outer\,ring} + 2J_{Overlap\,sheet} \tag{8.12}$$

Here, the outer ring and each of the overlap sheets, which were shown in Figure 8.10 and Figure 8.11 respectively, are treated approximately as hollow cylinder, as shown in Figure 8.14.

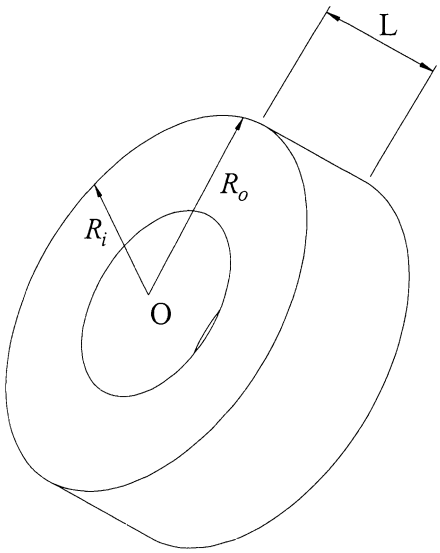

Figure 8.14. Cylinder model to calculate inertia moment

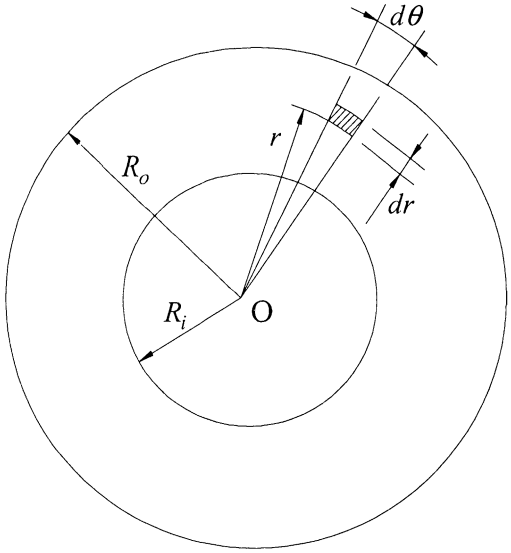

Figure 8.15. Mass element of cylinder

With a cylinder of mass m, length L and, outer radius R_o and inner radius R_i as shown in Figure 8.14 and the element of mass in Figure 8.15: $dm = \rho dV = \rho L r dr d\theta$ is chosen, ρ is the mass density of the cylinder and the equation $J_A = \int r^2 dm$ is used, the inertia of the cylinders can be calculated by:

$$J_O = \frac{1}{2} m(R_o^2 + R_i^2) \tag{8.13}$$

More detail of the equation (8.13) can be seen in Appendix B.

With parameters of outer ring and overlap sheet as shown in Table 8.2, the inertia moment of inner ring and each over lap sheet is calculated by equation (8.13), then, the inertia moment of ATVA J_A=0.021kgm^2 is calculated by equation (8.12).

Because there are eight MRE specimens in the ATVA, the ATVA torsional stiffness can be calculated by:

$$k_A = 8\frac{EA}{L}d \tag{8.14}$$

d is the distance from the centre of a MRE specimen to centre of the propeller shaft. In this design d=65mm, A=7mm×8mm is the cross section of a MRE specimen and E is MRE Young's modulus, which was shown in Figure 8.4.

With J_A=0.021kgm^2, the stiffness coefficient k_A calculated in equation (8.14) and damping ratio as shown in equation (8.4), the frequency of the designed ATVA is calculated by equation (5.9) in Chapter 5 and it is shown on Figure 8.16.

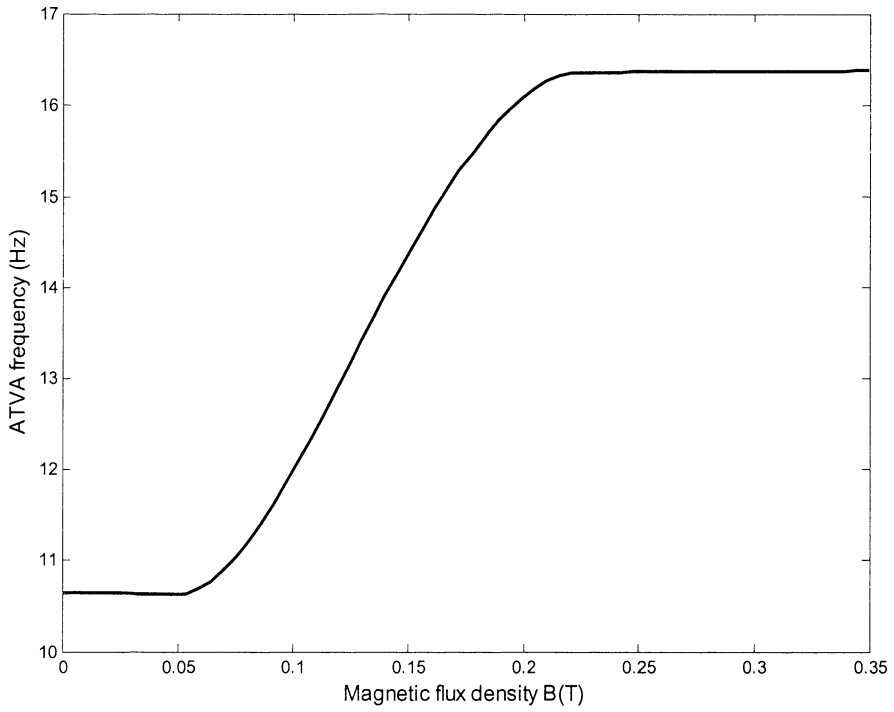

Figure 8.16. ATVA designed frequency

It can be seen that the interval [0.1-0.225T] will be effective for tuning ATVA frequency. In this interval, the MRE stiffness increases significantly and the damping ratio is nearly constant, as shown in Figures 8.4 and 8.5.

8.6 Discussions

A detailed design of a torsional ATVA using a MRE for UTS powertrain test rig was conducted in this chapter. The MRE used in this application was experimentally tested. The experimental results show that the MRE Young's modulus can be controlled from E_0=114.2kPa to E_{max}=270.9kPa in a magnetic field 0.35T, which is produced by two permanent magnets. In addition, it was found that the interval [0.1-0.225T] will be the effective range for tuning MRE frequency because in this interval, the Young's modulus increases significantly and the damping ratio is nearly constant.

From the experimental data, two effective formulas for both Young's modulus and damping ratio were derived to facilitate the ATVA design in this chapter, in which the Young's modulus is expressed as a cubic function of magnetic flux density as similarly described in Chapters 6 and 7. The damping ratio is expressed as a combination of cubic and quadratic polynomials of magnetic flux density. The effective formulas were experimentally validated and they are in a good agreement with the experimental results.

Ohm's law for the magnetic circuit was used to design the magnetic circuit of ATVA. With the specification of UTS powertrain test rig, ATVA geometry parameters are calculated and chosen. In this application, the magnetic circuit, which include a electromagnetic coil and mild steel cores, belongs to the stationary part of the ATVA that is fixed to the test bed of the UTS powertrain test rig. The designed magnetic circuit can product a uniform field across the MRE specimens.

The total cost of this device after fabricated is AU $1200. This value is not much compared to the cost of the vehicle if the device will be a commercial product. In addition, the cost is calculated in this study for a single device. The cost will be much reduced if a large number of the devices are manufactured.

8.6.1 Limitations

To measure the MRE properties, the MRE samples were placed in the middle plane of the two permanent magnets. The magnetic flux density on the surface of MRE sample

was controlled by varying the distance between two magnets, as shown in Figure 8.2. In fact, with the fixture in Figure 8.2, the minimum value of magnetic flux density on MRE surface is 0.05T. In other words, the MRE properties were not measured with the magnetic flux density under 0.05T. It can be seen that this limitation affects the MRE measured damping ratio, as shown in Figure 8.5, because in the range from 0 to 0.05T there are only two data points. However, the limitation may not affect the MRE Young's modulus as seen in Figure 8.4 as at B=0 and at B=0. 05T the measured Young's modulus of the MRE is the same. In other words, the Young's modulus of the MRE is not changed from 0 to 0.05T.

In addition, the temperature increase in the electric coil was not considered. For low current the temperature of the coil will not be high, but for high current, the high temperature of the coil will affect both the current and the magnetic field. If the magnetic coil is too hot, the current will fall significantly. As a result, the magnetic field will be reduced.

8.7 Summary

With the purpose of validating ATVA's effectiveness for the UTS powertrain test rig, an ATVA design was presented in this chapter. To design the ATVA, a MRE was fabricated and experimentally tested for measuring Young's modulus and damping ratio. From the specification of the UTS powertrain test rig, an actual MRE-based ATVA were designed. The designed ATVA consists of two main components, stationary and rotating ones. The magnetic circuit, which belongs to the stationary component, was designed to provide a uniform magnetic field across the MRE specimens. By varying the magnetic field, the Young's modulus of the MRE can be controlled. As a result, the torsional frequency of the rotating component can be tuned magnetically. With the designed parameters, ATVA's frequency is calculated and it can be tuned by the magnetic field.

Chapter 9 EXPERIMENTAL VALIDATION

9.1 Introduction

This chapter presents the experimental testing of the MRE-based ATVA for the UTS powertrain test rig, which was designed in Chapter 8. After the MRE-based ATVA was developed, the three stages of testing are discussed in this chapter. The first stage is to measure the magnetic field produced by electromagnetic coil. The dependence between the ATVA frequency and MRE magnetic flux density (input current as well) is then measured to compare with that of ATVA design. In the last stage, the ATVA's effectiveness for shifting the frequency of the UTS powertrain test rig is experimentally validated.

9.2 Measurement of magnetic field of ATVA magnetic circuit

9.2.1 Experimental set-up

In this section, after manufacture, the ATVA is assembled at the test bed of the UTS powertrain test rig to measure the magnetic field. The experimental set-up for the testing is shown in Figures 9.1 and 9.2. The electromagnetic coil of the powertrain is supplied by a DC power supply, SLIDER (type S-260-10 by YAMABISHI electric company, Japan). The maximum input current can be tuned up to 10A by the power supply.

In a similar method to the experiment conducted in Chapter 8, the device BELL 610 Gauss-meter with a Hall probe is used to measure the magnetic field on the surface of each MRE sample.

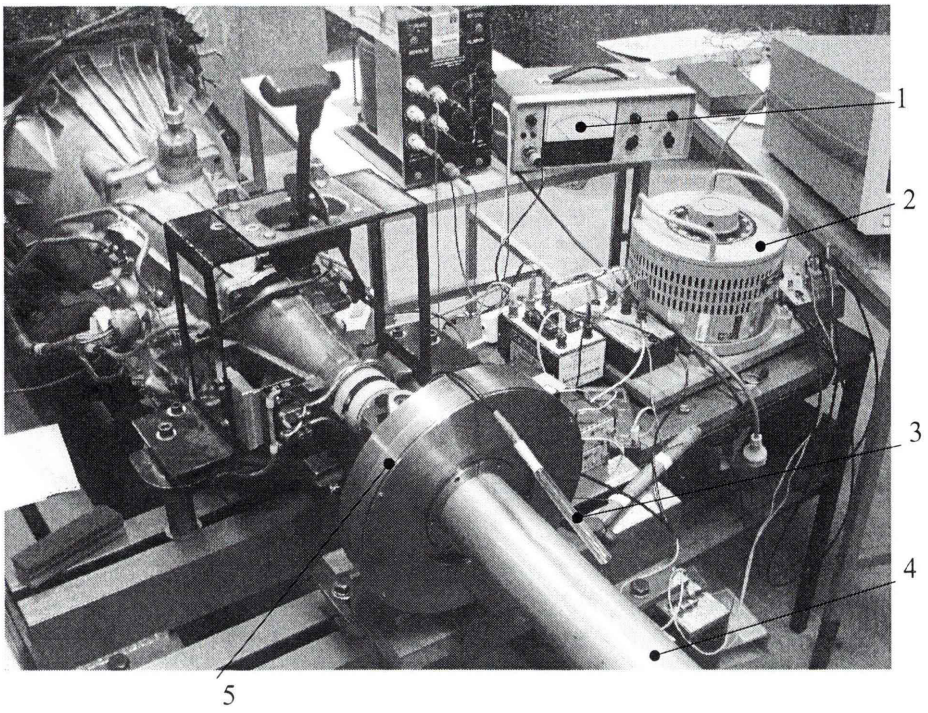

Figure 9.1. Experimental set-up for measuring magnetic field with mild steel cover
1. Gauss-meter; 2. DC power supply; 3. Hall probe; 4. Powertrain shaft; 5. ATVA

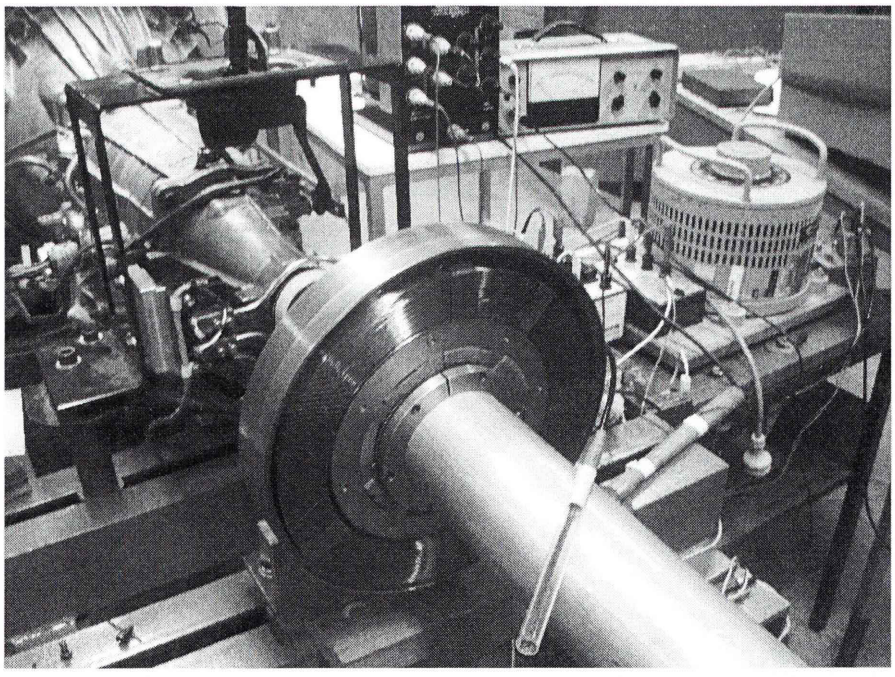

Figure 9.2. Experimental set-up for measuring magnetic field without mild steel cover

It can be seen that the MRE-based ATVA is mounted on the propeller shaft and next to the transmission of the UTS powertrain test rig. Also, the ATVA magnetic circuit including the coil and the steel core is stationary and is fixed on powertrain test bed.

9.2.2 Experimental results

The magnetic flux density was measured and it is shown in Figure 9.3.

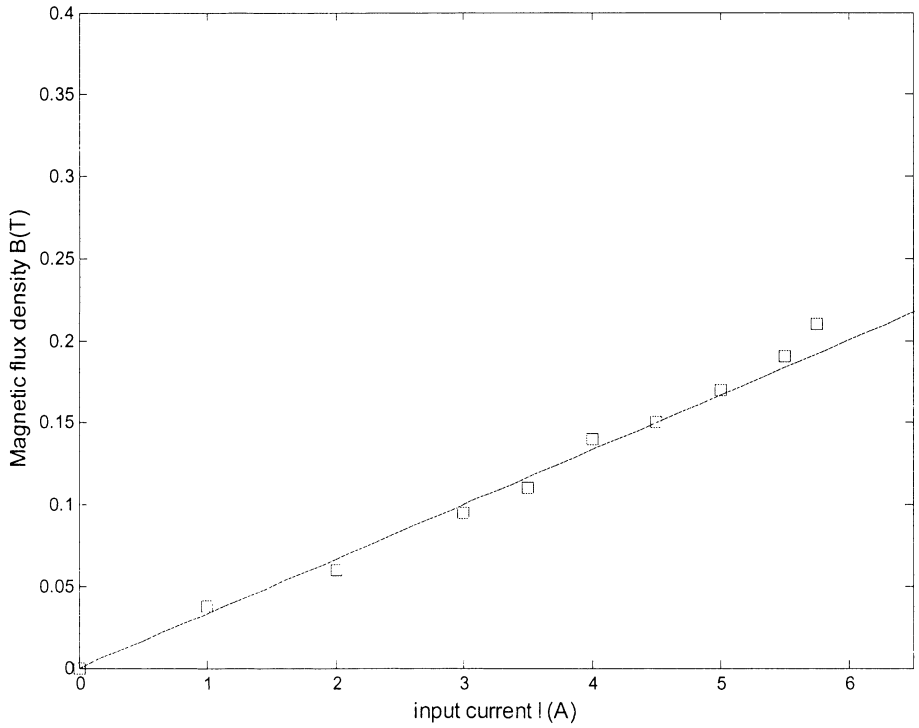

Figure 9.3. Dependence between measured magnetic flux density B and input current I

It can be seen that the magnetic flux density B of the magnetic circuit is proportional to the input current I, which is in the range from 0-5.75A. In this experiment, the highest current is 5.75A because at this current the electromagnetic coil is hot. Thus, the author could not increase the current further, because the temperature increase may damage the device.

From the experimental data, it is straightforward to have the relationship between the magnetic flux density B and input current I as follows:

$$B = \alpha I \tag{9.1}$$

Here α is a coefficient. By using the experiment data, α=0.0333 is calculated. Thus, equation (9.1) can be re-written as:

$$B = 0.0333I \tag{9.2}$$

From the experimental data it is found that the magnetic field of the magnetic circuit is relatively uniform on the MRE sample surface. For example, at I=3.5A the dependence

of magnetic flux density on the MRE specimen locations is shown on Figure 9.4.

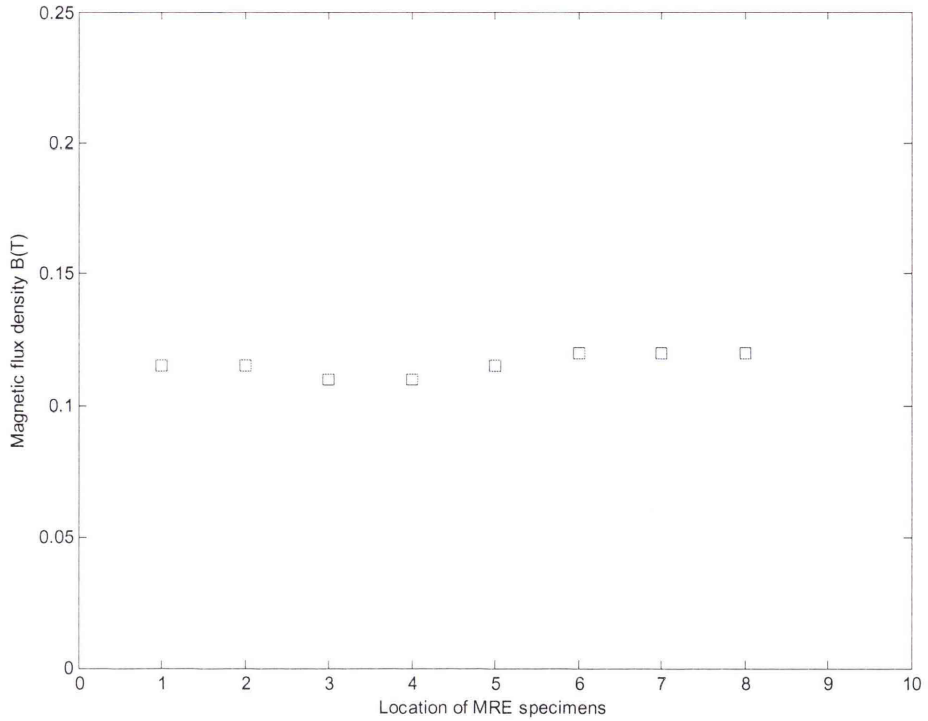

Figure 9.4. Measured magnetic flux density at locations of MRE specimens, I=3.5A

The index of MRE specimens from 1 to 8 is shown in Figures 9.5 and 9.6.

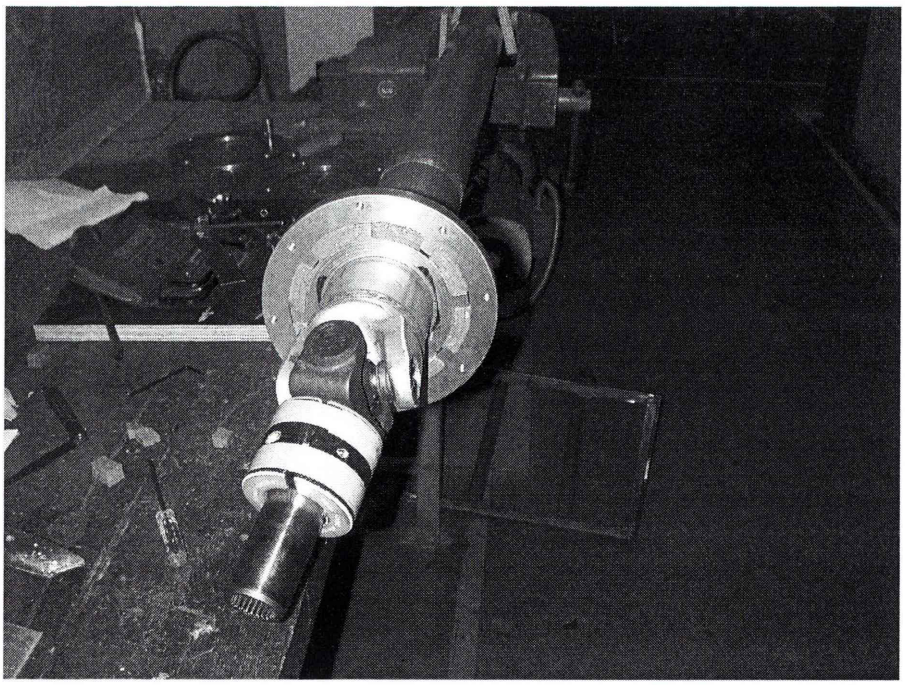

Figure 9.5. MRE specimens in ATVA

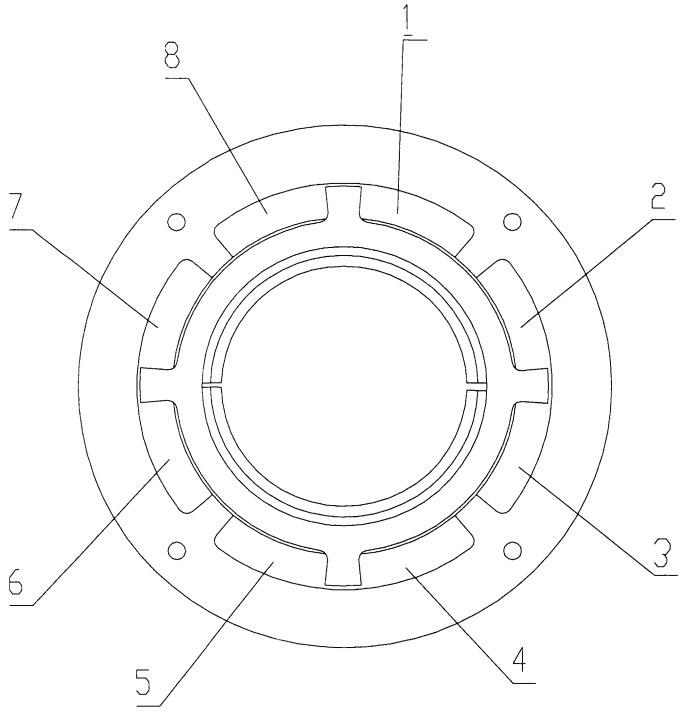

Figure 9.6. Location index of MRE specimens

9.3 Measurement of ATVA frequency

9.3.1 Experimental set-up

In this testing, two Crossbow CXL01LF1 accelerometers are used. These sensors are connected to the Dynamic Signal Analyser 35665A (Hewlett Packard). The Analyser has two channels 1 and 2 to connect to the accelerometers.

The experiment set-up for measuring the ATVA frequency is shown in Figure 9.7 and 9.8. As can be seen in Figure 9.7, the accelerometers are used to pick up the signal of acceleration in tangent directions and the signal is transferred to the channels of the Analyser. The data from the channel 1 and channel 2 are averaged in the time domain and then Fast Fourier Transformation (FFT) is used to obtain the frequency domain of the free vibration of the ATVA.

The acceleration of free vibration of the torsional vibration of the ATVA can be measured for impact excitation. As a result, the ATVA modal frequency can be obtained.

It is noted that to measure ATVA frequency, the propeller shaft was disconnected completely from the UTS powertrain test rig. This makes sure that the ATVA is tested separately with one end clamped, another end free. As a result, the free vibration of ATVA can be measured.

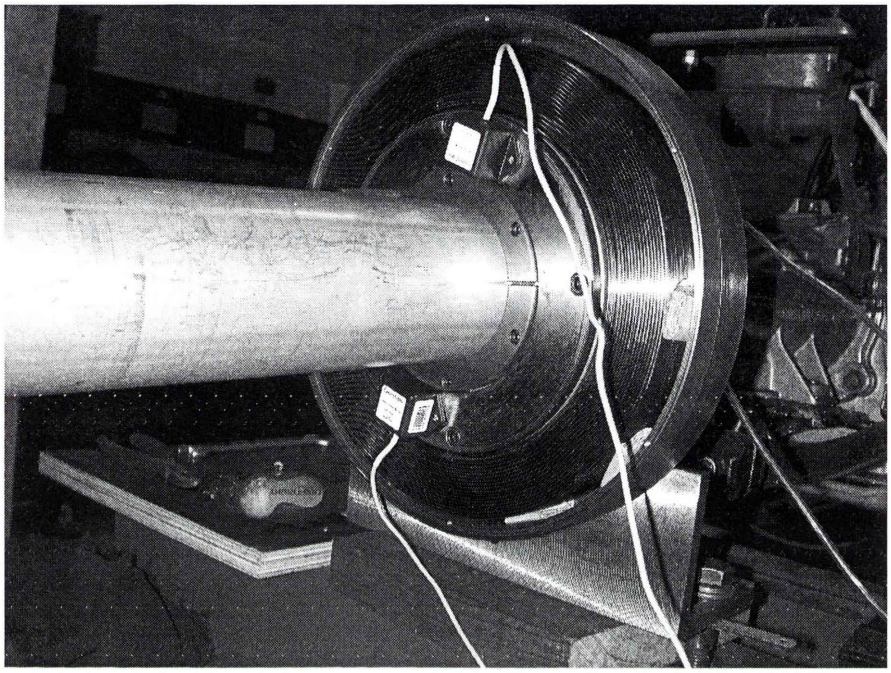

Figure 9.7. Accelerometers Crossbow CXL01LF1 for measuring the ATVA frequency

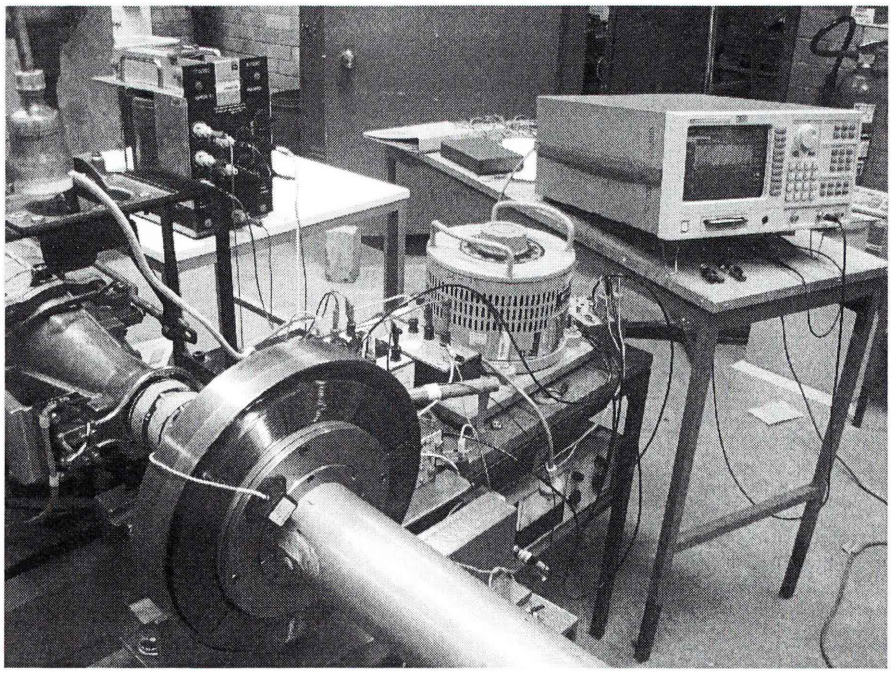

Figure 9.8. The experimental set-up for measuring the ATVA frequency

9.3.2 Experimental results

The free vibration of the ATVA at input current I=0A is shown in Figure 9.9 and the FFT is shown in Figure 9.10.

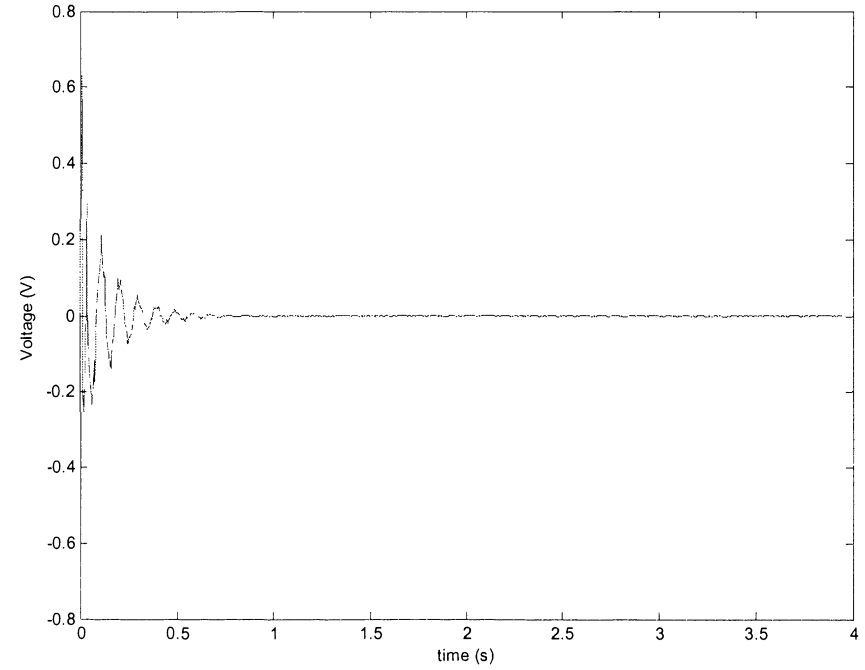

Figure 9.9. Powertrain decay vibration recorded by the Analyser, at I=0A

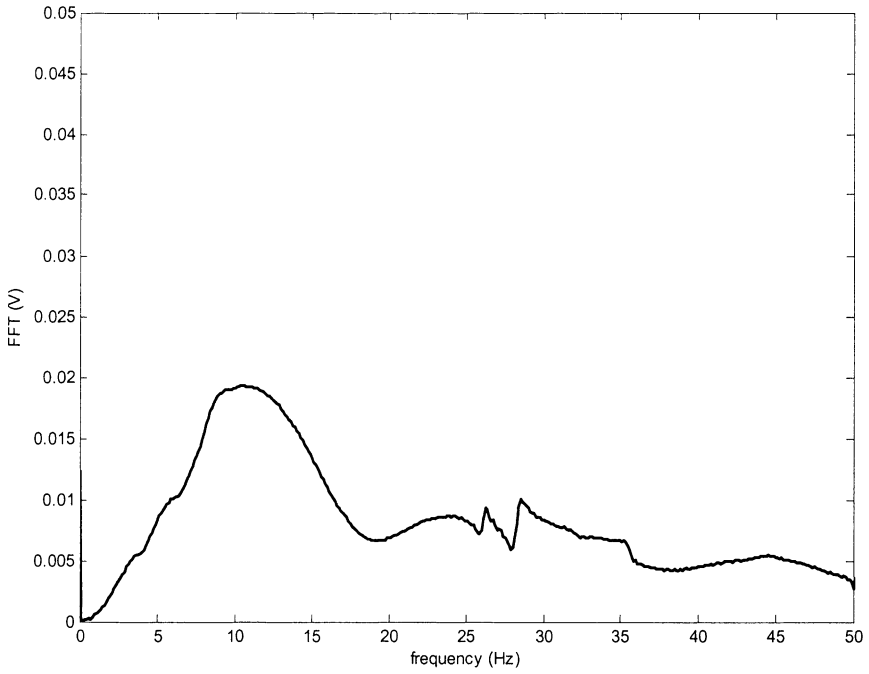

Figure 9.10. Frequency domain of the signal recorded by Analyser, at I=0A

The free vibration of the ATVA at input current I=5.75A is shown on Figure 9.11 and the FFT is shown in Figure 9.12.

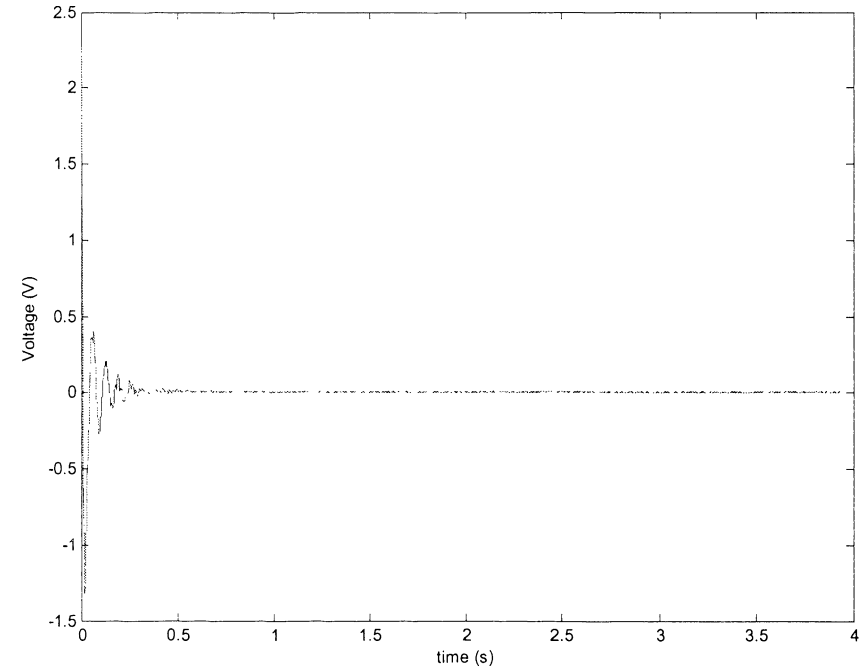

Figure 9.11. Powertrain decay vibration recorded by the Analyser, at I=5.75A

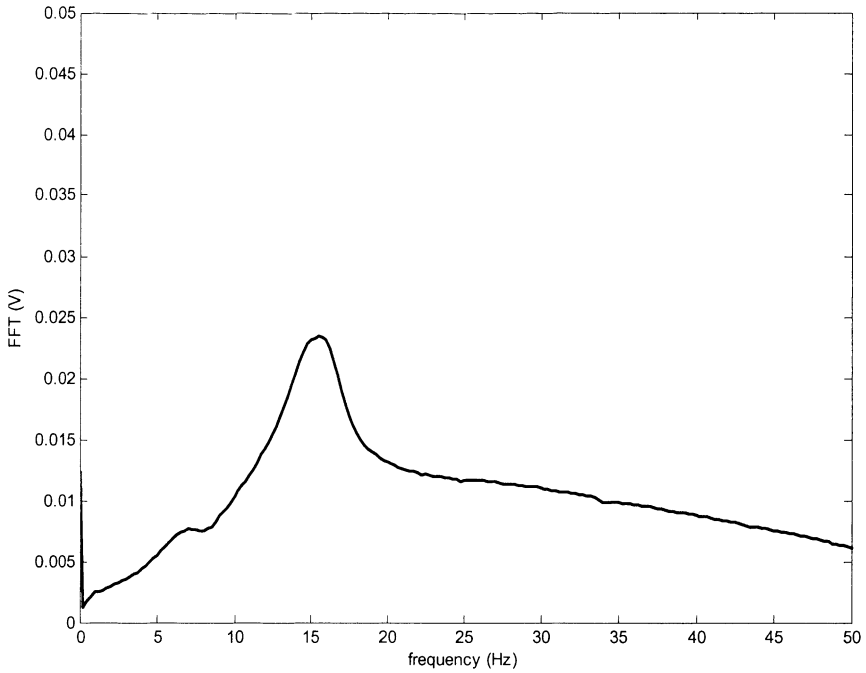

Figure 9.12. Frequency domain of the signal recorded by Analyser, at I=5.75A

It is noted that for this magnetic field circuit the input current can only be tested for

I=5.75A, because at this current, the coil is hot so that it is not permissible to test with higher current.

By varying the input current from 0-5.75A, the ATVA frequency is measured. The comparison of ATVA frequency between the design and the experiment is shown in Figure 9.13. It is noted that the ATVA designed frequency was calculated from the designed parameters and shown in Figure 8.16 in Chapter 8.

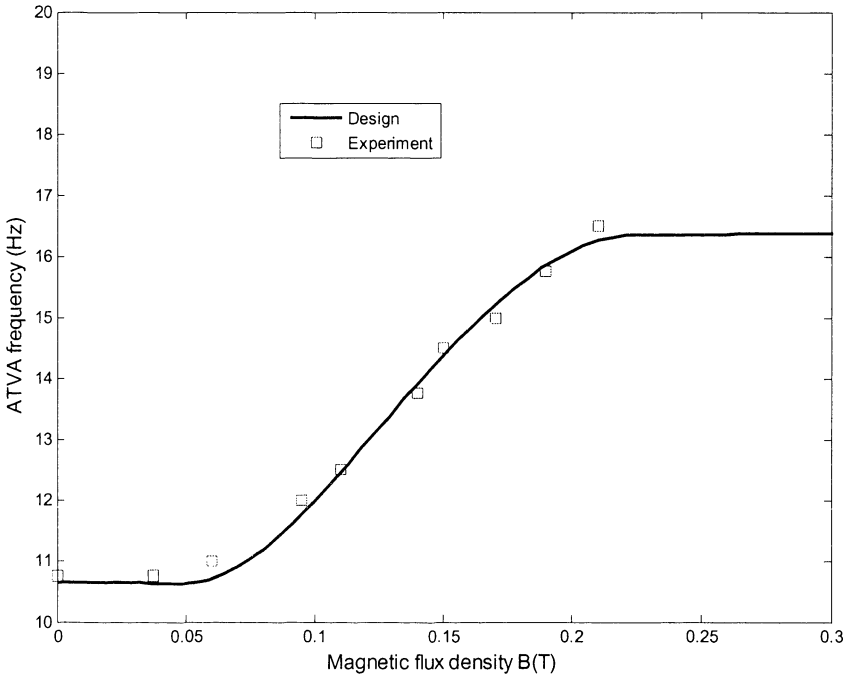

Figure 9.13. ATVA frequency relative to magnetic flux density B

It can be seen that the ATVA frequencies for both experimental data and the design are in a good agreement. The ATVA frequency range is from 10.75 to 16.5Hz. In other words, the relative change in the frequency is 53%. Also, it can be seen that the maximum frequency 16.5 Hz is measured at magnetic flux density B=0.21Tesla (at input current I=5.75A). The result as shown in Figure 9.13 confirms that the MRE-based ATVA is tunable in a frequency range [10.75 to 16.5Hz] and this frequency range is suitable for the UTS powertrain test rig, which will be discussed in section 9.4.

For more convenience and from the relationship between magnetic flux density B and input current in equation (9.2), the dependence of ATVA frequency on input current is shown in Figure 9.14. It is noted that in Figure 9.14, the solid line stands for the

dependence between the ATVA designed frequency and the input current, as shown in equation (9.2).

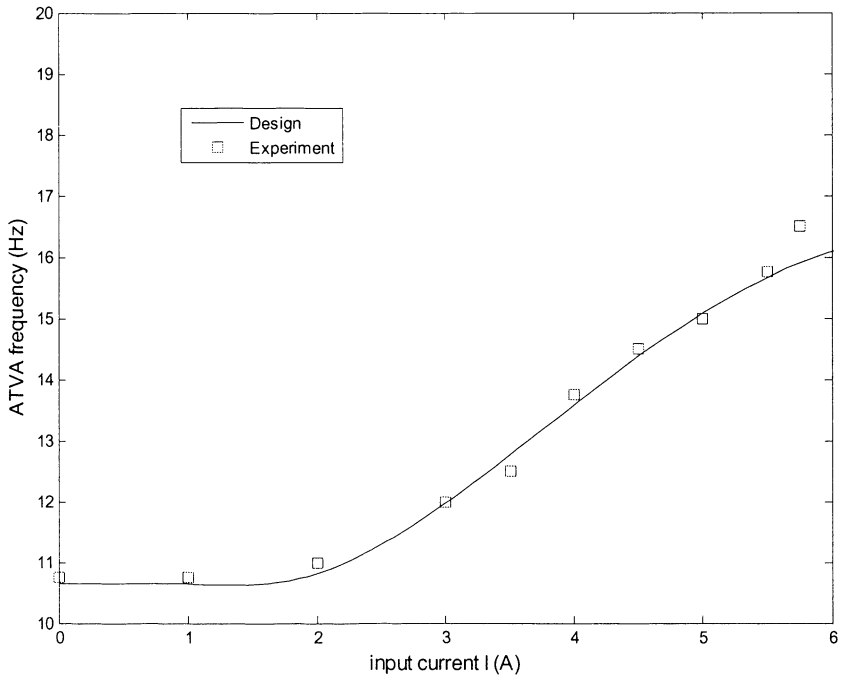

Figure 9.14. Dependence of ATVA frequency on input current I

It is obvious that the relationship between the ATVA frequency and input current I as shown in Figure 9.14 can be used to tune the ATVA frequency. In which, the interval [2-5.75] A is effective for controlling the ATVA frequency because the ATVA frequency increases significantly.

9.4 Measure UTS powertrain modal frequency before and after using the ATVA

9.4.1 Experimental set-up

Similar to the experiment used to measure the ATVA frequency in section 9.3, the experimental set-up for measuring the frequency of the UTS powertrain test rig is shown in Figure 9.15. There is only one difference, in this experiment, namely that, as shown in Figure 9.15, a torque transducer supplied by the Advanced Telemetrics International Company is used to pick up the free vibration of the UTS powertrain test rig instead of the sensor Crossbow CXL01LF1. The torque transducer, which is attached to the propeller shaft of the UTS Powertrain test rig, is used in this experiment because it is more effective for picking up the signal of the entire UTS powertrain vibration than the sensor Crossbow CXL01LF1 attached to ATVA.

It is noted that the torque transducer is connected to channel 1 of the Dynamic Signal Analyser 35665A. Thus, the time signal can be recorded and the frequency domain also obtained by using FFT method with sample time $\Delta t = 1.9531 \times 10^{-3}$ s, the sampling frequency $f_s = \frac{1}{\Delta t}$=256Hz, The display frequency span is 0-100Hz with 400 spectrum lines. Thus the resolution $\Delta f = 0.25$ Hz is obtained. With the configuration, the modal frequency of the UTS powertrain test rig can be measured.

To excite the free vibration of the UTS powertrain test rig, a thin steel bar is attached to the propeller shaft. An impact hammer is used to knock the steel bar. Thus, the free vibration of the powertrain can be excited. The torque transducer will pick up the signal and transfer the signal to channel 1 of the Dynamic Signal Analyser. As a result, the free vibration of the UTS powertrain test rig before and after adding the MRE-based ATVA can be measured.

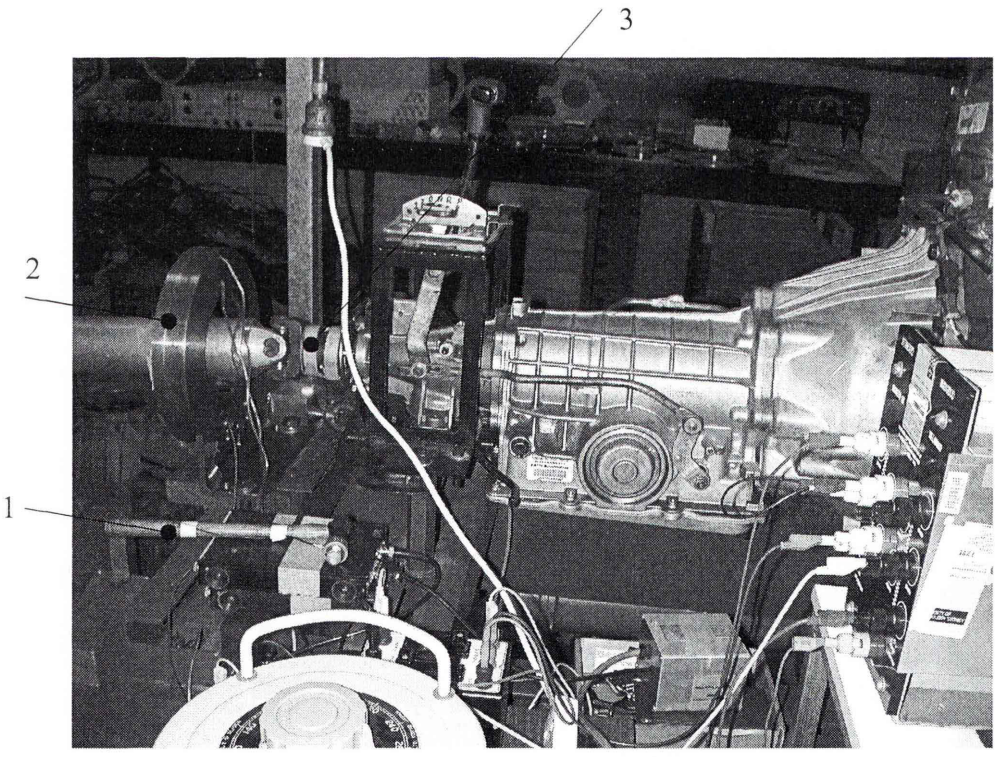

Figure 9.15. Experiment set-up for measuring powertrain modal frequency
1: Hammer; 2: ATVA; 3: Torque transducer

9.4.2 *Experimental results*

The free vibration response of the UTS powertrain test rig before adding the MRE-

based ATVA is shown in Figure 9.16 and the power spectrum is shown in Figure 9.17.

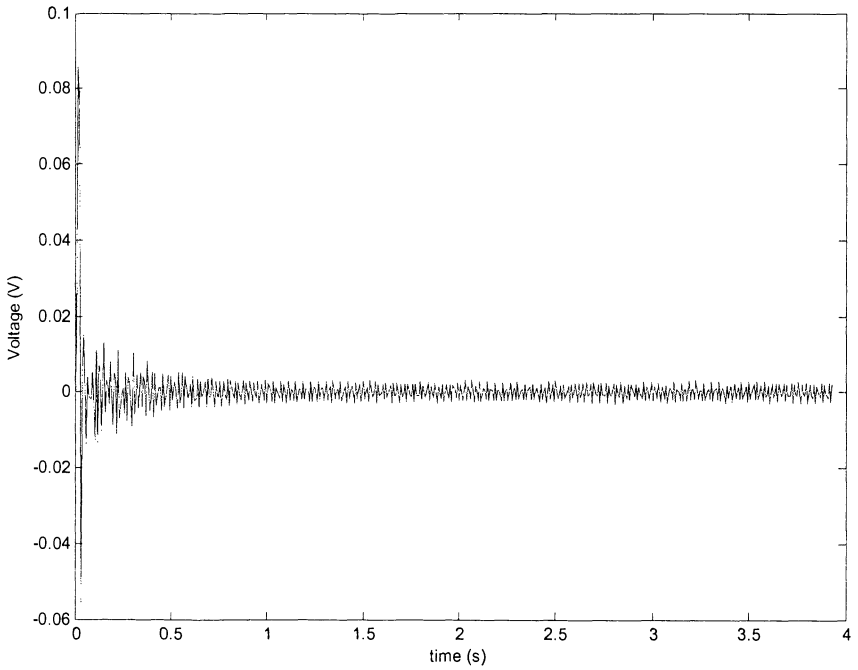

Figure 9.16. Powertrain free vibration response without ATVA

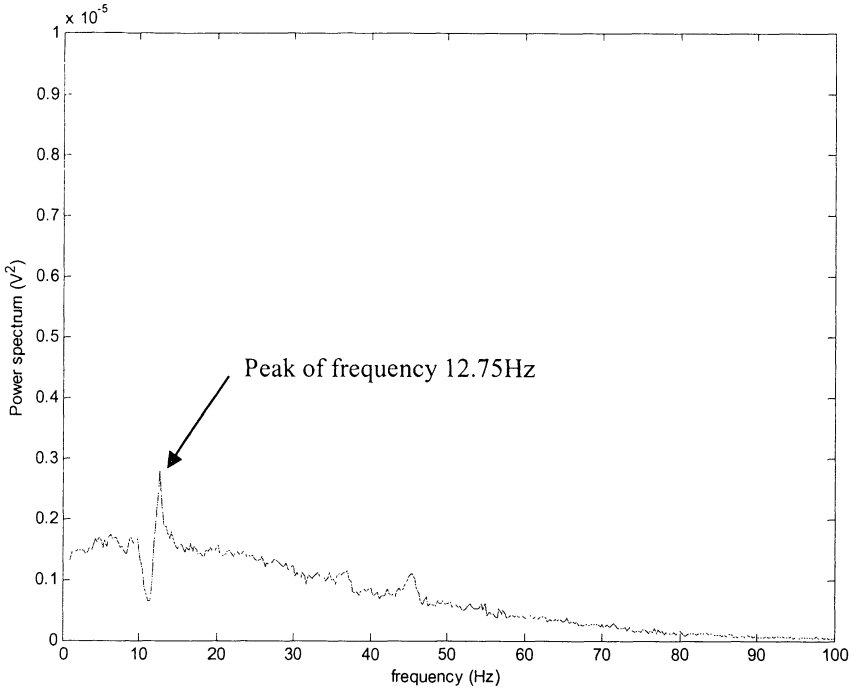

Figure 9.17. Power spectrum of powertrain free vibration response without ATVA

It can be seen that the powertrain fundamental torsional frequency peak is f=12.75Hz. This frequency will be used to validate the effectiveness of the MRE-based ATVA.

To show the ATVA's effectiveness, the ATVA frequency is tuned f_d=12.5Hz (at input current I=3.5A or magnetic flux density B=0.11T). After adding the ATVA, powertrain's free vibration response and its power spectrum are shown on Figures 9.18 and 9.19 respectively.

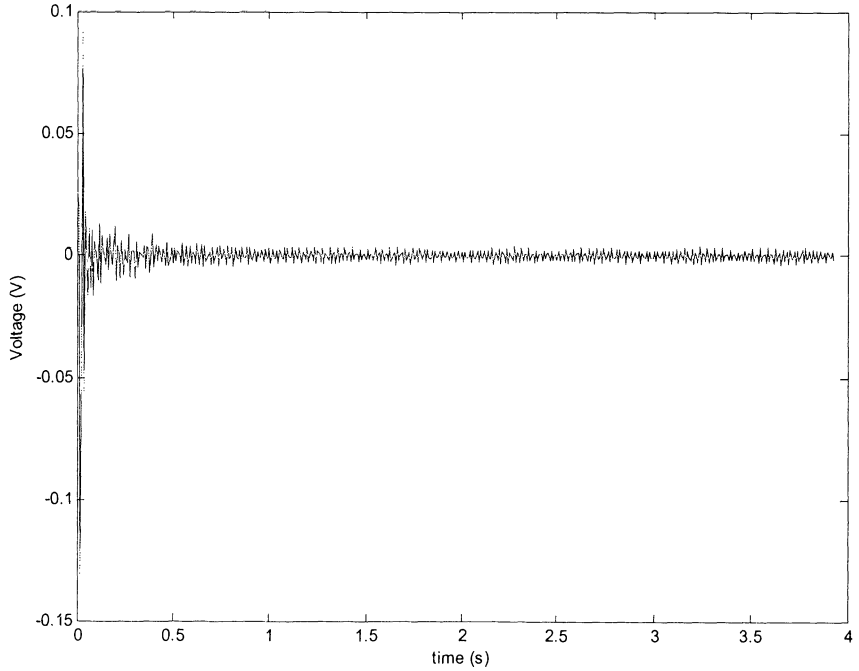

Figure 9.18. Powertrain free vibration response with ATVA

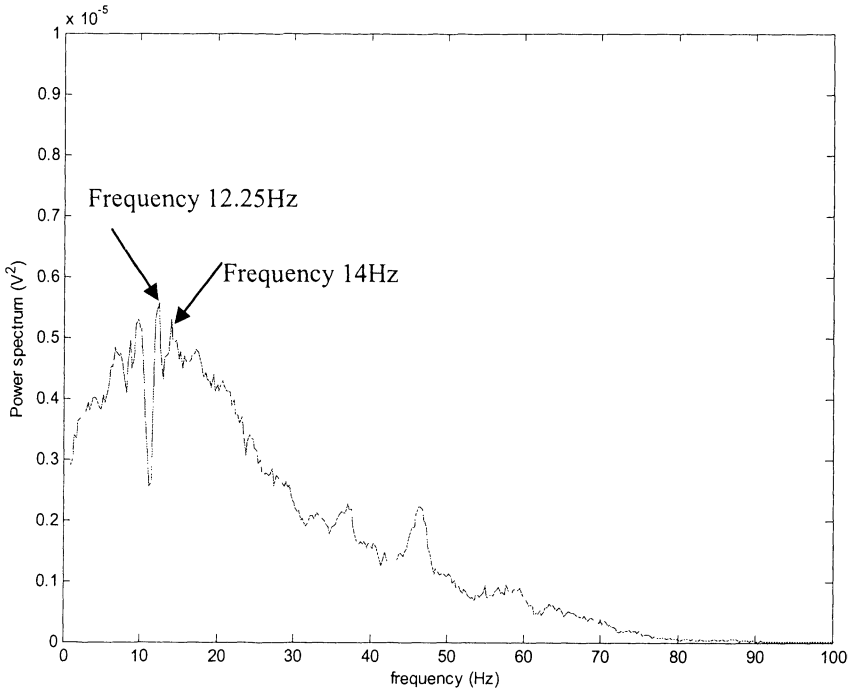

Figure 9.19. Power spectrum of powertrain free vibration response with ATVA

To show the ATVA's effectiveness more clearly, the power spectrum of the free vibration response of the UTS powertrain test rig before and after adding the MRE-based ATVA, from Figures 9.17 and 9.19, is shown in Figure 9.20 to compare.

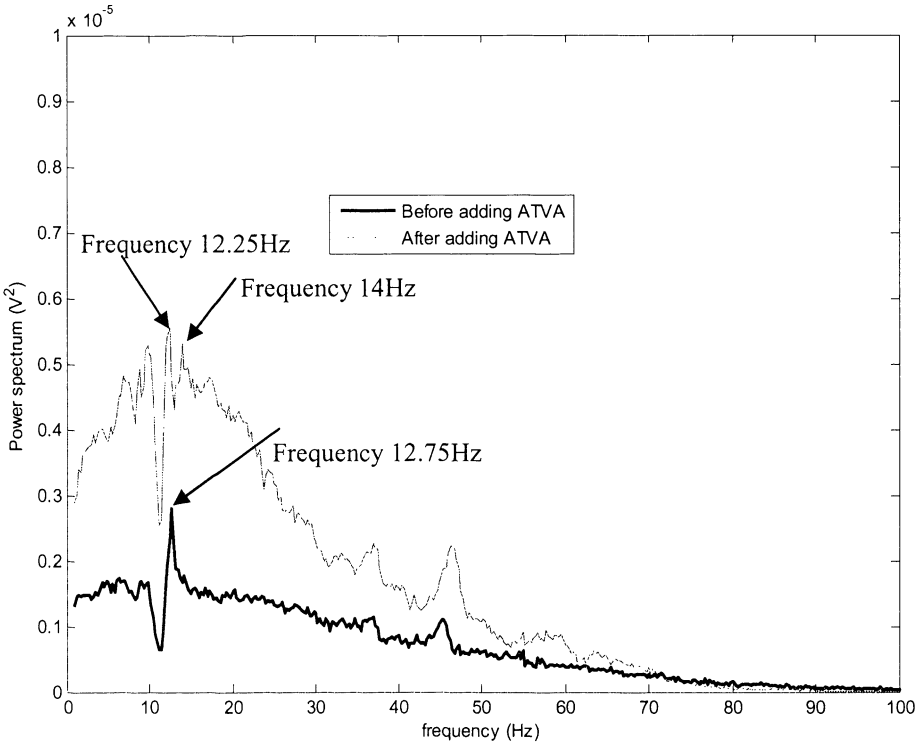

Figure 9.20. Power spectrum of powertrain vibration response with and without ATVA

It can be seen that before adding the ATVA, the powertrain modal frequency f=12.75Hz. After adding the ATVA, two new peaks were introduced, f_1=12.5Hz and f_2=14Hz. This means that the frequency is shifted 0.5Hz and 1.25Hz in the left side and right side respectively of the original frequency. This confirms that the ATVA works effectively. It is also noted that the ATVA inertia is much smaller than that of the transmission. Thus, the frequency of the UTS powertrain test rig can be shifted more if the ATVA inertia is increased. This should be done in further testing.

It is also noted that because the two initial conditions for the free vibration of the UTS powertrain test rig before and after adding the MRE-based ATVA are different, only the frequency values, which were shown in Figures 9.17, 9.19 and 9.20, are compared in this experiment. In contrast, the amplitudes of free vibration of the test rig were not compared because the amplitude of the spectra depends on the impact force amplitude.

9.5 Discussion

After the ATVA was developed, experimental testing was conducted to measure the magnetic field of the ATVA, which is produced by an electromagnetic coil. The maximum input current supplied for the magnetic circuit can be up to 10A. However, in this experiment, the maximum current was tested only 5.75A because of the increase of temperature of the coil.

Firstly, the experimental result shows that with the input current I=5.75A, the measured magnetic field in the surface of MREs is 0.21T. It was found that in the range of input current 0-5.75A, the relationship between magnetic flux density B and input current I is linear. In addition the magnetic field produced by the coil is uniform.

Secondly, the ATVA free vibration response is measured, and the ATVA frequency can be obtained. The experimental results show that the ATVA, which was developed in Chapter 8, can work in the frequency range 10.75-16.5Hz under the magnetic field of an electromagnetic coil, which is supplied by a DC current 0-5.75A. The increase in frequency of the ATVA is 53%. This confirms that the MRE-based ATVA is tunable.

Lastly, for input current I=3.5A (at which the magnetic flux density B=0.11T was measured), the original powertrain modal frequency f=12.75Hz was shifted to two new frequencies, f_1=12.25Hz and f_2=14Hz. This confirmed that the ATVA worked effectively. It is noted that the frequency of the test rig can be shifted more if the ATVA inertia is increased as well. This testing should be conducted in further experiments.

9.5.1 The experimental limitations

1. The design was conducted for 0.3T for MRE magnetic flux density; however, in the measured data, the value is only 0.21T at current 5.75A. Although, the higher current can be tested, the temperature increase was not allowed as it may have caused the damage to the MRE-based ATVA.

2. The MRE samples should be cut to fit in the gap to make sure that these samples work in the longitudinal direction only. If the working mode of MRE samples is a

combination of shear and longitudinal mode, the ATVA frequency may not be correct as designed.

3. Because the torsional forced vibration of the UTS powertrain test rig could not be measured in this chapter, the frequency response of the powertrain test rig before and after adding the MRE-based ATVA were not presented in this chapter. It would be useful to confirm the ATVA's effectiveness more convincing, for example, as shown in Figure 5.10 in Chapter 5. To be specific, the torsional vibration of the UTS powertrain test rig at a large number of engine speeds should be measured. At current state, only static test can be conducted. As a result, only modal frequency of the UTS test rig can be measured. To measure the forced vibration of the test rig, there is a need to be equipped for sensors to pick-up sensors to pic up the torsional powertrain vibration when the engine is running. These sensors are been available in Dynamic and Solid Mechanics Laboratory, UTS. The limitation will be overcome if such sensors are equipped and the experiment can be conducted. This should be carried out in a further study.

4. From the input current I=5.75A the temperature increase in the coil is high. Thus, the test can not be conducted for a long time. In fact, a test for measuring the frequency takes less than 100s. This shortcoming can be overcome if the input current is reduced by increasing the number of turns of the coil. The increase in number of turns of the coil should be conducted in future tests.

5. At a high current of electromagnetic coil, magnetic forces are applied to the mild steel overlap sheets. Consequently, the outer ring, which is bolted to both overlap sheets, may be pushed out of the concentric location and the vibration between the outer ring and inner ring can not be only torsional vibration.

9.6 Summary

This chapter conducted experimental testing to validate the ATVA's effectiveness for shifting the frequency of the UTS powertrain test rig. The ATVA frequency which depends on the magnetic field supplied by a DC current was experimentally validated. The experimental results show that the frequency range of the MRE-based ATVA is

from 10.75 to 16.5Hz (the relative increase in frequency is 53%). It was found that both predicted and experimental data are in a good agreement. To investigate the ATVA's effectiveness, the frequency of the UTS powertrain test rig before and after adding the MRE-based ATVA was measured and compared. The measured results confirm that the ATVA works effectively because the fundamental frequency of the UTS powertrain test rig was shifted from the original frequency 12.75Hz to be two new frequencies 12.25 and 14Hz with ATVA frequency f=12.5Hz tuned (at the input current I=3.5A).

Chapter 10 SUMMARY, CONCLUSIONS AND RECOMMENDATIONS

10.1 Summary of thesis

The content of this thesis is summarised as follows:

Chapter 1:

A brief introduction to the thesis was presented and the project definition including motivation, objectives and contributions of this work were outlined. The methods used to achieve the objectives of the thesis were also presented in this chapter.

Chapter 2:

A literature survey was conducted in Chapter 2. Key research topics relating to torsional vibration, the powertrain and powertrain vibration were provided. The MRE, a smart material, was introduced as a promising material for developing ATVAs, on which a great deal of MRE research was provided. In addition, the detailed review of ATVAs using MREs was conducted and the gaps in research knowledge were identified.

Chapter 3:

Fundamental characteristics of MRE were presented and the MRE properties such as stiffness and damping, which are two main factors for the mechanical vibration problem, were examined. In addition, the equivalent stiffness of MRE samples was provided for mechanical vibration problems.

Chapter 4:

The mathematical background of traditional TVAs was summarised in this chapter. The equation of motion for TVAs with and without damping was derived. The harmonics responses of the primary system and dynamic absorbers were determined and the effectiveness of TVAs was investigated. This chapter also presented the optimal parameters of TVA.

Chapter 5:

The principal concept of the thesis was examined by using numerical simulations in Chapter 5. A concept design of torsional ATVA using a soft MRE was proposed. With the proposed design, the MRE-based ATVA can work in a frequency range around 7 to 70Hz. Also, a simplified model of a powertrain was presented to numerically investigate the effectiveness of the MRE-based ATVA. It was found that the ATVA works effectively because the powertrain frequencies were shifted away from the resonant frequency; thus, the forced vibration of the powertrain was reduced significantly. In addition, the influence of ATVA parameters, such as inertia, damping and stiffness, on its effectiveness was investigated. Furthermore, the effect of locating the MRE-based ATVA, at different points in the powertrain, was examined.

Chapter 6:

The application of a dual MRE-based ATVA for powertrain system vibration control under multi-frequency excitation was simulated in Chapter 6. The dual ATVA consists of two single ATVAs with frequency ranging from 7-70Hz. The frequency of the dual ATVA can be tuned to deal with multi resonances occurring at the same time. With the ATVA, powertrain frequencies were shifted away from the resonant frequencies. As a result, the resonances were removed by using the dual ATVA.

Chapter 7:

Numerical simulations were conducted in Chapter 7 to validate the effectiveness of ATVA for powertrain vibration control under the acceleration of the engine which is different from the steady state in that the excitation frequency in the transient state varies with the time. In the transient state, the excitation frequency varies from 20 to 40Hz. As a result, the excitation frequency passes through powertrain modal frequency

f=28.5814Hz and powertrain transient response increases significantly. By using the MRE-based ATVA, the powertrain modal frequency can be moved away from the resonant area for the entire transient process. Thus, the transient vibration of powertrain is reduced significantly.

Chapter 8:

This chapter presented a proposed design of the MRE-based ATVA for the UTS powertrain test rig. The MRE used to develop the ATVA were experimentally tested to measure Young's modulus and damping ratio. Under the magnetic field 0.35 Tesla, the Young's modulus increase from 114.2 to 270.9kPa and the damping ratio is between 0.126 and 0.14. From the measured properties of a MRE and UTS powertrain specifications, both ATVA mechanical and magnetic parameters were designed. With ATVA designed parameters, the frequency range of the ATVA was presented. It was found that the ATVA frequency can be tuned effectively if the magnetic flux density varied from 0.1 to 0.2T.

Chapter 9:

Experimental testing to validate the ATVA's effectiveness was presented in this chapter. After the MRE-based ATVA was built, experimental testing was conducted to measure the frequency range of the ATVA. The experimental results show that the MRE-based ATVA can work from 10.75 to 16.5Hz. UTS powertrain test rig was experimentally investigated to show the ATVA's effectiveness. In the experimental validation, the free vibration of the test rig before and after adding the MRE-based ATVA was measured. In this way, the frequency of the UTS powertrain test rig could be obtained. The experimental results confirm that the ATVA works effectively because the frequency of the UTS powertrain test rig was shifted away from the resonant frequency.

10.2 Contributions of this thesis

Objectives of this thesis defined in Chapter 1 were achieved. The results are summarised below:

1. *To gain a comprehensive understanding of relevant research topics by investigation into previous research to identify the gap in current knowledge.*

This task was achieved through an extensive literature review that was conducted on several relevant research topics. Previous research about torsional vibration, powertrains and their vibration was reviewed. In addition, the study on MREs and application of MREs for developing ATVAs was investigated. From the review, the gap in current knowledge was highlighted. As a result, research definitions were established (Chapter 2).

2. *To numerically investigate the MRE-based ATVA's effectiveness for powertrain vibration for both steady and transient states. Also, the application of ATVA for powertrain vibration reduction in single or multi-frequency excitation is examined.*

This task was achieved through numerical simulations to evaluate the ATVA's effectiveness for vibration control of powertrain for both the steady state and transient states.

Firstly, a concept design of ATVA using a soft MRE was proposed and the ATVA's effectiveness was numerically investigated for vibration steady state control of the powertrain with a single harmonic excitation torque (Chapter 5 and Appendixes A1, A2, A3, A5 and A6). It was found that with a soft MRE, the ATVA can work in a frequency range around 7-70Hz. As a result, the ATVA frequency can be tuned for shifting powertrain modal frequency away from the resonant frequency and powertrain steady state vibration can be significantly reduced.

Secondly, the usage of dual ATVAs for dealing with multi-resonances at the same time was investigated (Chapter 6, Appendixes A1 and A4). By using a dual ATVA, which consists of two single MRE-based ATVAs at two different locations in a powertrain system, all resonances occurring in all vibration modes of powertrain can be removed. In particular, the modal frequencies of the dual ATVA can be tuned to deal with multi resonances occurring at the same time.

Finally, the application of ATVA for dealing with the resonance in the transient state, which has time-varying excitation frequency, was numerically examined

(Chapter 7 and Appendixes A1 and A7). In the transient state, as the excitation frequency increases from 20 to 40Hz, it passes through the powertrain modal frequency f=28.5814Hz, thus, the resonance occurs and powertrain transient vibration increases significantly. By actively turning the MRE-based ATVA frequency, this frequency of powertrain is shifted far away from the excitation frequency over the transient state. As a result, the powertrain transient vibration is reduced significantly. This confirms the ATVA work effectively.

3. *To measure the mechanical properties of a MRE material. The measured properties of the MRE include Young's modulus and damping ratio. These MRE properties will be used to design an ATVA. Also, theory models of the properties are derived to facilitate the ATVA design.*

This task was achieved through the experimental testing for measuring the properties of a MRE material. To measure the properties of the MRE, a test rig was designed and built. With the test rig, the magnetic field, which is produced by two permanent magnets, could be controlled. As a result, the Young's modulus and damping ratio of the MRE were measured and used to design a MRE-based ATVA for powertrain vibration control. In which, it was found that the Young's modulus increase from 114.2 to 270.9kPa as cubic function of magnetic flux density and the damping ratio increase from 0.126 to 0.142 up to B=0.1T and then decreases slightly to 0.138 until B=0.35T. Thus, proposed models for the experimental data of Young's modulus and damping ratio as functions of magnetic flux density were derived. The derived models and the experimental results are in a good agreement (Chapter 8). The models were used to facilitate the ATVA design.

4. *To propose an ATVA design using the MRE for vibration control of a powertrain test rig at the Dynamics Laboratory, Faculty of Engineering and Information Technology, University of Technology, Sydney (UTS). Accordingly, both mechanical and magnetic parameters are designed.*

This task was achieved through a detailed design of a torsional MRE-based ATVA for vibration control of the UTS powertrain test rig system. With the measured MRE

properties and UTS powertrain specification, a detailed design of MRE-based ATVA was proposed. In which both mechanical and magnetic parameters were determined. Consequently, an actual MRE-based ATVA was manufactured at UTS mechanical workshop (Chapter 8 and Appendix B).

5. *To measure the frequency of the MRE-based ATVA, in which, the dependence of ATVA frequency on magnetic flux density (or electric current) is presented.*

This task was achieved through the experimental testing of ATVA. In which the MRE-based ATVA frequency was measured. As a result, the dependence of ATVA frequency on the magnetic flux density (and the input current as well) was presented. The experimental results show that the ATVA range is from 10.75Hz to 16.5 Hz (The increase in frequency is 53%). The experimental and the designed ATVA frequencies were compared and they are in a good an agreement. This confirmed the ATVA is tunable in the frequency range, which is suitable for the powertrain (Chapter 8).

6. *To conduct the experimental validation to show the ATVA's effectiveness for shifting the frequency of the UTS powertrain test rig.*

This task was achieved through experimental testing of ATVA's effectiveness for UTS powertrain test rig. Firstly, the frequency of powertrain without ATVA was measured. The frequency of the UTS powertrain fitted with the ATVA was also measured and compared. The measured results show that the original frequency of the UTS powertrain test rig f=12.75Hz shifted to two new frequencies 12.25 and 14Hz after the ATVA was added to the test rig. This confirms that the ATVA works effectively (Chapter 9).

10.3 Recommendation for further studies

There are several research areas for further studies for both numerical simulation and experimental testing.

1. There is a need to use a MRE which has larger MR effect to test for developing MRE-based ATVA, because the ATVA works effectively in a frequency range from 10.75 to 16.5Hz (the increase in frequency is only 53%). This means that

the MRE used to validate the ATVA's effectiveness has the same MR effect as that of traditional MREs. With a MRE of a newer generation, the MRE-ATVA will be able to work in a wider frequency range.

2. Although it was experimentally validated that the powertrain modal frequency can be shifted by using the MRE-based ATVA, there is a benefit from testing the MRE-based ATVA for measuring the forced vibration of powertrain torsional vibration over a frequency range of excitation frequency (or over a range of powertrain engine speed). The frequency response of powertrain vibration over a frequency range should be further demonstrated.

3. The magnetic circuit of the ATVA should be improved to produce a magnetic field with higher magnetic flux density. There are two ways to do this. Firstly, the number of turns of the coil should be increased. In this way, the current may be reduced and the temperature rise will not be a problem. Secondly, the gap between the coil and the mild steel core should be reduced.

4. It would be useful to build an equivalent MDOF model of the UTS powertrain test rig, in which a number of powertrain fundamental frequencies are investigated. In other words, an equivalent model should be proposed from a real powertrain system. In the equivalent model, it may be that only the global modes of powertrain system are remained and local modes can be ignored. To do this, the compensation method could be used to build the equivalent model. The experiment testing and numerical method can be compared to show the ATVA's effectiveness.

5. It would be useful if the ATVA's effectiveness for transient vibration control of the UTS powertrain test rig can be experimentally validated during acceleration of the engine, in which the powertrain transient responses should be measured. In addition, experimental testing for multi ATVAs should be conducted.

6. The optimisation of ATVA parameters to obtain the optimal performance in experimental validation should be examined. To be specific, the input current

should be tuned to obtain ATVA frequency around 12.5Hz (at I=3.5A). For example, the shifting frequency of the UTS powertrain test rig should be conducted at several ATVA frequencies such as f=12, 12.25, 12.5, 12.75 and 13Hz to obtain the optimal value. This should be carried out in further testing.

Appendix A

Determination of powertrain vibration features

The equation of motion of the system in matrix form can be expressed as follows:

$$\mathbf{J}\ddot{\boldsymbol{\theta}} + \mathbf{C}\dot{\boldsymbol{\theta}} + \mathbf{K}\boldsymbol{\theta} = \mathbf{T} \tag{A.1}$$

The equation (A.1) can be obtained by using the Lagrange equation; the equation of the motion of the system can be expressed as below, [7]:

$$\frac{d}{dt}\left(\frac{\partial T}{\partial \dot{\theta}_i}\right) - \frac{\partial T}{\partial \theta_i} + \frac{\partial R}{\partial \dot{\theta}_i} + \frac{\partial V}{\partial \theta_i} = T_i \tag{A.2}$$

In which:

T: kinetic energy of the system, V: potential energy of the system

R: is the dissipation function, T_i : generalized force (torque) corresponding to the i^{th} generalized coordinate θ_i .

A1. Equation motion of powertrain without ATVA

The equation of motion of the powertrain which is expressed in equation (5.1) is explained in detail. It is noted that the model of the powertrain is shown in Figure (5.3).

With the parameters in Figure 5.3, the kinetic energy:

$$T = \frac{1}{2}J_1\dot{\theta}_1^2 + \frac{1}{2}J_2\dot{\theta}_2^2 + \frac{1}{2}J_3\dot{\theta}_3^2 + \frac{1}{2}J_4\dot{\theta}_4^2$$

Potential energy:

$$V = \frac{1}{2}k_1(\theta_1 - \theta_2)^2 + \frac{1}{2}k_2(\theta_2 - \theta_3)^2 + \frac{1}{2}k_3(\theta_3 - \theta_4)^2$$

Dissipation function:

$$R = \frac{1}{2}c_1(\dot{\theta}_1 - \dot{\theta}_2)^2 + \frac{1}{2}c_2(\dot{\theta}_2 - \dot{\theta}_3)^2 + \frac{1}{2}c_3(\dot{\theta}_3 - \dot{\theta}_4)^2$$

The generalized force: $T_1 = T_0\sin(\Omega t)$, $T_2 = 0$, $T_3 = 0$ and $T_4 = 0$.

Substitute T, V, R, T_i into equation (A.1), the equation of motion of the powertrain before adding the ATVA can be expressed as:

$$\begin{cases} J_1\ddot{\theta}_1 + k_1(\theta_1 - \theta_2) + c_1(\dot{\theta}_1 - \dot{\theta}_2) = T_1(t) \\ J_2\ddot{\theta}_2 - k_1(\theta_1 - \theta_2) + k_2(\theta_2 - \theta_3) - c_1(\dot{\theta}_1 - \dot{\theta}_2) + c_2(\dot{\theta}_2 - \dot{\theta}_3) = 0 \\ J_3\ddot{\theta}_3 - k_2(\theta_2 - \theta_3) + k_3(\theta_3 - \theta_4) - c_2(\dot{\theta}_2 - \dot{\theta}_3) + c_3(\dot{\theta}_3 - \dot{\theta}_4) = 0 \\ J_4\ddot{\theta}_4 - k_3(\theta_3 - \theta_4) - c_3(\dot{\theta}_3 - \dot{\theta}_4) = 0 \end{cases} \tag{A.3}$$

The equation of motion can be rewritten in the matrix form as (A.1) with the inertial matrix **J** and stiffness and damping matrices, **K** and **C,** have the following forms:

$$\mathbf{J} = \begin{bmatrix} J_1 & 0 & 0 & 0 \\ 0 & J_2 & 0 & 0 \\ 0 & 0 & J_3 & 0 \\ 0 & 0 & 0 & J_4 \end{bmatrix} \tag{A.3}$$

$$\mathbf{K} = \begin{bmatrix} k_1 & -k_1 & 0 & 0 \\ -k_1 & k_1 + k_2 & -k_2 & 0 \\ 0 & -k_2 & k_2 + k_3 & -k_3 \\ 0 & 0 & -k_3 & k_3 \end{bmatrix} \tag{A.4}$$

$$\mathbf{C} = \begin{bmatrix} c_1 & -c_1 & 0 & 0 \\ -c_1 & c_1 + c_2 & -c_2 & 0 \\ 0 & -c_2 & c_2 + c_3 & -c_3 \\ 0 & 0 & -c_3 & c_3 \end{bmatrix} \tag{A.5}$$

where $\boldsymbol{\theta} = [\theta_1\ \theta_2\ \theta_3\ \theta_4]^T$, $\mathbf{T} = [T(t)\ 0\ 0\ 0]^T$ are vectors of generalized coordinates and external torques.

Alternatively

Because in this study, the inertial matrix **J** and stiffness and damping matrices, **K** and **C** are symmetrical, these matrices can be determined directly by the following equations:

$$\mathbf{J} = [J_{ij}] = \left[\frac{\partial^2 T}{\partial \dot{\theta}_i \partial \dot{\theta}_j}\right],\ \mathbf{K} = [k_{ij}] = \left[\frac{\partial^2 V}{\partial \theta_i \partial \theta_j}\right],\ \mathbf{C} = [c_{ij}] = \left[\frac{\partial^2 R}{\partial \dot{\theta}_i \partial \dot{\theta}_j}\right] \tag{A.6}$$

It is straightforward to check the coefficients of inertia matrix **J**:

$J_{11} = J_1, J_{12} = J_{13} = J_{14} = 0; J_{21} = 0,\ J_{22} = J_2, J_{23} = J_{24} = 0; J_{31} = J_{32} = 0,\ J_{33} = 0$

$J_{34} = 0;\ J_{41} = J_{42} = J_{43} = 0,\ J_{44} = J_4;$

The coefficients of stiffness matrix **K**:

$k_{11}=k_1$, $k_{11}=-k_1$, $k_{13}=k_{14}=0$; $k_{21}=-k_1$, $k_{22}=k_1+k_2$, $k_{23}=-k_2$; $k_{24}=0$; $k_{31}=0$, $k_{32}=-k_2$, $k_{33}=k_2+k_3$; $k_{34}=0$; $k_{41}=0$, $k_{42}=0$, $k_{43}=-k_3$; $k_{44}=k_3$.

The coefficients of damping matrix **C**:

$c_{11}=c_1$, $c_{11}=-c_1$, $c_{13}=c_{14}=0$; $c_{21}=-c_1$, $c_{22}=c_1+c_2$, $c_{23}=-c_2$; $c_{24}=0$; $c_{31}=0$, $c_{32}=-c_2$, $c_{33}=c_2+c_3$; $c_{34}=0$; $c_{41}=0$, $c_{42}=0$, $c_{43}=-c_3$; $c_{44}=c_3$.

Consequently, **J**, **K** and **C** are in the form as in equations (A.4) and (A.5).

A2. Equation motion of powertrain with ATVA at location A

If the ATVA is added to the powertrain system as shown in Figure 5.8, the kinetic energy, potential energy and dissipation function of the system can be calculated by:

$$T=\frac{1}{2}J_1\dot{\theta}_1^2+\frac{1}{2}J_2\dot{\theta}_2^2+\frac{1}{2}J_3\dot{\theta}_3^2+\frac{1}{2}J_4\dot{\theta}_4^2+\frac{1}{2}J_A\dot{\theta}_A^2$$

$$V=\frac{1}{2}k_1(\theta_1-\theta_2)^2+\frac{1}{2}k_2(\theta_2-\theta_3)^2+\frac{1}{2}k_3(\theta_3-\theta_4)^2+\frac{1}{2}k_A(\theta_3-\theta_A)^2$$

$$R=\frac{1}{2}c_1(\dot{\theta}_1-\dot{\theta}_2)^2+\frac{1}{2}c_2(\dot{\theta}_2-\dot{\theta}_3)^2+\frac{1}{2}c_3(\dot{\theta}_3-\dot{\theta}_4)^2++\frac{1}{2}c_A(\dot{\theta}_3-\dot{\theta}_A)^2$$

By using the equation (A.6), the inertia matrix, stiffness and damping matrix can be obtained as:

$$\mathbf{J}=\begin{bmatrix} J_1 & 0 & 0 & 0 & 0 \\ 0 & J_2 & 0 & 0 & 0 \\ 0 & 0 & J_3 & 0 & 0 \\ 0 & 0 & 0 & J_4 & 0 \\ 0 & 0 & 0 & 0 & J_A \end{bmatrix} \tag{A.7}$$

$$\mathbf{K}=\begin{bmatrix} k_1 & -k_1 & 0 & 0 & 0 \\ -k_1 & k_1+k_2 & -k_2 & 0 & 0 \\ 0 & -k_2 & k_2+k_3+k_A & -k_3 & -k_A \\ 0 & 0 & -k_3 & k_3 & 0 \\ 0 & 0 & -k_A & 0 & k_A \end{bmatrix} \tag{A.8}$$

$$\mathbf{C}=\begin{bmatrix} c_1 & -c_1 & 0 & 0 & 0 \\ -c_1 & c_1+c_2 & -c_2 & 0 & 0 \\ 0 & -c_2 & c_2+c_3+c_A & -c_3 & -c_A \\ 0 & 0 & -c_3 & c_3 & 0 \\ 0 & 0 & -c_A & 0 & c_A \end{bmatrix} \tag{A.9}$$

A3. Equation motion of powertrain with ATVA at location B

If the ATVA is added to the powertrain system as shown in Figure 5.14, the kinetic energy, potential energy and dissipation function of the system can be calculated by:

$$T = \frac{1}{2}J_1\dot{\theta}_1^2 + \frac{1}{2}J_2\dot{\theta}_2^2 + \frac{1}{2}J_3\dot{\theta}_3^2 + \frac{1}{2}J_4\dot{\theta}_4^2 + \frac{1}{2}J_A\dot{\theta}_A^2$$

$$V = \frac{1}{2}k_1(\theta_1 - \theta_2)^2 + \frac{1}{2}k_2(\theta_2 - \theta_3)^2 + \frac{1}{2}k_3(\theta_3 - \theta_4)^2 + \frac{1}{2}k_A(\theta_2 - \theta_A)^2$$

$$R = \frac{1}{2}c_1(\dot{\theta}_1 - \dot{\theta}_2)^2 + \frac{1}{2}c_2(\dot{\theta}_2 - \dot{\theta}_3)^2 + \frac{1}{2}c_3(\dot{\theta}_3 - \dot{\theta}_4)^2 + +\frac{1}{2}c_A(\dot{\theta}_2 - \dot{\theta}_A)^2$$

By using the equation (A.6), the inertia matrix remains the same as equation (A.7), but the stiffness and damping matrix are determined as:

$$\mathbf{K} = \begin{bmatrix} k_1 & -k_1 & 0 & 0 & 0 \\ -k_1 & k_1 + k_2 + k_A & -k_2 & 0 & -k_A \\ 0 & -k_2 & k_2 + k_3 & -k_3 & 0 \\ 0 & 0 & -k_3 & k_3 & 0 \\ 0 & -k_A & 0 & 0 & k_A \end{bmatrix} \tag{A.10}$$

$$\mathbf{C} = \begin{bmatrix} c_1 & -c_1 & 0 & 0 & 0 \\ -c_1 & c_1 + c_2 + c_A & -c_2 & 0 & -c_A \\ 0 & -c_2 & c_2 + c_3 & -c_3 & 0 \\ 0 & 0 & -c_3 & c_3 & 0 \\ 0 & -c_A & 0 & 0 & c_A \end{bmatrix} \tag{A.11}$$

A4. Equation motion of powertrain with dual ATVA

With the dual ATVA as in shown Figure 6.2, the kinetic energy, potential energy and dissipation function of the system can be calculated by:

$$T = \frac{1}{2}J_1\dot{\theta}_1^2 + \frac{1}{2}J_2\dot{\theta}_2^2 + \frac{1}{2}J_3\dot{\theta}_3^2 + \frac{1}{2}J_4\dot{\theta}_4^2 + \frac{1}{2}J_{A1}\dot{\theta}_{A1}^2 + +\frac{1}{2}J_{A2}\dot{\theta}_{A2}^2$$

$$V = \frac{1}{2}k_1(\theta_1 - \theta_2)^2 + \frac{1}{2}k_2(\theta_2 - \theta_3)^2 + \frac{1}{2}k_3(\theta_3 - \theta_4)^2 + \frac{1}{2}k_{A1}(\theta_3 - \theta_{A1})^2 + +\frac{1}{2}k_{A2}(\theta_2 - \theta_{A2})^2$$

$$R = \frac{1}{2}c_1(\dot{\theta}_1 - \dot{\theta}_2)^2 + \frac{1}{2}c_2(\dot{\theta}_2 - \dot{\theta}_3)^2 + \frac{1}{2}c_3(\dot{\theta}_3 - \dot{\theta}_4)^2 + \frac{1}{2}c_{A1}(\dot{\theta}_3 - \dot{\theta}_{A1})^2 + +\frac{1}{2}c_{A2}(\dot{\theta}_2 - \dot{\theta}_{A2})^2$$

By using the equation (A.6), the inertia matrix, stiffness and damping matrix can be

obtained as:

$$\mathbf{J}=\begin{bmatrix} J_1 & 0 & 0 & 0 & 0 & 0 \\ 0 & J_2 & 0 & 0 & 0 & 0 \\ 0 & 0 & J_3 & 0 & 0 & 0 \\ 0 & 0 & 0 & J_4 & 0 & 0 \\ 0 & 0 & 0 & 0 & J_{A1} & 0 \\ 0 & 0 & 0 & 0 & 0 & J_{A2} \end{bmatrix} \tag{A.12}$$

$$\mathbf{K}=\begin{bmatrix} k_1 & -k_1 & 0 & 0 & 0 & 0 \\ -k_1 & k_1+k_2+k_{A2} & -k_2 & 0 & 0 & -k_{A2} \\ 0 & -k_2 & k_2+k_3+k_{A1} & -k_3 & -k_{A1} & 0 \\ 0 & 0 & -k_3 & k_3 & 0 & 0 \\ 0 & 0 & -k_{A1} & 0 & k_{A1} & 0 \\ 0 & -k_{A2} & 0 & 0 & 0 & k_{A2} \end{bmatrix} \tag{A.13}$$

$$\mathbf{C}=\begin{bmatrix} c_1 & -c_1 & 0 & 0 & 0 & 0 \\ -c_1 & c_1+c_2+c_{A2} & -c_2 & 0 & 0 & -c_{A2} \\ 0 & -c_2 & c_2+c_3+c_{A1} & -c_3 & -c_{A1} & 0 \\ 0 & 0 & -c_3 & c_3 & 0 & 0 \\ 0 & 0 & -c_{A1} & 0 & c_{A1} & 0 \\ 0 & -c_{A2} & 0 & 0 & 0 & c_{A2} \end{bmatrix} \tag{A.14}$$

A5. Solution to free vibration of powertrain

Let N be the number of degrees of freedom of a system, which has the EOMs as in equation (A.1). The free vibration of the powertrain can be obtained by solving the following equation:

$$\mathbf{J}\ddot{\boldsymbol{\theta}}+\mathbf{C}\dot{\boldsymbol{\theta}}+\mathbf{K}\boldsymbol{\theta}=\mathbf{0} \tag{A.15}$$

For convenience, equation (A.15) can be expressed as:

$$\dot{\mathbf{z}}=\mathbf{A}\mathbf{z} \tag{A.16}$$

With $\mathbf{z}=[\boldsymbol{\theta}\ \ \dot{\boldsymbol{\theta}}]^{\mathrm{T}}$ is the state vector, matrix $\mathbf{A}$ is called the system matrix

$$\mathbf{A}=\begin{bmatrix} \mathbf{0} & \mathbf{I} \\ -\mathbf{J}^{-1}\mathbf{K} & -\mathbf{J}^{-1}\mathbf{C} \end{bmatrix} \tag{A.17}$$

Here $\mathbf{I}$ is the identity matrix sizes N×N.

The solution for equation (A.16) can be predicted in this form $\mathbf{z} = \mathbf{z}_0 e^{\lambda t}$. Thus, equation (A.16) becomes:

$$[\mathbf{A} - \lambda\mathbf{I}]\mathbf{z}_0 = \mathbf{0} \tag{A.18}$$

To make sure the equation (A.18) has non-zero solutions, the determinant of system matrix is equal to zero:

$$\det[\mathbf{A} - \lambda\mathbf{I}] = 0 \tag{A.19}$$

By solving equation (A.19), mechanical vibration features of the powertrain can be obtained. The features include powertrain natural frequencies, damped natural frequencies, damping ratios and powertrain mode shapes.

The j^{th} root of eigenvalues can be expressed in complex form:

$$\lambda_j = h_j \pm i\omega_{dj} \tag{A.20}$$

$$\omega_{nj} = \sqrt{h_j^2 + \omega_{dj}^2} \tag{A.21}$$

$$\varsigma_j = \frac{-h_j}{\omega_{nj}} \tag{A.22}$$

j=1..N and $i = \sqrt{-1}$.

It is noted that the mode shapes of the mechanical system in equation (A.15) can also be obtained from eigenvector of equation (A.18).

To solve equation (A.18), it is convenient to use the Matlab software; more detail can be seen in references [100, 101].

A6. Solution to steady state response of powertrain under harmonic excitation

If the powertrain, which has the EOMs as in equation (A.1), is under the excitation of a harmonics with magnitude and frequency are T_0 and Ω, respectively, the forced vibration response of the powertrain can be calculated by using the complex magnitude method as follows:

The particular solutions of equation (A.1) can be determined by using the complex form: $\boldsymbol{\theta} = \boldsymbol{\Theta} e^{i\Omega t}$, $\mathbf{T} = \mathbf{T}_0 e^{i\Omega t}$. Equation (A.1) will be rewritten as:

$$\mathbf{J}\ddot{\boldsymbol{\theta}} + \mathbf{C}\dot{\boldsymbol{\theta}} + \mathbf{K}\boldsymbol{\theta} = \mathbf{T}_0 e^{i\Omega t} \tag{A.23}$$

The steady vibration responses of powertrain are determined by:

$$\theta = \mathrm{Re}(\boldsymbol{\Theta})\cos(\Omega t) - \mathrm{Im}(\boldsymbol{\Theta})\sin(\Omega t) \tag{A.24}$$

With $\boldsymbol{\Theta}$ is the vector of complex magnitude and it can be calculated by:

$$\boldsymbol{\Theta} = [-\Omega^2\mathbf{J} + i\Omega\mathbf{C} + \mathbf{K}]^{-1}\mathbf{T}_0 = \mathbf{R}\mathbf{T}_0 \tag{A.25}$$

$\mathbf{R} = \mathbf{R}(i\Omega) = [-\Omega^2\mathbf{J} + i\Omega\mathbf{C} + \mathbf{K}]$ is called as matrix of transfer functions.

Equation (A.24) is the solution for steady state vibration of powertrain under a single harmonics excitation. If there are more than one harmonics in the vector of excitation torque, the total responses of powertrain will be the combination of each separated component, which is calculated from equation (A.24). More detail of solving the equation of motion under harmonics excitations can be seen in reference [101].

A7. Solution to transient response of powertrain using numerical integration

In the general case of excitation torque, the forced vibration response of powertrain must be solved by a numerical method. In this case, the equation (A.1) is rewritten in the following form:

$$\begin{bmatrix}\dot{\theta}\\ \ddot{\theta}\end{bmatrix} = \begin{bmatrix}[0] & [I]\\ -\mathbf{J}^{-1}\mathbf{K} & -\mathbf{J}^{-1}\mathbf{C}\end{bmatrix}\begin{bmatrix}\theta\\ \dot{\theta}\end{bmatrix} + \begin{bmatrix}[0] & [0]\\ [0] & -\mathbf{J}^{-1}\end{bmatrix}\begin{bmatrix}0\\ \mathbf{T}\end{bmatrix} \tag{A.26}$$

Or:

$$\dot{\mathbf{z}} = \mathbf{A}\mathbf{z} + \mathbf{B}\mathbf{q}(\mathbf{t}) \tag{A.27}$$

In which **A** is the system matrix, **z** is the state vector

$$\mathbf{B} = \begin{bmatrix}[0] & [0]\\ [0] & -\mathbf{J}^{-1}\end{bmatrix} \text{ and } \mathbf{q(t)} = \begin{bmatrix}0\\ \mathbf{T}\end{bmatrix}$$

It is noted that the form in equation (A.27) is the standard form for an ODE system. It can be solved directly by using the ODE 45 solver Matlab software. More detail can be seen in reference [102].

It should be noted that if the inertia matrix, stiffness matrix and damping matrix are determined, all mechanical vibration features of the powertrain can be obtained.

Appendix B

Inertia moment of a cylinder with a centred circular hole

To determine the moment of inertia of a cylinder with a centred circular hole, as in Figure 8.14, let m and ρ be the mass and mass density of the cylinder, respectively. From Figure 8.15, the element of mass is expressed as

$$dm = \rho dV = \rho L r dr d\theta \tag{C.1}$$

The inertia of the holed cylinder can be calculated:

$$J_O = \int r^2 dm = \rho L \int_0^{2\pi} \int_{R_i}^{R_o} r^3 dr d\theta = \rho L \int_0^{2\pi} d\theta \int_{R_i}^{R_o} r^3 dr = 2\pi\rho L \int_{R_i}^{R_o} r^3 dr \tag{C.2}$$

It is straightforward to obtain:

$$J_O = \frac{\pi\rho L}{2}(R_o^4 - R_i^4) = \frac{\pi\rho L}{2}(R_o^2 - R_i^2)(R_o^2 + R_i^2) \tag{C.3}$$

It is noted that $m = \pi\rho L(R_o^2 - R_i^2)$ is the mass of the cylinder, thus, the moment of inertia:

$$J_O = \frac{1}{2} m(R_o^2 + R_i^2) \tag{C.4}$$

In two particular cases: if $R_i \approx R_o$ (for thin shell) the equation (C.4) becomes:

$$I_O \approx mR_o^2 \approx mR_i^2 \tag{C.5}$$

If R_i=0 (the cylinder becomes the solid cylinder) the equation (C.4) becomes:

$$J_O = \frac{1}{2} mR_o^2 \tag{C.6}$$

Equations (C.5) and (C.6) are confirmed in classic books of Engineering mechanics such as Meriam and Kraige [103] and Hibbeler [104].

Alternative:

The inertia J_O can be derived by:

$$J_O = J_{solid} - J_{hole} \tag{C.7}$$

It is noted that $m_{solid} = \rho V_{solid}$, $m_{hole} = \rho V_{hole}$, $V_{solid} = \pi R_o^2 L$, $V_{hole} = \pi R_i^2 L$

$$m_{solid} = \frac{V_{solid}}{V} m = m\frac{R_0^2}{R_0^2 - R_i^2}, \quad m_{hole} = \frac{V_{hole}}{V} m = m\frac{R_i^2}{R_0^2 - R_i^2}$$

Thus equation (C.7) is re-arranged to become equation (C.4)

$$J_O = J_{solid} - J_{hole} = \frac{1}{2} m_{solid} R_o^2 - \frac{1}{2} m_{hole} R_i^2 = \frac{1}{2} m\left(\frac{R_0^4 - R_i^4}{R_0^2 - R_i^2}\right) = \frac{1}{2} m(R_o^2 + R_i^2)$$

Appendix C

Publication from this work

International journal papers

C1

Hoang, N., Zhang, N. and Du, H. 2009, 'A dynamic absorber with a soft magnetorheological elastomer for powertrain vibration suppression', Smart Materials and Structures, vol. 18, no. 7, (074009). (Chapter 5)

C2

Hoang, N., Zhang, N. and Du, H. 2011, 'An adaptive tunable vibration absorber using a new magnetorheological elastomer for vehicular powertrain transient vibration reduction', Smart Materials and Structures, vol. 20, no. 1, (015019). (Chapter 7)

C3

Hoang, N., Zhang, N., Li, W.H and Du, H. 2011, 'Development of a torsional dynamic absorber using a magnetorheological elastomer for vibration reduction of a powertrain test rig', Journal of Intelligent Material Systems and Structures, submitted and under review. (Chapter 8 and Chapter 9)

International conference papers

C4

Zhang, N., Hoang, N. and Du, H. 2008, 'A novel dynamic absorber using enhanced magnetorheological elastomers for powertrain vibration control, proceedings of Advanced Materials Research, vol. 1, Hong Kong, China, pp. 117-120. (Chapter 5)

C5

Hoang, N., Zhang, N. and Du, H. 2009, 'The damping effect of magnetorheological elastomers on dynamic absorber for powertrain vibration reduction', The 13th Asia Pacific Vibration Conference, November 22-25, Christchurch, New Zealand, pp. 1-10. (Chapter 5)

C6

Hoang, N., Zhang, N. and Du, H. 2010, 'A dual adaptive tunable vibration absorber using MREs for vehicle powertrain vibration control', SPIE Symposium on Active and Passive Smart Structures and Integrated Systems, volume 7643, March 7-11, San Diego, CA, USA, pp.76430Z. (Chapter 6)

C7

Hoang, N., Zhang, N. and Du, H. 2009, 'An adaptive tunable dynamic absorber using magnetorheological elastomers for vehicle powertrain transient vibration control', 15th Asia Pacific Automotive Engineering Conference, October 26-28, Hanoi, Vietnam, pp.1-6. (Chapter 7)

C8

Hoang, N., Zhang, N., Li, W.H and Du, H. 2010, 'Application of a magnetorheological elastomer to develop a torsional dynamic absorber for vibration reduction of powertrain', The 12th International Conference on Electrorheological (ER) Fluids and Magnetorheological (MR) Suspensions, August 16 - 20, Philadelphia, USA (In press) (Chapter 8 and Chapter 9).

References

[1] Crowther, A.R. 2004, 'Transient vibration in powertrain systems with automatic transmissions', Doctoral thesis, University of Technology, Sydney.

[2] Zhang, N., Crowther, A., Liu, D.K. and Jeyakumaran, J. 2003, 'A finite element method for the dynamic analysis of automatic transmission gear shifting with a four-degree-of-freedom planetary gearset element', Proceedings of the Institution of Mechanical Engineers, Part D: Journal of Automobile Engineering, vol. 217, no. 6, pp. 461-473.

[3] Couderc, P., Callenaere, J., Der Hagopian, J., Ferraris, G., Kassai, A., Borjesson, Y., Verdillon, L. and Gaimard, S. 1998, 'Vehicle driveline dynamic behaviour experimentation and simulation', Journal of Sound and Vibration, vol. 218, pp. 133-157.

[4] Wachel, J.C. and Szenasi, F.R. 1993, 'Analysis of torsional vibrations in rotating machinery', Proceedings of 22nd Turbomachinery Symposium, Texas A&M. University September 13-16, pp. 127-151.

[5] Den Hartog, J.P. 1985, Mechanical vibrations, Dover, p. 436.

[6] William, J.P. 2007, Mechanical vibration, John Wiley & Sons, p. 700.

[7] Rao, S.S. 2004, Mechanical vibrations, Addison-Wesley Publishing, p. 1078.

[8] Kallio, M. 2005, The elastic and damping properties of magneto rheological elastomers, VTT Technical Research Centre of Finland, p. 146.

[9] Carlson, J.D. and Jolly, M.R. 2000, 'MR fluid, foam and elastomer devices', Mechatronics, vol. 10, no. 4-5, pp. 555-569.

[10] Zhou, G.Y. 2003, 'Shear properties of a magneto rheological elastomer', Smart Materials and Structures, vol. 12, pp. 139-146.

[11] Walker, D.N. 2004, Torsional vibration of turbomachinery, McGraw-Hill, p. 189.

[12] Friswell, M.I., Penny, J.E.T., Garvey, S.D. and Lees, A.W. 2010, Dynamics of Rotating Machines, Cambridge University Press, p. 526.

[13] Shaver, R. 1997, Manual Transmission Clutch Systems, The Society of Automotive Engineers, p. 191.

[14] Kienckle, U. and Nielsen, L. 2000, Automotive Control Systems for Engine, Driveline and Vehicle, Springer, p. 412.

[15] Crouse, W.H. 1971, Automotive Transmissions and Power Trains, McGrav-Hill, p. 466.

[16] Larew, W.B. 1966, Automatic Transmissions, Chilton, p. 209.

[17] Gillespie, T.D 1999, Fundamentals of Vehicle Dynamics, The Society of Automotive Engineers, p. 495.

[18] 'How Manual Transmissions Work', viewed 20-11 2010 <http://auto.howstuffworks.com/transmission1.htm>

[19] Reik, W. 1990, 'Torsional Vibration in the drive train of Motor Vehicles Principle Considerations', 4th International Symposium on Torsional Vibration in the drive train, 20 April, Baden-Baden, Germany, pp. 5-28.

[20] Reik, W. 1990, 'Torsional Vibration Isolation in the Drive Train, An Evaluative Study', 4th International Symposium on Torsional Vibration in the drive train, 20 April, Baden-Baden, Germany, pp. 125-146.

[21] Karl, K. 1990, 'Torsional vibrations in Tractor Drive Trains damping options', 4th International Symposium on Torsional Vibration in the drive train, 20 April, Baden-Baden, Germany, pp. 29-54.

[22] Schnurr, M. 1990, 'Development of Super-Long-Travel Dual Mass Flywheel', 4th International Symposium on Torsional Vibration in the drive train, 20 April, Baden-Baden, Germany, pp. 55-80.

[23] Albers, A. 1990, 'Torque Control Isolation (TCI) The Smart Clutch', 4th International Symposium on Torsional Vibration in the drive train, 20 April, Baden-Baden, Germany, pp. 81-107.

[24] Maucher, P. 1990, 'Clutch chatter', 4th International Symposium on Torsional Vibration in the drive train, 20 April, Baden-Baden, Germany, pp. 109-124.

[25] Hwang, S.J., Chen, J.S., L, L. and Ling, C.C. 2000, 'Modelling and simulation of a powertrain-vehicle system with automatic transmission', International Journal of Vehicle Design, vol. 23, pp. 145-160.

[26] Wang, M. 2002, 'Design and torsional vibration analysis of a complex vehicle powertrain system test rig', Master thesis, University of Technology, Sydney.

[27] Fredriksson, J., Weiefors, H. and Egardt, B. 2002, 'Powertrain Control for Active Damping of Driveline Oscillations', Vehicle System Dynamics, vol. 37, no. 5, pp. 359-376.

[28] Imtiaz, A. 1999, 'Feasibility of utilizing active control to minimize torsional vibration of drivelines ', Doctorage thesis, University of Cincinnati Ohio, the USA.

[29] Schankin, D.P., Ranex, M.N. and Sagady, D.V. 2006, Torsional active vibration

control system – US Patent 7004291 B2, pp. 1-7.

[30] 'Dampers for powertrain' 2011, Dampers for powertrain, viewed 1-1 2011 http://www.luk.de/content.luk.de/en/products/dampers/dampers.jsp

[31] Sun, J., Jolly, M. and Norris, M.A. 1995, 'Passive, adaptive and active tuned vibration absorbers—a survey', Journal of Vibration and Acoustics vol. 117, pp. 234-242.

[32] Ram, Y.M. and Elhay, S. 1996, 'The theory of the multi-degree-of-freedom dynamic absorber', Journal of Sound and Vibration, vol. 95, pp. 607-615.

[33] Hadi, M.N.S. and Arfiadi, Y. 1998, 'Optimum design of absorber for MDOF structures', Journal of Structural Engineering, vol. 124 pp. 1272-1280.

[34] Ozer, M.B. and Royston, T.J. 2005, 'Extending Den Hartog's vibration absorber technique to multi-degree-of-freedom systems', Journal of Vibration and Acoustics, vol. 127, pp. 341-350.

[35] Ozer, M.B. and Royston, T.J. 2005, 'Application of Sherman-Morrison matrix inversion formula to damped vibration absorbers attached to multi-degree of freedom systems', Journal of Sound and Vibration, vol. 283, pp. 1235-1249.

[36] Kitis, L., Wang, B.P. and Pilkey, W.D. 1983, 'Vibration reduction over a frequency range', Journal of Sound and Vibration, vol. 89, pp. 559-569.

[37] Asami, T., Nishihara, O. and Baz, A.M. 2002, 'Analytical solutions to H∞ and H2 optimization of dynamic vibration absorbers attached to damped linear systems', Journal of Vibration and Acoustics, vol. 124, no. 2, pp. 284-295.

[38] Vakakisa, A.F. and Paipetisa, S.A. 1986, 'The effect of a viscously damped dynamic absorber on a linear multi-degree-of-freedom system', Journal of Sound and Vibration, vol. 105, no. 2, pp. 49-60

[39] Agnes, G.S. and Inman, D.J. 2001, 'Performance of Nonlinear Vibration Absorbers for Multi-Degrees-of-Freedom Systems Using Nonlinear Normal Modes', Nonlinear Dynamics, vol. 25, pp. 275-292.

[40] M. J. Brennan, M.J. and Dayou, J. 2000, 'Global control of vibration using a tunable vibration neutralizer', Journal of Sound and Vibration vol. 232, no. 3, pp. 585-600.

[41] Bonello, P., Brennan, M.J. and Elliott, S.J. 2005, 'Vibration control using an adaptive tuned vibration absorber with a variable curvature stiffness element', Smart Materials and Structures, vol. 14, pp. 1055-1065.

[42] Davis, C.L. and Lesieutre, G.A. 2000, 'An actively tuned solid-state vibration absorber using capacitive shunting of piezoelectric stiffness', Journal of Sound and Vibration, vol. 232, no. 3, pp. 601-617.

[43] Franchek, M.A., Ryan, M.W. and Bernhard, R., J 1995, 'Adaptive-passive vibration control', Journal of Sound and Vibration, vol. 189 (5), pp. 565-585.

[44] Flatau, A.B., Dapino, M.J. and Calkins, F.T. 2000, 'High bandwidth tunability in a smart vibration absorber', Journal of Intelligent Material Systems and Structures, vol. 11, no. 12, pp. 923-929

[45] Walsh, P.L. and Lamancusa, J.S. 1992, 'A variable stiffness vibration absorber for minimization of transient vibrations', Journal of Sound and Vibration, vol. 158, pp. 195-211.

[46] Williams, K.A., Chiu, G.T.C. and Bernhard, R.J. 2001, Vibration absorber using shape memory material, US Patent 6,290,037 B1, p. 17.

[47] Williams, K., Chiu, G. and Bernhard, R. 2002, 'Adaptive-passive absorbers using shape-memory', Journal of Sound and Vibration, vol. 249, no. 5, pp. 835-848.

[48] Williams, K.A., Chiu, G.T.-C. and Bernhard, R.J. 2005, 'Dynamic modelling of a shape memory alloy adaptive tuned vibration absorber', Journal of Sound and Vibration vol. 280, pp. 211-234.

[49] Rustighi, E., Brennan, M.J. and Mace, B.R. 2005, 'Real-time control of a shape memory alloy adaptive tuned vibration absorber', Smart Materials and Structures, vol. 14, pp. 1184.

[50] Liu, B., Li, W.H., Kosasih, P.B. and Zhang, X.Z. 2006, 'Development of an MR-brake-based haptic device', Smart Materials and Structures, vol. 15, pp. 1960-1966.

[51] Li, W.H. and Du, H. 2003, 'Design and Experimental Evaluation of a Magnetorheological Brake', The International Journal of Advanced Manufacturing Technology, vol. 21, no. 7, pp. 508-515.

[52] Huang, J., Zhang, J.Q., Yang, Y. and Wei, Y.Q. 2002, 'Analysis and design of a cylindrical magneto-rheological fluid brake', Journal of Materials Processing Technology vol. 129, pp. 559-562.

[53] Kavlicoglu, B., Gordaninejad, F., Evrensel, C.A., Cobanoglu, N., Xin, M., Heine, C., Fuchs, A. and Korol, G. 2002, 'A High-Torque Magneto-Rheological Fluid Clutch', Proceedings of SPIE Conference on Smart Materials and Structures, 17

March, San Diego, CA, USA.

[54] Jolly, M.R., Carlson, J.D. and Munoz, B. 1996, 'A model of the behaviour of magnetorheological materials', Smart Materials and Structures, vol. 5 pp. 607-614.

[55] Davis, L.C. 1999, 'Model of magnetorheological elastomers', Journal of Applied Physics, vol. 85, no. 6, pp. 3348-3351.

[56] Shiga, T., Okada, A. and Kurauchi, T. 1995, 'Magnetroviscoelastic Behavior of Composite Gels', Journal of Applied Polymer Science, vol. 58 no. 4, pp. 787-792.

[57] Zhou, G.Y. 2004, 'Complex shear modulus of a magnetorheological elastomer', Smart Materials and Structures, vol. 13, pp. 1203-1210.

[58] Lokander, M. and Stenberg, B. 2003, 'Performance of isotropic magnetorheological rubber materials', Polymer Testing, vol. 22, pp. 245–251.

[59] Lokander, M. and Stenberg, B. 2003, 'Improving the magnetorheological effect in isotropic magnetorheological rubber materials', Polymer Testing, vol. 22, no. 6, pp. 677-680.

[60] Hu, Y., Wang, Y.L., Gong, X.L., Gong, X.Q., Zhang, X.Z., Jiang, W.Q., Zhang, P.Q. and Chen, Z.Y. 2005, 'New magnetorheological elastomers based on polyurethane/Si-rubber hybrid', Polymer Testing, vol. 24, no. 3, pp. 324-329.

[61] Chen, L., Gong, X.L. and Li, W.H. 2008, 'Effect of carbon black on the mechanical performances of magnetorheological elastomers', Polymer Testing, vol. 27, no. 3, pp. 340-345.

[62] Jiang, W.Q., Yao, J.J., Gong, X.L. and Chen, L. 2008, 'Enhancement in Magnetorheological Effect of Magnetorheological Elastomers by Surface Modification of Iron Particles', Chinese Journal of Chemical Physics, vol. 21, no. 1, pp. 87-91.

[63] Farshad, M. and Benine, A. 2004, 'Magnetoactive elastomer composites', Polymer Testing, vol. 23, no. 3, pp. 347-353.

[64] Zhang, X., Li, W. and Gong, X.L. 2008, 'An effective permeability model to predict field-dependent modulus of magnetorheological elastomers', Communications in Nonlinear Science and Numerical Simulation, vol. 13, no. 9, pp. 1910-1916.

[65] Nikitin, L.V., Korolev, D.G., Stepanov, G.V. and Mironova, L.S. 2006, 'Experimental study of magnetoelastics', Journal of Magnetism and Magnetic Materials, vol. 300, no. 1, pp. 234-238.

[66] Abramchuk S, Kramarenko E, Stepanov G, Nikitin, L.V., Filipcsei G., Khokhlov, A.R. and Zrinyi, M. 2007, 'Novel highly elastic magnetic materials for dampers and seals: part I. Preparation and characterisation of the elastic materials', Polymers for Advanced Technologies, vol. 18, pp. 883–890.

[67] Abramchuk S, Kramarenko E, Stepanov G, Nikitin, L.V., Filipcsei G., Khokhlov, A.R. and Zrinyi, M. 2007, 'Novel highly elastic magnetic materials for dampers and seals: Part II. Material behaviour in a magnetic field', Polymers for Advanced Technologies, vol. 18, pp. 513–518.

[68] Stepanov, G.V., Borin, D.Y., Raikher, Y.L., Melenev, P.V. and Perov, N.S. 2008, 'Motion of ferroparticles inside the polymeric matrix in magnetoactive elastomers', Journal of Physics: Condensed Matter, vol. 20, 204121.

[69] Stepanov, G.V., Abramchuk, S.S., Grishin, D.A., Nikitin, L.V., Kramarenko, E.Y. and Khokhlov, A.R. 2007, 'Effect of a homogeneous magnetic field on the viscoelastic behavior of magnetic elastomers', Polymer, vol. 48, pp. 488-495.

[70] Abramchuk, S.S., Grishin, D.A., Kramarenko, E.Y., Stepanov, G.V. and Khokhlov, A.R. 2006, 'Effect of a homogeneous magnetic field on the mechanical behavior of soft magnetic elastomers under compression', Polymer Science Series A, vol. 48, no. 2, pp. 138-145.

[71] Chertovich, A.V., Stepanov, G.V., Kramarenko, E.Y. and Khokhlov, A.R. 2010, 'New Composite Elastomers with Giant Magnetic Response', Journal of Macromolecular Materials and Engineering, vol. 295, no. 4, pp. 336 - 341.

[72] Ginder, J.M., Schlotter, W.F. and Nichols, M.E. 2001, 'Magnetorheological elastomers in tunable vibration absorbers', SPIE, Smart Structures and Materials: Damping and Isolation vol. 4331, Newport Beach, CA, USA pp. 103-110.

[73] Ginder, J.M., Clark, S.M., Schlotter, W.F. and Nichols, M.E. 2002, 'Magnetostrictive Phenomena in Magnetorheological Elastomers', International Journal of Modern Physics B, vol. 16, no. 17-18, pp. 2412-2418.

[74] Deng, H.X., Gong, X.L. and Wang, L.H. 2006, 'Development of an adaptive tuned vibration absorber with magnetorheological elastomer', Smart Materials and Structures, vol. 15, pp. 111–116.

[75] Deng, H.X. and Gong, X.L. 2008, 'Application of magnetorheological elastomer to vibration absorber', Communications in Nonlinear Science and Numerical Simulation, vol. 13, no. 9, pp. 1938-1947.

[76] Ni, Z.C., Gong, X.L., Li, J.F. and Chen, L. 2010, 'Study on a dynamic stiffness-tuning absorber with squeeze-strain enhanced magnetorheological elastomer', Journal of Intelligent Material Systems and Structures, vol. 21, pp. 1039-1047.

[77] Holdhusen, M.H. and Cunefare, K.A. 2003, 'Damping effects on the state-switched absorber used for vibration suppression', Journal of Intelligent Material Systems and Structures, vol. 14, pp. 551-561.

[78] Albanese, A.M. and Cunefare, K.A. 2003, 'Properties of a magnetorheological semi-active vibration absorber', SPIE Symposium on Smart Structures and Materials, volume 5052, pp. 36-43.

[79] Lerner, A.A. 2008, 'Tunability and sensitivity investigation of MREs in longitudinal vibration absorbers', Doctorate thesis, Georgia Institute of Technology.

[80] Albanese, A.M. 2005, 'The Design and Implementation of a Magnetorheological Silicone Composite State-Switched Absorber', Master of Science thesis, Georgia Institute of Technology.

[81] Lerner, A.A. and Cunefare, K.A. 2008, 'Performance of MRE-based Vibration Absorbers', Journal of Intelligent Material Systems and Structures, vol. 19, pp. 551-563.

[82] García Tárrago, M.J., Karil, L., Viñolas, J. and Gil-Negrete, N. 2007, 'Torsion stiffness of a rubber bushing: a simple engineering design formula including the amplitude dependence', The Journal of Strain Analysis for Engineering Design, vol. 42, no. 1, pp. 13-21.

[83] Park, E.J., Stoikov, D., Falcao, L. and Suleman, A. 2006 'A performance evaluation of an automotive magnetorheological brake design with a sliding mode controller', Mechatronics vol. 16, pp. 405-416.

[84] Wang, M.Y., Manoj, R. and Zhao, W. 2001, 'Gear rattle modelling and analysis for automotive manual transmissions', Proceedings of the Institution of Mechanical Engineers, Part D: Journal of Automobile Engineering, vol. 215, pp. 241-258.

[85] Chen L, G.X., Li X 2008, 'Damping of Magnetorheological Elastomers', Chinese Journal of Chemical Physics, vol. 21, pp. 581-585.

[86] Sun, H.L., Zhang, P.Q., Gong, X.L. and Chen, H.B. 2007, 'A novel kind of active resonator absorber and the simulation on its control effort', Journal of Sound and Vibration, vol. 300 pp. 117-125.

[87] Yamashita, S., Seto, K. and Hara, F. 1990, 'Vibration control in piping system by dual dynamic absorber (Realization of piping systems with unresonant characteristics)', JSME international journal, vol. 33, no. 4, pp. 488-494.

[88] Yan, T.H. and Lin, R.M. 2004, 'Dual-Mass Dynamic Absorber for the Head Actuator Assembly in Hard Disk Drives', Mechanics based design of structures and machines, vol. 32 no. 2, pp. 119-132.

[89] Burdisso, R.A. and Heilmann, J.D. 1998, 'A new dual-reaction mass dynamic vibration absorber actuator for active vibration', Journal of sound and vibration, vol. 214, no. 5, pp. 817-831.

[90] Iwanami, K. and Seto, K. 1984, 'An optimum design method for the dual dynamic damper and its effectiveness', Bulletin of JSME, vol. 27, no. 231, pp. 1965-1973.

[91] Al-Bedoor, B.O., Moustafa, K.A. and Al-Hussain, K.M. 1999, 'Dual dynamic absorber for the torsional vibrations of synchronous motor-driven compressors', Journal of Sound and Vibration, vol. 220, no. 4, pp. 729-748.

[92] Citron, S.J. and O'higgins, J.E. 1989, Cylinder-by-cylinder engine pressure and pressure torque waveform determination utilizing crankshaft speed fluctuations, US Patent: 4,843,870.

[93] Brennan, M.J. 1997, 'Vibration control using a tunable vibration neutralizer', Proceedings of the Institution of Mechanical Engineers - Part C: Journal of Mechanical Engineering Science, vol. 211, no. 2, pp. 92-108.

[94] White, R.G. and Pinnington, R.J. 1982, 'Practical application of the rapid frequency sweep technique for structural frequency response measurement', Aeronautical Journal vol. 86 pp. 179-199.

[95] The MathWorks 2011, Find root of continuous function of one variable, viewed Jan 25 2011 http://www.mathworks.com/help/toolbox/optim/ug/fzero.html.

[96] McLyman, C.W.T. 2002, High Reliability Magnetic Devices: Design and Fabrication, Marcel Dekker, Inc, pp.115.

[97] Kusko, A. and Wroblewski, T. 1969, Computer-aided design of magnetic circuits, MIT Press, pp. 109.

[98] Kazimierczuk, M.K. 2009, High-Frequency Magnetic Components, John Wiley & Sons, pp. 485.

[99] Members of the Staff of the Department of Electrical Engineering, M. 1943, Magnetic Circuits and Transformers A First Course for Power and

Communication Engineers, MIT Press, pp. 718.

[100] The MathWorks 2011, Eigenvalues and eigenvectors, viewed January 20 2011 <http://www.mathworks.com/help/techdoc/ref/eig.html>.

[101] Krodkiewski, J. 2008, Lecture notes, Mechanics Unit 4: Mechanical vibration, viewed 15-01 2008 <http://www.mame.mu.oz.au/dynamics/page14.html.>.

[102] The MathWorks 2011, Solve initial value problems for ordinary differential equations, viewed Jan 25 2011 <http://www.mathworks.com/help/techdoc/ref/ode45.html>.

[103] Meriam, J.L. and Kraige, L.G. 1993, Engineering Mechanics, Dynamics (Volume 2) Third edition, John Wiley & Sons, pp. 719.

[104] Hibbeler, R.C. 2004, Engineering Mechanics, Dynamics, Third edition, Prentice Hall, pp. 688.